ADVANCEMENTS IN MULTINUCLEAR MULTICHANNEL NMR AND MRI

A Dissertation

by

STEPHEN EDWIN OGIER

Submitted to the Office of Graduate and Professional Studies of
Texas A&M University
in partial fulfillment of the requirements for the degree of

DOCTOR OF PHILOSOPHY

Chair of Committee,	Steven M. Wright
Committee Members,	Mary P. McDougall
	Christian Hilty
	Samuel Palermo
Head of Department,	Miroslav M. Begovic

December 2019

Major Subject: Electrical Engineering

ABSTRACT

The introduction of receive arrays revolutionized ^{1}H MRI and *in vivo* NMR by increasing SNR and enabling accelerated imaging. All MRI scanners manufactured today are equipped to receive signals from ^{1}H array coils, but few support multi-channel reception for other nuclei. The extension of receive arrays to non-^{1}H nuclei has proven difficult because of the lack of broadband array receivers. These nuclei often have low sensitivity and stand to benefit greatly from the increase in SNR arrays provide.

This dissertation presents a variety of technologies that have been developed to enable the development and use of X-nuclear and multi-nuclear arrays. Frequency conversion receiver front-ends provide a straightforward and cost-effective approach for adapting standard ^{1}H multi-channel array receivers for use with other nuclei. Two generations of frequency translation receiver front-ends have been developed that use active mixers to convert the received signal from a non-^{1}H array to the ^{1}H frequency for reception by the host system receiver. This first-generation system has been demonstrated on 4.7T and 7T systems without any decrease in SNR as compared to the stock systems, and has been shown to be capable of accommodating ^{1}H decoupling. The second-generation receiver was developed to add the capability to simultaneously convert signals received from multiple nuclei as well as to streamline the setup and use of the translation system. Frequency translation has been shown to be able to convert ^{1}H-only multi-channel receivers for use with other nuclei with minimal degradation of SNR.

In addition, a standalone broadband system capable of simultaneous multi-nuclear imaging and spectroscopy at 1T and 4.7T has been developed. This system can either operate completely independently or interface with existing systems. The broadband system has been demonstrated with simultaneous imaging and spectroscopy of three nuclei.

This work allows existing multi-channel MRI receivers to be adapted to receive signals from nuclei other than hydrogen, allowing for the use of receive arrays for in vivo multi-nuclear NMR.

DEDICATION

"Let the favor of the Lord our God be upon us,

and establish the work of our hands upon us;

yes, establish the work of our hands!"

Psalm 90:17

ACKNOWLEDGEMENTS

I would first like to thank my committee chair, Dr. Wright, for his support and wisdom over the past several years. Without his experienced advice, none of this would have ever worked. Additionally, I wish to thank Dr. McDougall for her relentless enthusiasm and encouragement.

I am forever indebted to Dr. John Bosshard and Dr. Neal Hollingsworth, who have helped me to become a good engineer, and more importantly provided good council and stimulating conversation during the highs and lows of research.

Thanks to Matthew Wilcox for being the other half of the translation project and accompanying me on many, many trips to Dallas.

I would like to thank our collaborators at University of Texas-Southwestern Medical center, specifically Dr. Sergey Cheshkov, Dr. Ivan E. Dimitrov, and Dr. Craig Malloy for their generosity with magnet time and trusting me with their 7T system.

I would also like to thank my parents for their support and encouragement and for never questioning why I decided to get a PhD.

Finally, I'd like to thank my wife, Kathrine, for her incredible patience and unwavering support.

CONTRIBUTORS AND FUNDING SOURCES

Contributors

This work was supervised by a dissertation committee consisting of Dr. Steven Wright [advisor] and Dr. Samuel Palermo of the Department of Electrical and Computer Engineering, Dr. Mary McDougall of the Department of Biomedical Engineering, and Dr. Christian Hilty of the Department of Chemistry.

I would like to acknowledge the assistance of Sandeep Ganji of Philips Healthcare in loading and reformatting the 7 T spectroscopic data.

I was assisted in development of the multinuclear frequency translation system in Chapter 4 by Dr. Neal Hollingsworth.

Dr. John Bosshard was instrumental in the development of the broadband system described in Chapter 5, and substantial contributions were also made by Dr. Neal Hollingsworth, Scott Blaczyk, and Brian Bass. The triple-tuned coil was developed principally by Hongli Dong, and the triple-nucleus receiver front-end was developed by Dr. Chung-Huan “Tim” Huang.

All other work conducted for the dissertation was completed by the student independently.

Funding Sources

Graduate study was supported by a Graduate Merit Fellowship from Texas A&M University.

This work was also made possible in part by the National Institutes of Health under Grant Number R21HL120064 and the Cancer Prevention Research Institute of Texas under Grant Number RP150456. Its contents are solely the responsibility of the authors and do not necessarily represent the official views of the sponsors.

NOMENCLATURE

^{1}H	Hydrogen, Protium isotope, commonly referred to as Proton
^{2}H	Hydrogen, Deuterium isotope, commonly referred to as Deuterium
^{13}C	Carbon-13
^{15}N	Nitrogen-15
^{23}Na	Sodium-23
^{31}P	Phosphorus-31
B_0	Static Magnetic Field
B_1	Transmit RF Magnetic Field
B_2	Decoupling RF Magnetic Field
CSV	Comma-Separated Value
DDS	Direct Digital Synthesis
DNP	Dynamic Nuclear Polarization
FID	Free Induction Decay
FOV	Field-of-View
FPGA	Field-Programmable Gate Array
FTW	Frequency Tuning Word
I^2C	Inter-Integrated Circuit
IF	Intermediate Frequency
LNA	Low Noise Amplifier
FTU	Frequency Translation Unit

LO	Local Oscillator
MRSL	Magnetic Resonance Systems Lab
MRI	Magnetic Resonance Imaging
NMR	Nuclear Magnetic Resonance
PHIP	Parahydrogen-Induced Polarization
PLL	Phase-Locked Loop
ppm	Parts-per-Million
RF	Radiofrequency
RFPA	Radiofrequency Power Amplifier
RMS	Root Mean Square
SABRE	Signal Amplification by Reversable Exchange
SAW	Surface Acoustic Wave
SDR	Software Defined Radio
SFDR	Spurious-Free Dynamic Range
SNR	Signal-to-Noise Ratio
SPDT	Single-Pole Double-Throw
SPI	Serial Peripheral Interface
TCXO	Temperature-Controlled Crystal Oscillator
TTL	Transistor-Transistor Logic
VGA	Variable-Gain Amplifier

TABLE OF CONTENTS

Page

LIST OF FIGURES

Page

LIST OF TABLES

Page

1. INTRODUCTION

1.1. Nuclear Magnetic Resonance Spectroscopy

Nuclear Magnetic Resonance was first demonstrated in liquids and solids by Bloch and Purcell in 1946 [1, 2]. Since then, NMR spectroscopy has become one of the most powerful techniques in analytical chemistry.

Early NMR was done with ^{1}H, but NMR was quickly extended to other nuclei (commonly denoted as X-nuclei), and ^{13}C, ^{15}N, ^{23}Na, and ^{31}P are in common use [3-6]. For a variety of reasons, NMR of non-^{1}H nuclei is often more challenging than study of ^{1}H nuclei. Nearly all non-^{1}H nuclei have a lower gyromagnetic ratio than ^{1}H. SNR is related to gyromagnetic ratio, so nuclei with lower gyromagnetic ratios are less sensitive than those with higher ratios. Sensitivity is further reduced by the low natural abundance of many X-nuclei. For example, while ^{1}H has a natural abundance of 99.99%, ^{13}C has a natural abundance of just 1.1%. The remaining 98.9% is ^{12}C, which is not sensitive to NMR.

An additional complication for many X-nuclei is ^{1}H coupling, which further reduces SNR by splitting individual resonances in the spectra of many X-nuclei into multiple peaks, further reducing the signal intensity.

NMR was quickly applied to biological samples and extracts, and it soon began to be applied *in vivo* to ^{31}P [7, 8] and ^{13}C [9]. *In vivo* NMR of X-nuclei has the promise to provide a great deal more information than is available from ^{1}H NMR alone. ^{31}P has a

relatively high sensitivity compared to other X-nuclei studied *in vivo* and can provide incredible insights into metabolic activity and pH [10].

In vivo ^{13}C is especially tantalizing, as ^{13}C is enormously important metabolically and ^{13}C spectra can be clearer and easier to interpret than ^{1}H spectra [11]. Additionally, ^{13}C is amenable to the use of hyperpolarized agents *in vivo*, which allows biological probes to be used that are much more sensitive than standard ^{13}C NMR.

1.2. Parallel MRI

Early work in NMR and MRI was performed using a single RF coil to receive the signal from the sample, but it was proposed to use multiple RF coils and receive channels to improve the sensitivity or accelerate imaging or spectroscopy. When using a single volume coil to receive the NMR signal, signal only comes from the excited voxel or region of interest while noise is not localized and arises from the entire sample. This can be overcome by using an array of smaller coils to receive the NMR signal. Because smaller coils have a more limited region of sensitivity, they do not collect noise from the entire sample. By performing an optimized combination of the signal from the receive array elements, one can improve the sensitivity of the NMR experiment [12, 13]. Techniques were later developed to allow imaging to be accelerated – using information about the structure of the array, one could undersample the imaging matrix and recover the missing data using the geometry of the array. Two early techniques were Simultaneous Imaging of Multiple Spatial Harmonics (SMASH) and Sensitivity Encoding (SENSE) [14, 15], which paved the way for the development of an enormous number of parallel imaging sampling and reconstruction schemes. With the development of Single Echo Acquisition

(SEA) in the MRSL, parallel imaging was taken to the extreme – phase encoding could completely be eliminated by using arrays of as many as 64 elements [16].

Almost immediately, receive array technology was applied to spectroscopy to improve SNR [17-21]. X-nuclei are excellent candidates for the improvement of sensitivity with the use of array coils, as their low sensitivity makes any technology that improves SNR an enormous boon. Development of receive array coils for X-nuclei is frequently easier than development of similar coils for ^{1}H, as all X-nuclei of interest *in vivo* are at a lower frequency than ^{1}H for a given field strength. For thermally polarized X-nuclei, the use of receive arrays has the potential to greatly reduce the number of averages required. For experiments in which hyperpolarization techniques have been used to greatly increase the available signal, arrays can be used to increase resolution through undersampling much as they are for ^{1}H [18, 22].

However, the uptake of array technology for X-nuclei has been slow. This can potentially be attributed to a relative dearth of *in vivo* applications for X-nuclei, but because of the enormous information available from X-nuclei this explanation falls flat. Instead, one of the primary reasons for the lack of array coils for X-nuclei is that until the most recent generation of scanners, most MRI systems were not capable of receiving more than a single X-nuclear channel – if they could receive X-nuclei at all. Without systems capable of receiving signals from X-nuclear arrays, there was no reason to develop X-nuclear array coils. Without the sensitivity improvements X-nuclear arrays can provide, development of clinical applications for *in vivo* NMR of X-nuclei has been difficult. Without applications, there is no reason to develop X-nuclear coils or receivers. This cycle

can be broken, in part, by the development of add-on systems to enable the use of X-nuclear coils with existing NMR/MRI systems.

1.3. Dissertation Organization

This dissertation describes the development of two generations of frequency translation receiver front-ends that were designed to adapt multi-channel ^{1}H-only receivers for use with X-nuclei. Today, multi-channel receivers are ubiquitous on clinical MRI scanners, but most are limited to only receiving ^{1}H. Using a frequency translation front-end can adapt these receivers for use with X-nuclei.

After this chapter follows a chapter on the background theory of NMR and MRI and the technologies used to implement the frequency translation system as well as a brief overview of NMR/MRI spectrometer architecture.

Chapters 3 covers the first-generation 16-channel frequency translation system. Different approaches to adding multichannel multinuclear receive to an existing system are discussed, and two frequency translation-based architectures are introduced. Results are shown from single coils at 4.7T and single coils and a 16-element array at 7T.

Chapter 4 discusses a second-generation 16-channel frequency translation system that was developed to expand on the capabilities of the original translation system as well as address some of its shortcomings.

Chapter 5 describes the architecture of a standalone broadband MRI system that was developed to enable simultaneous multinuclear imaging and the development of related technologies. Results are shown from of simultaneous images and spectra from three nuclei.

The dissertation is concluded with discussion of the systems developed, their applications, and potential future work.

1.4. Dissertation Style

The format used for reference notations follows that used by the journals of the Institute of Electrical and Electronics Engineers (IEEE). Additionally, each of the main body chapters is based on a stand-alone paper intended for publication in an IEEE journal.

2. BACKGROUND AND MOTIVATION

2.1. Nuclear Magnetic Resonance

2.1.1. Fundamentals of NMR

2.1.1.1. Spins, Polarization, and Precession

Nuclear Magnetic Resonance Spectroscopy and Imaging are based on the study of nuclei with non-zero nuclear spin. When placed into a static magnetic field, commonly referred to as B_0, the spins polarize into different states determined by their nuclear spin state. For nuclei with spin equal to ½ (e.g. ^{1}H, ^{13}C, ^{15}N, and ^{31}P), there are only two spin states, +½ and -½.

When placed in a magnetic field with strength B_0, the spins precess at a nucleus-specific frequency governed by the Larmour equation:

$$f = \gamma B_0$$

where γ is the gyromagnetic ratio, given in MHz/T.

The two spins states are at slightly different energy levels, and because of this they develop slightly different populations, described by [11]:

$$\frac{n_{+\frac{1}{2}} - n_{-\frac{1}{2}}}{n} \approx \frac{h\gamma B_0}{2kT}$$

where n is the total number of spins in a sample and $n_{+\frac{1}{2}} - n_{-\frac{1}{2}}$ is the difference in population between the two spin states.

For nuclei at reasonably obtainable field strengths and biologically compatible temperatures, the developed polarization is not very large. The polarizations for

commonly used nuclei at the field strengths considered in this dissertation can be seen in Table 2.1.

Nucleus	Polarization in ppm		
	1T	4.7T	7T
^{1}H	3.39	15.95	23.75
^{13}C	0.85	4.01	5.97
^{15}N	0.34	1.62	2.41
^{31}P	1.37	6.46	9.62

Table 2.1: Polarizations for common nuclei at assorted B_0 field strengths.

2.1.1.2. RF Pulses

Spins are excited by use of pulses at the Larmour frequency, which is in the 10s to 100s of MHz for the nuclei and B_0 encountered in this work. An oscillating magnetic field, B_1 is applied at the Larmour frequency to tip the spins from their relaxed state along the B_0 axis (typically denoted z) to the transverse (x-y) plane, where they can emit a Free Induction Decay (FID) or be further manipulated by additional RF pulses or radiofrequency gradients.

The magnetic field required to excite the spins is fairly high. The amount of power required to generate the required B_1 field depends on the RF pulse type and the coil size, shape, and efficiency, but a small 6 cm birdcage coil typically requires on the order of 50 W, and the breast array coil used for 7T work often required 1000 W. It is not uncommon for the full-body coils built into the bore of clinical MRI systems to be driven by amplifiers capable of producing over 10 kW.

The amount of power needed to excite the spins is enormous in comparison to the signal the spins produce, which rarely exceeds 1 μV. The massive discrepancy in signal level between the transmitted and received signals drives a great deal of NMR and MRI system design, as the sensitive receive electronics must be protected against the powerful transmit RF pulses.

2.1.1.3. Chemical Shift

One of the fundamental methods by which NMR spectroscopy is able to provide insight into the structure of molecules is through chemical shift. Chemical shift, measured in parts-per-million and commonly denoted by δ, is the difference in frequency between different nuclei in a molecule caused by non-uniformity in electron density. Differences in electron density cause different nuclei to experience slightly different static magnetic fields, which causes them to have slightly different precession frequencies.

The range of common chemical shifts varies between different nuclei. Most ^{1}H resonances fall within an approximately 10 ppm range, whereas the full ^{13}C chemical shift range covers approximately 220 ppm.

2.1.2. Hyperpolarization

Hyperpolarization refers to a group of techniques that allow the polarization of a sample of spins to be increased greatly beyond what thermal equilibrium polarization would be at that temperature [23].

Multiple nuclei can be hyperpolarized simultaneously, but after polarization, they undergo T_1 relaxation, so it is imperative that the nuclei are imaged/interrogated rapidly and simultaneously.

2.1.2.1. Hyperpolarization Techniques

A large number of hyperpolarization techniques have been developed. Discussion here will be limited to brute-force polarization, dynamic nuclear polarization, and parahydrogen techniques.

Brute-force polarization uses low temperatures (~ 4.2 K) and high magnetic fields to increase the polarization of a sample of spins [24]. Brute-force polarization doesn't require complicated equipment, but it can be very slow, as the polarization build-up is T_1-dependent, and T_1 increases at low temperatures.

Dynamic nuclear polarization (DNP) uses RF irradiation in combination with low temperatures and high magnetic fields to greatly accelerate the hyperpolarization process. DNP is done in the solid state, so for use in *in vivo* applications, the sample is melted by superheated water in a technique known as dissolution DNP, which has seen some use in clinical research [23, 25].

Parahydrogen-induced polarization (PHIP), signal amplification by reversable exchange (SABRE), and signal amplification by reversable exchange in shield enables alignment transfer to heteronuclei (SABRE-SHEATH) are a set of related techniques that use the spin order from parahydrogen to increase the polarization of other nuclei [26-29].

2.1.2.2. Limitations of Hyperpolarization

Although hyperpolarization can provide immense enhancements in signal-to-noise ratio, it has a number of limitations that limit its application to *in vivo* NMR and MRI.

T_1 has a large impact on how quickly the hyperpolarized signal decays, limiting the time in which data can be acquired and constraining the selection of compounds that

are well suited to hyperpolarization. T_1 limits the acquisition time in two ways: the polarization decays as with T_1 after the sample is removed from the polarizer, and every RF excitation irreversibly converts some of the longitudinal magnetization to transverse magnetization. For *in vivo* applications, it is important that the hyperpolarized substrate has a long enough T_1 for the sample to be ejected, transferred to the imaging suite, and injected into the subject.

Hyperpolarization also requires dedicated equipment. Although instructions for the construction of hyperpolarization systems have been published [28], the equipment for hyperpolarization is still very specialized and requires cryogenic temperatures, necessitating either the use of liquid helium or a helium cold head, both of which add considerable cost and complexity.

2.1.3. ^{1}H Decoupling

^{3}J coupling between ^{1}H nuclei is an important part of interpreting ^{1}H NMR spectra. ^{1}J coupling between protons and directly-bound heteronuclei is also important for the interpretation of NMR spectra, but eliminating the effects of ^{1}J-coupling of protons on heteronuclei is often important to simplify spectra and improve SNR.

The effects of ^{1}H coupling can be virtually eliminated by the use of ^{1}H decoupling. ^{1}H decoupling uses RF irradiation at the ^{1}H frequency to reduce the effects of coupling. Rapidly inverting the ^{1}H spins at a frequency much greater than the ^{1}J coupling frequency averages out the effect of proton coupling. A variety of decoupling pulse sequences have been developed to efficiently decouple protons over a broad bandwidth [30-32].

2.1.4. NMR Imaging

By using pulsed gradient fields, spatial information can be encoded into the NMR signal [33]. This can be used to simply image the relaxation-weighted density of ^{1}H spins, as is done in MRI, or spectral information can be preserved, as in chemical shift imaging (CSI) [34].

2.2. Radiofrequency Mixers

Radiofrequency mixers are non-linear 3-port devices designed to convert between different frequencies. They have long been a core component of many transmitter and receiver architectures.

2.2.1. Theoretical Basis

RF mixers are based on the trigonometric product and sum identities. Essentially, by multiplying the RF signal at frequency f_{RF} with a local oscillator at frequency f_{LO}, the output, commonly referred to as the intermediate frequency (IF), will contain mixing products at two intermediate frequencies given by:

$$f_{IF} = f_{RF} + f_{LO}$$

and

$$f_{IF} = f_{RF} - f_{LO}$$

Because of this property, mixers can be used in both transmitters and receivers: in transmit they can convert a signal at a baseband or low IF to a higher frequency for broadcasting, and in receive they can convert a high frequency signal down to a lower frequency for digitization.

2.2.2. Spurious Signals

Because practical RF mixers are constructed using non-linear devices, the output is complicated by additional spurious signals, commonly referred to as spurs. The outputs of a realistic mixer occur at frequencies given by

$$f = mf_{RF} + nf_{LO}$$

where m and n are integers. The most commonly desired mixing products occur for $m = \pm 1$ and $n = \pm 1$.

The outputs for all n with $m = 0$ and for all m with $n = 0$ represent the LO and RF bleed-through, respectively. These can be minimized through the use of balanced and doubly-balanced mixers.

The outputs for $|m| > 1$ and $|n| > 1$ are typically considered spurious outputs. The magnitude of these outputs is dependent on the exact design of the mixer and the non-linear devices used to implement it.

2.2.3. Phase in RF Mixers

If the derivation of the output of an ideal RF mixer performed with the addition of phase terms for both the RF and LO, we can find that the phases of the mixing products are dependent on the phases of the RF inputs.

Let us begin with the expression of the output voltage P of an ideal mixer as

$$P = \cos(2\pi f_{RF} t + \phi_{RF}) \cos(2\pi f_{LO} t + \phi_{LO})$$

where f_{RF} and ϕ_{RF} are the frequency and phase, respectively of the RF input and f_{LO} and ϕ_{LO} are the frequency and phase, respectively, of the LO input. Using the trigonometric product and sum identities, we can split the product into outputs at two frequencies.

$$P = \frac{1}{2}[\cos(2\pi f_{RF}t + \phi_{RF} + 2\pi f_{LO}t + \phi_{LO}) + \cos(2\pi f_{RF}t + \phi_{RF} - 2\pi f_{LO}t - \phi_{LO})]$$

Combining similar terms, we arrive at the two primary mixing products

$$P = \frac{1}{2}[\cos(2\pi(f_{RF} + f_{LO})t + \phi_{RF} + \phi_{LO}) + \cos(2\pi(f_{RF} - f_{LO})t + \phi_{RF} - \phi_{LO})]$$

Each cosine term is one of the primary mixing products, at frequencies $\omega_{RF} + \omega_{LO}$ and $\omega_{RF} - \omega_{LO}$. The phase of each output is dependent on both ϕ_{RF} and ϕ_{LO}.

2.2.4. Passive and Active Mixers

Mixers have been implemented in a wide variety of ways, from single diodes, to vacuum tubes, to integrated circuits. The most common architecture based on a passive component is the doubly-balanced diode mixer, which can be seen in Figure 2.1.

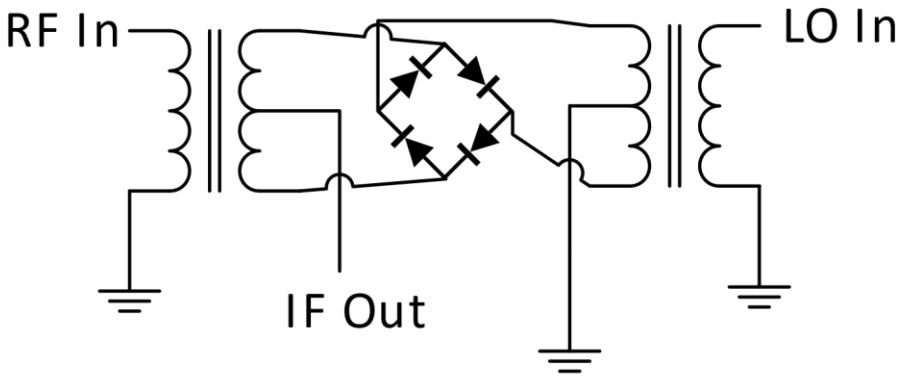

Figure 2.1: Doubly-balanced diode mixer.

If broadband performance is desired, the baluns on the RF and LO ports must be constructed with ferrite cores. Additionally, the LO drive level must be substantially larger

than the maximum RF amplitude in order for this circuit to function as a good approximation of an ideal mixer. Also, because the diode mixer contains no devices capable of producing gain, this type of mixer invariably results in an IF output at a lower amplitude than the RF input, which can lead to more gain being required in the circuit to achieve the desired signal level.

If a similar circuit is implemented with transistors, one arrives at the doubly-balanced Gilbert cell mixer [35]. Active mixers have several potential advantages over passive diode mixers. They do not require as much LO power to operate and can also provide conversion gain. Most importantly for our application, they often do not require use of magnetic components to achieve broadband performance.

Active mixers do have a few disadvantages. They typically require a DC power supply to operate, and they are often more expensive then doubly-balanced diode mixers.

2.2.5. Importance of Phase Coherence

Phase coherence is necessary for any technique that requires the processing of complex echoes or FIDs. Phase coherence can be foregone for looking at spectra acquired with a single acquisition and projection imaging.

The importance of phase coherence can be easily demonstrated with averaging. If the phase of each acquired average is randomly different, then as the number of averages increases, the sum of the averages will tend towards zero.

Commercial NMR and MRI scanners are phase coherent by design. When inserting hardware into the transmit or receive path or substituting the transmitter or receiver with custom hardware, care must be taken to maintain phase coherence.

2.3. Direct Digital Synthesis

Direct Digital Synthesis (DDS) is a technology by which waveforms are generated digitally before being converted to an analog output. DDS allows for precise control of frequency and phase and easily accommodates locking to an external frequency reference.

In a DDS system, a numerically controlled oscillator (also called a phase accumulator), whose frequency is controlled by a frequency tuning word (FTW), keeps track of the phase of the system. The numerically controlled oscillator's phase is fed into a lookup table which converts the phase to the appropriate amplitude of a sinusoid. This digital amplitude is then converted to an analog output. A block diagram of a basic DDS synthesizer can be seen in Figure 2.2.

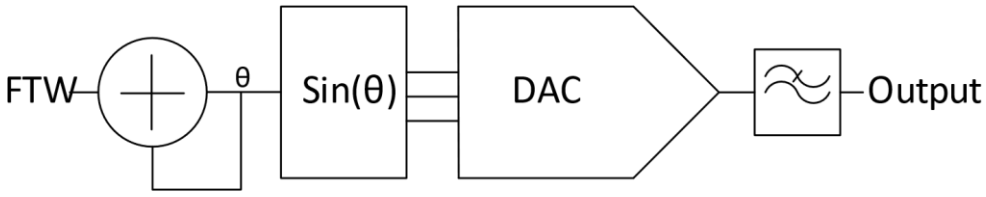

Figure 2.2: Block diagram of a basic DDS synthesizer.

The analog output contains a fundamental output at a frequency below the Nyquist frequency as well as a large number of images above the Nyquist frequency. For low frequency operation (typically <40% the system clock), a low-pass filter can be used to suppress the images, but it is possible to make use of the image outputs, albeit with increased phase noise and reduced SFDR [36].

2.4. Magnetic Resonance Systems

An overview of the major subsystems of an NMR/MRI scanner can be seen in Figure 2.3.

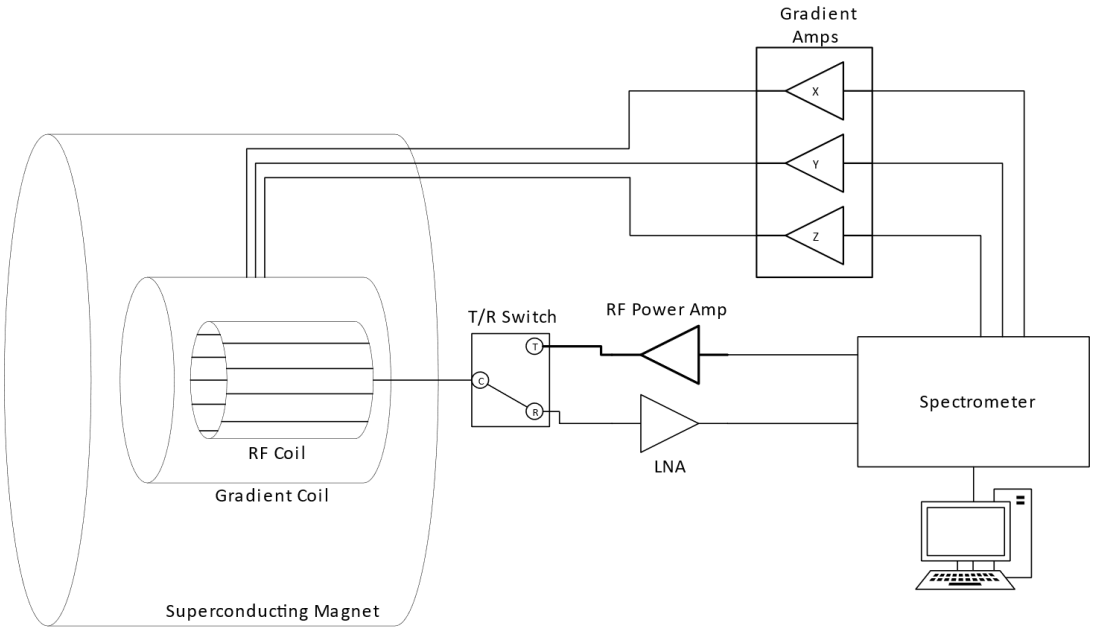

Figure 2.3: Overview of a MRI system.

2.4.1. Receivers

The receiver in an MRI system is responsible for digitizing the signal produced by the NMR experiment. The first stage of an MRI receiver is invariably a low-noise amplifier (LNA), but after that, the receiver architectures can vary greatly.

2.4.1.1. Receiver Requirements

Because the signal produced by the NMR experiment is so small, the receiver must meet some strict requirements. The noise figure of the receiver should be as low as possible, and it is essential that the system be phase coherent. Additionally, the system

must be capable producing a complex dataset, that is the resulting data must have in-phase (I) and quadrature (Q) information.

2.4.1.2. Receiver Architectures for MRI

2.4.1.2.1. Conversion to Baseband

In the oldest receiver architecture, the received signal is mixed to baseband before digitization. This can be done using a single conversion stage (aka a homodyne receiver), but it is common to use two conversion stages (aka a heterodyne architecture).

In order to obtain both I and Q data, it is common in the final mixing stage to split the signal and use two local oscillators at the same frequency to mix to baseband, one a sine and the other a cosine. The baseband output of each mixer is filtered, digitized, and combined in memory to form I/Q data. This is the architecture used by the Varian Unity Inova system.

This architecture does not require ADCs with high sample rate, as the sampling rate of each digitizer simply needs to equal the spectral width. However, it is prone to artifacts arising from DC offsets in the digitized signal and amplitude or phase imbalance between the quadrature mixing stages. These can be corrected for in post processing or by using techniques such as phase cycling.

2.4.1.2.2. Conversion to IF

A more advanced approach is to use a mixing stage to convert the received signal to some lower IF before digitizing the IF directly. The digitized IF can then be digitally demodulated and filtered digitally to obtain I/Q data in much the same fashion as the two mixers were used in the baseband conversion heterodyne architecture. This approach was

used in the MRSL stand-alone 64-channel receiver system, which uses a 500 kHz IF and 2.5 MHz sampling rate [37, 38].

This architecture is not susceptible to DC offset and quadrature artifacts, but the sampling rate requirement can be much higher depending on the IF used. In order to avoid aliasing, it is best to fully sample the IF, so the required sample rate is at least twice the IF frequency. The IF can be undersampled, but that can potentially reduce SNR and introduce artifacts if care is not taken. Due to the high sampling rate, the data processing requirements are higher than baseband sampling, at least until the signal has been digitally demodulated, filtered, and decimated.

2.4.1.2.3. Direct Sampling and Undersampling

The point of digitization can be pushed further towards the LNA to get direct sampling. In this architecture, the received signal is preamplified before being directly digitized by the ADC. After digitization, the signal is digitally demodulated. This is the approach used in the Medusa console [39] and the MRSL broadband system.

This architecture requires a minimum of RF hardware, but does require a very fast digitizer to fully sample the received signal, as the Nyquist rate is two times the Larmour frequency. Alternately, it is possible to intentionally undersample the received signal. Using a sampling rate less than the Nyquist rate will result in the received signal aliasing. If the digitizer has a fast enough front-end and the received signal has been well-filtered, this can be done without significant reduction in SNR.

Direct sampling or undersampling also produces the largest data files if digital demodulation and decimation is not performed in the receiver itself. Efficient

implementations of direct sampling use FPGAs built into the receiver to perform this conversion in hardware before the file is saved. This can greatly reduce the size of the raw data files produced.

2.4.2. Transmitters

The small-signal portions of the MRI transmit system are essentially the same as those in the receive system, but with the signal flow reversed. A modulated RF signal needs to be produced at the Larmour frequency. This small signal is then inserted into a high-power amplifier, which drives the RF coil, producing the B_1 field. The amplitude of the RF pulse is typically controlled by a variable attenuation or gain stage between the RF waveform generator and the RF power amplifier.

2.4.2.1. Transmitter Requirements

Like the receiver, the transmitter must be phase coherent. For any sequence that requires shaped RF pulses, such as most imaging and localizes spectroscopy sequences, it is also important that the transmit system be linear, as distortion of the RF pulses will result in distorted slice profiles and incorrect voxel shapes.

2.4.2.2. Transmitter Small-Signal Architectures for MRI

MRI Transmit architectures are essentially the dual of MRI receiver architectures. DACs replace ADCs, and up-conversion replaced down-conversion, but the overall picture is overall the same.

Two important transmit architectures will be discussed in detail. A single-conversion (homodyne) architecture can be implemented using a vector modulator, which encapsulates the two mixers and power combiner into the same package. Depending on

the design, either a single LO or two LOs in quadrature are input as well as baseband I and Q analog waveforms.

A more recent development is to use DDS to generate the RF waveform. DDS modulators allow for control of the amplitude and phase of the synthesized signal over a digital interface. This allows for full modulation of the synthesized RF waveform.

3. A FREQUENCY TRANSLATION SYSTEM[1]

3.1. Introduction

The introduction of array coils and multi-channel receivers dramatically changed the nature of MRI. Sensitivity was improved, and the increase in available information enabled images to be more quickly obtained without any change in contrast [12]. Techniques were developed to accelerate imaging using arrays of receive coils [14, 15]. Furthermore, it has been shown that the benefits of array coils and multi-channel receivers extend to *in vivo* ^{1}H NMR spectroscopy [13].

In order to use an array of coils to improve signal-to-noise ratio (SNR) or accelerate imaging, a multi-channel receiver is necessary. The first receivers for large ^{1}H arrays were stand-alone add-on systems [37, 40], but they are now standard on clinical MRI scanners.

In vivo NMR spectroscopy has long been a goal of the magnetic resonance community. The increasing popularity of 3T scanners and introduction of 7T whole-body research systems has done a great deal to bring *in vivo* NMR spectroscopy within reach, and an enormous amount of research is being done to realize clinical ^{1}H spectroscopy *in vivo*. The study of other nuclei has been less successful, as X-nuclei (nuclei other than ^{1}H) have lower gyromagnetic ratios and are therefore less sensitive. Additionally, some X-nuclei, such as ^{13}C and ^{15}N have low natural abundance, i.e. in a naturally occurring sample

[1] This chapter is based on a draft of a paper intended for submission in IEEE Transactions on Biomedical Imaging entitled "A Frequency Agile Mixing Front End for Multi-Channel, Multi-Nuclear Spectroscopy"

of one of these elements, the majority of the nuclei will not be NMR sensitive. As one of the most extreme examples, ^{13}C is enormously significant metabolically but has a low natural abundance (1.1%) and gyromagnetic ratio (~1/4 that of ^{1}H) which combine to give it sensitivity approximately 5700 times lower than that of ^{1}H [11].

A logical step is to develop array coils for nuclei such as ^{13}C and ^{31}P to improve their detectability. Presently, most available large array receivers (16 channels or greater) are limited to receiving ^{1}H signals. Although nearly all 3T and 7T systems have at least 16 channels of ^{1}H receive, until recently, even most 7T systems only shipped with a small (1-4) number of broadband receive channels.

The lack of broadband multi-channel receivers makes the use of array coils for X-nuclei difficult or impossible, has made the development of these coils difficult due to the fewer number of systems on which to test and apply them. Without X-nuclear array coils, there is less motivation to develop multi-nuclear receivers or develop protocols that could benefit from the improved sensitivity provided by multi-channel coils for X-nuclei such as ^{13}C, and the cycle may be slow to be broken without a solution to retrofit or augment current systems. The ubiquity of ^{1}H receivers with 16 or more channels presents a solution – when used with a translation system to modify the ^{1}H array receivers for use with other nuclei.

3.2. Methods and Materials

3.2.1. Approaches to Receive Technology

There are several possible ways in which 16 channels of multi-nuclear receive capability could be added to a system with a multi-channel receiver limited to ^{1}H. This

could be accomplished by constructing a standalone receiver [39], but adding the capability to the host system receiver has several advantages. Integrating with the receiver eliminates the considerable expense and complexity of adding a 16-channel standalone digitizer. Additionally, integration makes the system much easier to use, as the scan results are immediately available on the host system console.

A variety of receiver topologies are possible [38], but a single frequency conversion stage to convert the received signal from the frequency of the X-nucleus to the ^{1}H frequency was chosen, a method referred to here as frequency translation [41].

3.2.2. Overview of Frequency Translation

Frequency translation has been used to adapt scanners for use with 4-channel ^{31}P and ^{23}Na coils in the past [42]. This work aims to use recent developments in commodity electronics to extend this to 16 channels in a compact form. Our primary target is ^{13}C, so accommodation of ^{1}H decoupling is crucial. This leads to the following set of requirements, justified and discussed below:

- Compact – The frequency translation unit (FTU), which contains translation hardware for 16 channels should be able to fit in a reasonably sized enclosure (here, a 2U 19-inch rack). The control equipment should be similarly compact as to not take up too much space in a crowded equipment room
- B_0-tolerant – The FTU should be able to be located in the scan room, adjacent to the bore of magnet. This is necessary as the FTU needs to be inserted between the coil and the host system receiver. The easiest place to intercept the received signal

is before the host's coil interface, which requires the FTU to be located in the magnet room to minimize the distance the signal must travel.

- Broadband – The system should be able to translate most nuclei used for *in-vivo* spectroscopy (e.g. ^{2}H, ^{13}C, ^{15}N, ^{23}Na, ^{31}P) at frequencies up to those used at 7T. The use of narrow-band components should be minimized, and any required filters should be modularized to enable them to be easily replaced.
- Phase Coherent – To perform averaging of real spectra or most localization techniques, it is necessary that the phase of the received signal be consistent from acquisition to acquisition.
- Interference Interference Immune – The system should be able to tolerate and reject the strong signals required for ^{1}H decoupling.
- Low Noise – The introduction of any additional stages to the receive path will reduce the SNR of the received signal, but this should be minimized. Our objective was that the system should not degrade the overall noise figure of the receive system by more than 0.5dB, or more than 5.6%.
- Easily Integrated – The system should be easy to transport and to integrate with a variety of MRI systems. Here we demonstrate the use of a frequency translation system on both Philips Achieva 7T and Varian Unity Inova 4.7T scanners

The frequency translation front-end fundamentally consists of a single radiofrequency mixer followed by a bandpass filter inserted into each receive channel after

low-noise amplification. The same local oscillator (LO) is used to drive all of the translation channels to allow conversion of the received ^{13}C signal to ^{1}H.

The LO is generated by direct digital synthesis (DDS) which reduces the size and cost of the translation system. More importantly, use of DDS allows for control of the LO phase, which simplifies the translation system by eliminating the requirement that the excitation pulse is translated along with the received signals.

Radiofrequency mixers are non-linear devices used to convert an RF frequency, f_{RF}, to an intermediate frequency (IF), f_{IF}. Mixers have long been used in radiofrequency systems and have been a key part of MRI receiver architecture up until the latest generation of receivers.

In order to convert from one frequency to another, the mixer must be provided with a second input, a local oscillator (LO) at a frequency (f_{LO}) such that either of the two following conditions are met:

$$f_{IF1} = f_{LO} + f_{RF}$$

$$f_{IF2} = f_{LO} - f_{RF}$$

An ideal mixer would produce only two mixing products at the frequencies given by the above equations; however, practical RF mixer implementations also produce a large number of spurious signals over a wide range of frequencies, commonly referred to as spurs [43]. These are found at frequencies described by:

$$f_{\text{Spur m,n}} = mf_{\text{LO}} + nf_{\text{RF}}$$

where *m* and *n* are integers. Because of the large number of different signals present at the mixer output, it is typically necessary to use a bandpass filter to select the desired output product, which for this application is f_{IF1}.

B_0	f_{IF}	f_{RF}	f_{LO}
4.7 T	200.1 MHz	50.3 MHz	149.8 MHz
7 T	297.9 MHz	74.9 MHz	223.0 MHz

Table 3.1: Local Oscillator Frequencies for ^{13}C

In our application of frequency translation, the RF input to the mixer is the signal received from the X-nucleus after preamplification, and the IF is the ^{1}H frequency, the frequencies of which are given in Table 3.1. For our implementation, the first condition was chosen because it requires a much lower LO frequency (223 MHz vs. 373 MHz for ^{13}C at 7T) and preserves the orientation of the spectrum. Using the higher LO frequency reverses the translated spectrum in the frequency domain. Had the chosen option presented problems due to spurious signals from the mixer, it would be straightforward to switch to the higher LO frequency and correct the reversal in the post-processing code.

The noise figures of RF mixers are typically poor (5-12 dB) [44]. Thus, it is important that frequency translation occur after the low-noise amplifier (LNA) to reduce the impact of the noise figure of the mixer, as cascading a noisy device after a gain stage greatly reduces the noise contribution of the noisy device [45]. The increase in noise figure of an amplifier with gain G_A and noise figure NF_A cascaded into a mixer with noise figure NF_M is given by [46]:

$$NF = 10 * \log_{10}\left[10^{\frac{NF_A}{10}} + \frac{\left(10^{\frac{NF_M}{10}} - 1\right)}{10^{\frac{G_A}{10}}}\right] - NF_A$$

In our application, inserting a mixer with a noise figure of 16 dB after an LNA with 26 dB of gain and a 1.0 dB noise figure would increase the noise figure by 0.32 dB.

Following translation, the signal is inserted into the input of the ^{1}H array receiver of the host system. The transmit pulse can be generated by either the system at the ^{13}C frequency or at the ^{1}H frequency, in which case an additional mixing stage is used to convert it to the ^{13}C frequency. The architecture for these two variations can be seen in Figure 3.1.

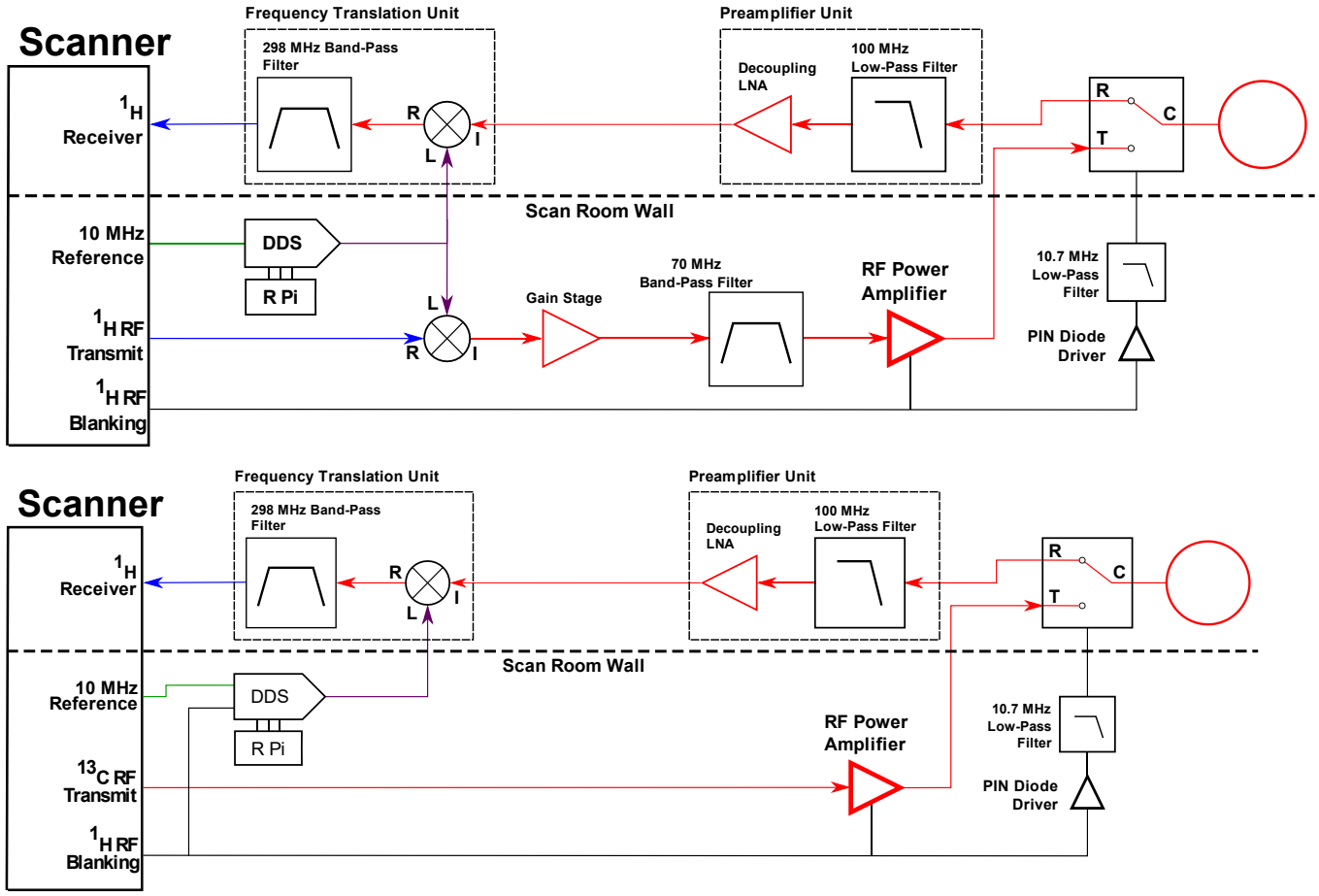

Figure 3.1: Two approaches to frequency translation. The top approach uses frequency translation of both the transmitted and received signals, and phase coherence is maintained through use of a common LO for both sides. The bottom approach only mixes on receive and resets the phase of the DDS with each acquisition to maintain coherence.

3.2.3. Maintaining Phase Coherence – Two Approaches

Although it is possible to collect magnitude NMR spectra without phase coherence, phase coherence is essential if one wishes to perform averaging of real (not magnitude) spectra or use more sophisticated pulse sequences which require the addition and subtraction of spectra, such as ISIS, PRESS, or Chemical Shift Imaging (CSI) [34, 47, 48]. The low sensitivity of 13C makes averaging essential, so phase coherence was a primary concern in the design of the system.

To maintain phase coherence, a high-stability oscillator is required for use in generating the LO. Nearly all NMR and MRI systems use a 10 MHz reference oscillator to synthesize RF signals and digital clocks, so this signal was used as the high-stability reference oscillator. Many systems have a spare 10 MHz reference output, and in the case that one is not present, it is straightforward to use a tee or splitter to tap into the reference signal.

The second important factor for maintaining phase coherence is accounting for the phase shift introduced by mixing. The phase of the output of an RF mixer is dependent on the phase of both the RF input and the LO [49]. To resolve this in hardware, this phase shift must either be cancelled out or kept constant. It can also be corrected in post-processing by use of navigators [49], parameter fitting [50], or by prospectively incrementing the phase of the transmitted pulse [51]. For this application, a hardware approach was chosen because navigators and parameter fitting require a high SNR to provide robust results, and ^{13}C does not have nearly enough SNR to ensure consistent results. Prospective correction is dependent on exact knowledge of the actual TR used by

the system and requires the TR to remain stable on a sub-nanosecond scale over the entire acquisition. If TR is timed by software instead of hardware timers in a system, the TR may not be sufficiently consistent to allow for prospective correction. Additionally, prospective correction requires modification of the pulse sequence for any change in any of the frequencies used or the TR, and we wished to be able to avoid sequence modifications at all if possible. Another approach could be to perform a similar TR-dependent phase correction retrospectively, but this has many of the same limitations as prospective correction and additionally requires saving each acquisition separately, which can greatly increase data throughput requirements if averaging is required.

Approaches for maintaining phase coherence have been developed for both of the architectures shown in Figure 3.1. Both approaches have been demonstrated on two systems – a 4.7T Varian Unity Inova system and a 7T Philips Achieva system.

In the first approach, which was used by Lee et al., phase coherence is maintained by mixing both the transmit pulse and the received signal to cancel out the phase shift introduced by mixing [42]. The host system operates in a normal 1H mode. The 1H transmit pulse from the host system is mixed down to the frequency of the X-nucleus. On receive, the received signal is mixed up to the 1H frequency using the same LO. As long as the LO is sufficiently stable (which is achieved by using a 10 MHz reference derived from the host system), any phase shift acquired mixing the transmitted signal down will be undone when mixing the received signal up to the 1H frequency.

In the second approach, phase coherence is maintained by holding the phase of the LO constant for each acquisition. Using a trigger from the system, the phase of the LO is

reset to the same point before each acquisition. This causes the phase shift generated by mixing to be identical between acquisitions, which ensures phase coherence. To accomplish this, Direct Digital Synthesis (DDS) is used to generate the LO, as this allows both locking to an external reference and arbitrary resetting of the LO phase. A spare digital line from the host system can be used to trigger the phase reset immediately before the acquisition, or the host's RF power amplifier blanking control line can simply be used to provide a reliable time point to reset the phase. The addition of a static phase shift to the received signal has no negative effects, as zero and first-order phase corrections are typically applied to spectra in post-processing [52]. The static phase shift from frequency translation simply changes the zero-order correction term in the same way using a different length of cable between the coil and the receiver would.

3.2.4. The 16-Channel Frequency Translation System

It is desirable to have the translation system in the scan room, close to the coil and host system receiver to minimize cable runs, noise, and the potential for interference. The control unit, which contains power supplies, the LO source, the LO control and monitoring equipment, and the transmit-side mixer, shown in Figure 3.2, is located in the equipment room, while the 16-channel FTU, shown in Figure 3.3, is located in the scan room. There are three required connections that must enter the scan room from the equipment room:

- DC power supplies to provide the required +15 V, +7.5 V, and -7.5 V DC voltages.
- Local oscillator
- TTL control line for coil detuning

Figure 3.2: Equipment room frequency translation rack. Units are, from top to bottom: Transmit translation stage, LO source, and power supplies and LO control and monitoring. The touchscreen in the monitoring unit shows the LO output being monitored with FreqShow.

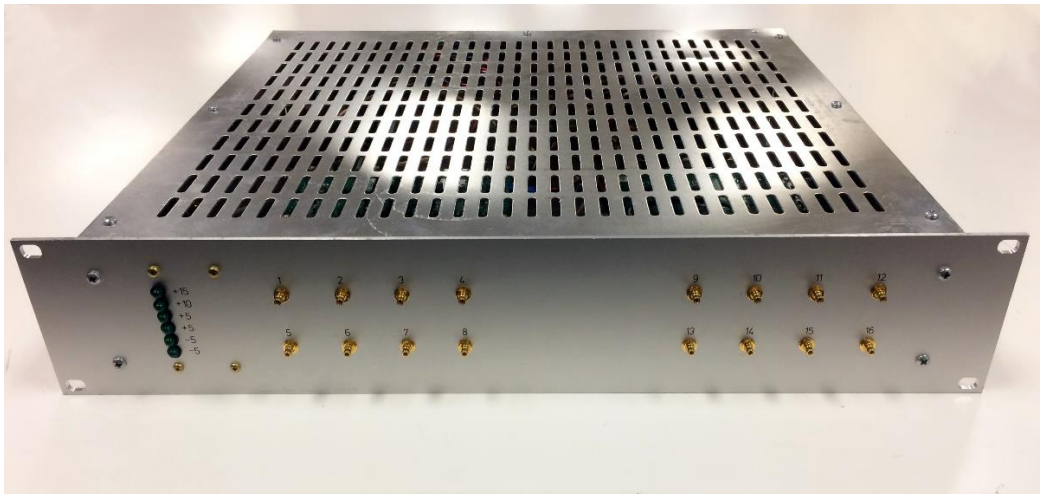

Figure 3.3: 16-channel frequency translation system. Front panel shows power supply indicators and RF inputs to the translation system. This unit is non-magnetic and operates in the scan room.

To prevent the introduction of extraneous noise, the DC power supplies and TTL detuning line are low-pass filtered on the equipment room side of the penetration panel. The TTL detuning line is brought in through a BNC connector and is filtered by a 10.7 MHz lowpass filter (BLP-10.7, Mini-Circuits). The LO is also brought in over a BNC connector, and the DC power supplies are brought in over a filtered DE-9 connector.

The only connections the frequency translation system requires to the host system are a 10 MHz clock and a TTL control line for coil detuning. If the system is configured to only mix the received signal, a TTL trigger for phase resetting is also necessary - the coil detuning signal can often be used in practice.

In In order to be able to operate in such a strong magnetic field and maintain a sufficient degree of compactness, it was decided to forgo the use of packaged, connectorized modules (which are bulky and sensitive to strong magnetic fields, e.g. ZAD-1-1+, Mini-Circuits, Brooklyn, NY, USA) and instead develop and construct boards in-house that would be populated with B0-toleran mixers, filters, and the required support components.

The ADL5801 (Analog Devices, Norwood, MA, USA) was chosen as the active mixer because it requires a single +5V power supply, is unconditionally stable, and has a high maximum operating frequency (600 MHz). This device performs better when driven differentially, so high-speed fully differential op-amps (ADA4932, Analog Devices) were used to convert the single-ended LO and RF inputs to differential, and a high-speed

conventional op-amp (ADA4857, Analog Devices) was used to convert the differential IF output of the mixer to a single-ended output.

In order to balance between size and ease of construction/repair, circuit boards were designed and fabricated in-house that each contain four frequency conversion channels, one of which can be seen in Figure 3.4. Each channel has its own LO and RF inputs for flexibility and includes a socket to install a filter for the IF output. Four of these were installed into the frequency translation unit seen in Figure 3.3, along with a power regulation board and small boards for LO amplification and distribution. Additionally, we designed and incorporated a standalone PIN diode driving circuit for detuning a transmit coil and up to 16 receive elements [53]. It has two complementary outputs to ensure the transmit coils and receive array are never tuned simultaneously. The driver takes a TTL-compatible input and is typically driven from the host's coil detune or RF transmit blanking signal. It is designed to be compatible with active-high or active-low control signals to best support a variety of host systems. To maintain compatibility with the Philips Achieva system for reference and calibration scans, the driver and coil use -5 V for forward bias and +15 V for reverse bias. The output for the transmit coils can supply a minimum of 200 mA, and the output for the receive array can supply a minimum of 1.6 A.

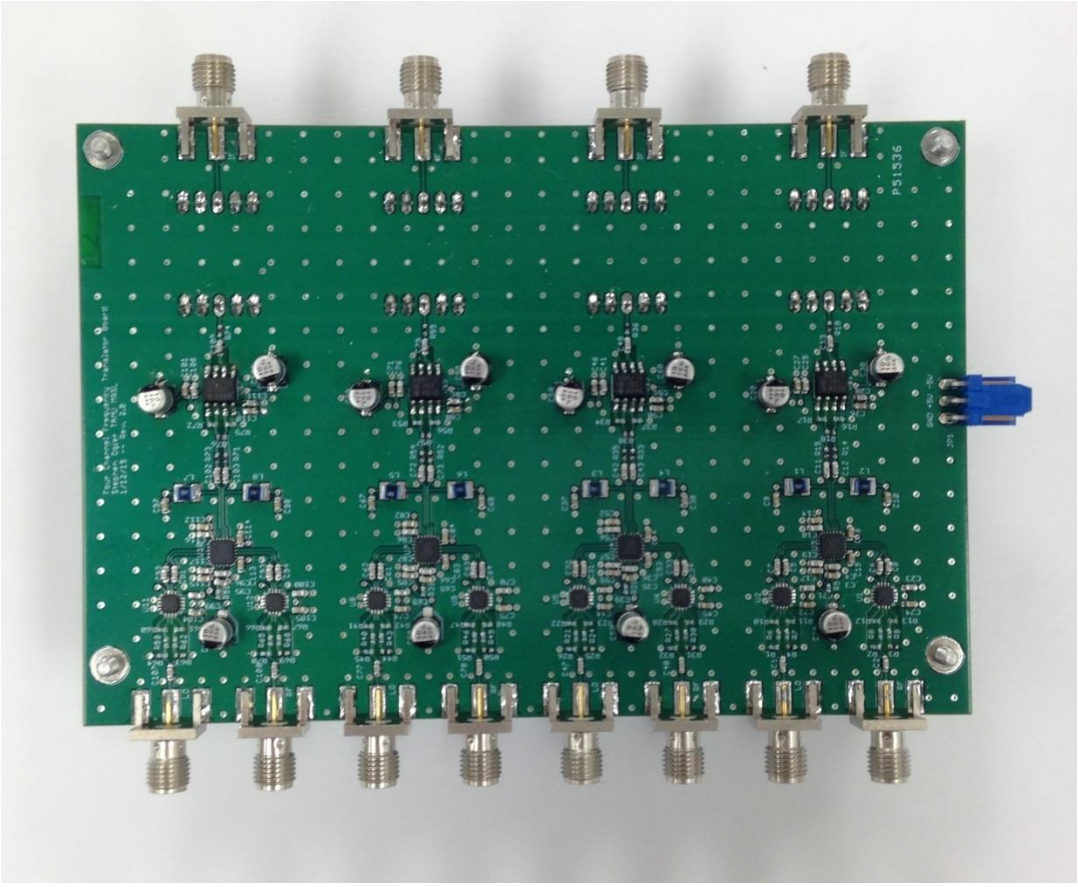

Figure 3.4: Four-channel frequency translation board. RF and LO inputs are on the bottom edge, and IF outputs are on the top edge.

The only narrow-band components in the FTU are the bandpass filters inserted after the mixing stage. These are centered on the ^{1}H frequency and are modular so that the FTU can be adapted for use with different systems simply by switching out the filters. At 4.7T, prepackaged 50Ω 200 MHz LC bandpass filters were used (KR2800, KR Electronics, Avenel, NJ, USA). At 7T, 298 MHz Surface Acoustic Wave (SAW) filters were used (SF1120B, Murata Electronics, Nagaokakyo, Kyoto, Japan). Daughter boards

were designed and constructed to match these filters to the modular form factor and, in the case of the 298 MHz filter, to 50Ω.

In the equipment room, a 4U 19-inch rack case holds the power supply, the LO source, the LO monitoring hardware, and the transmit-side translation channel, which can be seen in Figure 3.2. The power supply unit contains DC power supplies at +15 and ±7.5 V. Within the FTU, these are regulated down to +12 and ±5 V.

The LO source is based on the AD9915 DDS device (Analog Devices). This is controlled over the Serial Peripheral Interface (SPI) by a Raspberry Pi single-board computer (Raspberry Pi Foundation, Cambridge, UK) equipped with a touchscreen and keyboard, which runs in-house software to program the AD9915. The AD9915 was chosen because it has a maximum clock frequency of 2.5 GHz, which is more than sufficient for generating a high quality LO for up to a 21T system, and 32 bits of frequency control, which give a frequency resolution of ~0.56 Hz. It has a built-in phase-locked loop (PLL) clock multiplier that allows it to run off of the 10 MHz system reference without any external components, and it is easily programmable over the SPI. In order to accommodate arbitrary resetting of the LO phase, the AD9915 is operated with a 2.4 GHz clock, as the control inputs are sampled at 1/16 of the DDS core frequency, and this divided-down clock must be a multiple of 10 MHz for stable phase resetting.

The Raspberry Pi was used to control the LO source and monitor the output of the LO source. The output of the LO source was monitored using a built-in directional coupler (ZFDC-20-1H+, Mini-Circuits). The coupled output was attenuated then monitored with an RTL-SDR based USB software defined radio (SDR) receiver connected to the

Raspberry Pi running the FreqShow software [54]. This allowed us to monitor the output of the LO source, ensuring the source was at the right power level and frequency.

The transmit-side translation channel uses a passive mixer (ADE-1L+, Mini-Circuits) and a monolithic gain stage (TQ3PM9009, Qorvo, Greensboro, NC, USA). It also includes built-in power splitters (ADP-2-1W+, Mini-Circuits) for monitoring the transmitted pulse during debugging. Because it resides outside of the magnet room, ferrite-based mixers and power splitters can be used.

3.2.5. Accommodating ^{1}H Decoupling

^{1}H decoupling uses irradiation at the ^{1}H frequency during the acquisition time to simplify the spectrum of some X-nuclei and increase SNR. Although not essential, ^{1}H decoupling can be useful for ^{31}P spectroscopy and is extremely beneficial to ^{13}C spectroscopy. Because the primary aim for this system was ^{13}C spectroscopy at 7T, it was a requirement that the translation system be able to accommodate ^{1}H decoupling.

^{1}H decoupling of ^{13}C requires high degrees of RF power during the ^{13}C acquisition time, such that

$$\frac{\gamma \mathrm{B}_2}{2\pi} \gg {}^{1}J_{\mathrm{CH}}$$

where γ is the ^{1}H gyromagnetic ratio, B_2 is the ^{1}H decoupling field strength in T, and ${}^{1}J_{\mathrm{CH}}$ is the single-bond ^{1}H-^{13}C coupling coefficient in Hz [32]. For the WALTZ-16 decoupling sequence, which is commonly used *in vivo*, the required B_2 field strength to decouple isopropyl alcohol was found to be approximately 37 μT at 4.7T [55]. This is on the same order of field strength as is applied to excite the ^{13}C spins, but it is applied while receiving ^{13}C.

Thus, ^{1}H decoupling creates an enormous potential for signal interference with the translated ^{13}C signal in a variety of ways. The ^{1}H decoupling pulses can be picked up by the ^{13}C coil and bleed through the translation channel. This can be countered by using a bandpass or lowpass filter on the received ^{13}C signal, which also serves to protect the LNA from being saturated by the ^{1}H signal. Even with this filtering stage, ^{1}H signal can still couple into the translated signal, and this is more problematic because these two signals are now at the same frequency and cannot be separated by filtering. This interference can occur through the mixer, which only provides about 40 dB of isolation between RF and IF, or through coupling of nearby cables. The signal from ^{1}H decoupling is strong enough to make completely eliminating interference very difficult.

This was overcome by mixing the received ^{13}C signal to a frequency offset from the ^{1}H frequency by a few hundred kilohertz, as depicted in Figure 3.5. The receiver bandwidth of the 7T Philips Achieva system is 2 MHz, while the maximum bandwidth of the ^{13}C spectrum is 220 ppm, which at 7T is approximately 16.5 kHz, so the translated ^{13}C spectrum can easily be shifted away from interference from the ^{1}H decoupling signal while remaining within the receiver's bandwidth. This change was made by adjusting the system receiver frequency to 100-200 kHz away from the ^{1}H frequency and adjusting the LO frequency by the same amount.

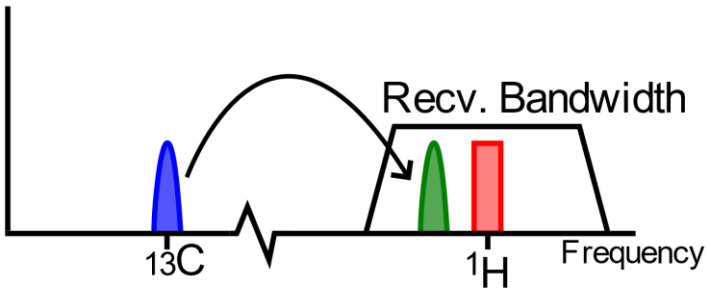

Figure 3.5: Spectral diagram of mixing ^{1}H-decoupled signal off-resonance.

3.2.6. Setup and Testing Procedure

The system shown in Figs. 2 and 3 was used to collect data from both the 4.7T and 7T systems. The appropriate output filters were installed in the translation system for each field strength before setting up the translation system. After the hardware was in place and connected, the only configuration necessary was programming the local oscillator frequency. As discussed previously, the LO was set to the difference between the ^{1}H frequency and the frequency of the X-nucleus (with an offset if performing ^{1}H decoupling). The exact frequencies must be obtained from the system settings. Simply using the nominal field strength of the system to compute the LO is unlikely to be successful because of the narrow widths of the NMR spectrum and receiver bandwidth. After the LO had been computed, it was programmed into the DDS synthesizer using the built-in Raspberry Pi.

To ensure proper functioning of the LO, a monitoring system was included in the LO source as described above. The active mixers are relatively insensitive to the signal strength of the LO, so the primary concern was the frequency of the LO. Checking the LO

with the monitoring system allowed for straightforward detection of errors in LO programming. Additionally, if the 10 MHz reference was faulty or disconnected, the LO output would be at a visibly incorrect frequency.

3.2.7. System Integration

Integration with the 4.7T Varian Unity Inova system was straightforward for single-channel testing of noise performance and isolation. The system includes a spare output for its 10 MHz reference, and a spare digital line was programmed to control the resetting of the phase. The only other change required was the insertion of the FTU in the Varian receiver between the preamp and the IF conversion stage. This was easily done by opening the magnet leg, disconnecting the cable that runs between these modules, and inserting the FTU between those units. The pulse sequence required slight modification to set the transmit to ^{13}C and receive to ^{1}H and to insert statements to turn on and off the spare digital line to reset the phase, but these changes are very easily made in the pulse programming environment.

Integration with the 7T Philips Achieva system was slightly more complicated. On the Varian it is simple to modify pulse sequences to transmit on one frequency and receive on another. This is not as straightforward on clinical systems and certainly would require a research agreement. Thus, the approach of mixing of both transmit and receive was used to avoid being required to modify the pulse sequence. The 10 MHz reference was split with a tee from a board in the Philips acquisition system. For transmit, the input to the ^{1}H RF power amplifier (RFPA) was disconnected and routed to the transmit-side translation channel. The output of this was routed into the RFPA's input. The Achieva's transmit path

includes a bandpass filter and a narrow-band RF circulator that protects the RFPA from reflected power, both which must be bypassed. This does not present additional risk, as the system automatically bypasses these when operating in a non-^{1}H mode. In the scan room, the transmit output was accessed by taking the transmitted pulse from within the Philips ^{1}H interface box. This signal was routed through a quad hybrid (10011-3, Anaren, East Syracuse, NY) to the quadrature ^{13}C transmit coil.

On receive, the signals from the receive array were lowpass filtered (in-house designed and constructed 100-MHz lowpass filters) and then preamplified with low input impedance preamps (WMA74D, WanTcom, Chanhassen, MN, USA). The preamplified signal was then routed through the FTU, the output of which was fed into the inputs of the Philips 16-channel ^{1}H interface box.

To ensure the translated RF pulse is of the correct amplitude, it is necessary as part of system integration testing to calibrate the RF pulse after setting up the translation system. Because access to the 7T system was limited, the RF pulse was calibrated conventionally when acquiring reference data using the volume coil. Once a calibration has been found with the volume coil, the RF transmit signal is measured with an oscilloscope, either at the input to the RF amp, or at the output of the coil interface through a high-power attenuator. After the translation system had been inserted into the transmit path, the attenuation, drive scale, or flip angle were adjusted until the measured transmit pulse matched what was previously measured. Calibrating in this manner allowed us to verify the transmit translation system and calibrate the RF pulse at the same time. In

clinical use, the host system is unaware of the insertion of the translation system, so a conventional RF calibration procedure can be used.

3.3. Results and Discussion

3.3.1. System Performance

The performance of the translation system was first characterized on the bench, using a test signal and spectrum analyzer. The conversion gain, 0.1 dB compression point, and channel-to-channel isolation were characterized for ^{13}C at both 4.7T and 7T, the results of which can be seen in Table 3.2. Noise performance was evaluated through comparison of the translation system with the stock Varian and Philips systems.

A high 0.1 dB compression point is important so that the received NMR signal is not distorted. Insufficient linear head-room will cause the signal to clip, which leads to distortion in the spectrum.

The isolation between the RF input and IF output of the translation system at the ^{1}H frequency is crucial for the accommodation of ^{1}H decoupling. Although filters are included to help suppress the ^{1}H signal, rejection of the ^{1}H signal by the translation system is important to achieve sufficient rejection of the decoupling signal. A small amount of residual ^{1}H signal at the IF output is acceptable, as mixing off-resonance eliminates the residual interference.

Performance of the system at 4.7T and 7T is similar. The difference in gain can mostly be attributed to the much higher insertion loss of the filter used for 7T. The KR2800 filter used at 4.7T has a specified typical insertion loss of 5 dB, while the SF1120B used at 7T has a specified maximum insertion loss of 12 dB.

Given that worst-case inter-coil coupling within the receive array is typically on the order -20 dB, it is unlikely that inter-channel coupling would degrade the isolation between received signals. This was verified on the bench by characterizing the outputs from an input from a single channel on an entire full 4-channel board as well as a single channel of an adjacent board. The worst-case coupling between channels for a simulated ^{13}C signal was -77.98 dB at 4.7T and -64.92 at 7T, far less than what will arise within the receive array.

	^{13}C AT 4.7 T	^{13}C AT 7 T
Noise Figure		
Conversion Gain	0.8642 dB	-8.349 dB
0.1 dB Input Compression Point	-1.762 dBm	-2.742 dBm
Isolation at ^{1}H frequency	27.18 dB	39.01 dB

Table 3.2: Translator Performance

3.3.2. 4.7 T Results

To demonstrate the efficacy of the previously described method of accommodating ^{1}H decoupling, proton-decoupled ^{13}C spectra were acquired on a 4.7T Varian Unity Inova system using frequency translation on receive. Spectra were acquired with the receive frequency set to the ^{1}H frequency (200.222 MHz) and set approximately 100 kHz below the ^{1}H frequency (200.122 MHz). Two 100 MHz lowpass filters (BLP-100+, Mini-Circuits) were used to reject interference from ^{1}H decoupling: one in front of the LNA to prevent it from saturating, the other at the translator input to block any ^{1}H signal that may have coupled in after the LNA. These filters provide approximately 50 dB each of rejection at 200 MHz.

Figure 3.6 shows the results of this experiment. Comparison of the top and bottom spectra shows that the translation system provides 98.0% of the SNR of the Varian, a degradation of 0.18 dB. This is less than the maximum desired degradation of 0.5 dB. The middle and bottom spectra demonstrate the necessity of mixing off-frequency when ^{1}H decoupling. The middle spectrum shows significant interference from the decoupling signal that occurs even with two low-pass filters when the received signal is translated exactly to the ^{1}H frequency. The spurs in the signal are from ^{1}H decoupling signal that has coupled into the translated output, and the loss in SNR is due to these spurs increasing the quantified noise level. Shifting the receiver and LO frequencies approximately 100 kHz lower solved this problem, as seen in the bottom spectrum.

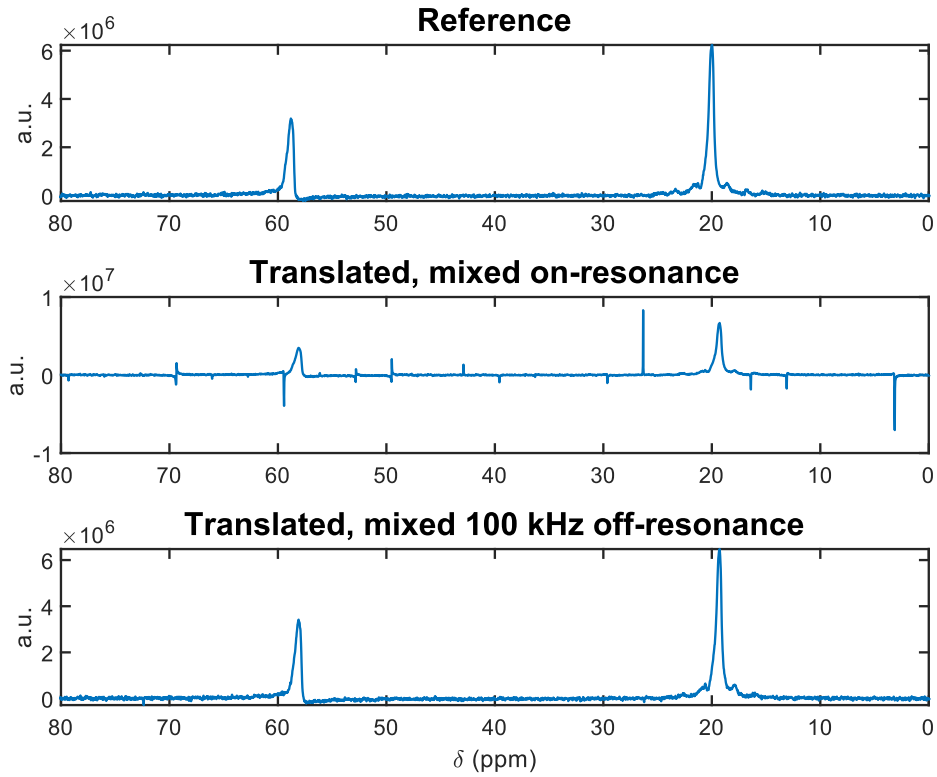

Figure 3.6: Translator performance for ^{1}H decoupled ^{13}C at 4.7T. From top-to-bottom, reference spectrum acquired with stock Varian system, spectrum acquired with the translator mixing to the ^{1}H frequency, spectrum acquired with the translator mixing 100 kHz below the ^{1}H frequency. Sample was 91% isopropanol in water. Spectra were acquired with 16 averages and normalized to the intensity of the Varian reference spectrum. WALTZ-16 ^{1}H decoupling and 3 Hz Gaussian line broadening were used.

3.3.3. 7 T Performance

To demonstrate noise performance of the translation system at 7T, data from a single ^{13}C coil was acquired with and without the translation system. For reference, the stock 7T system was configured for ^{13}C and data were acquired from a sample of ^{13}C-enriched acetic acid. The system was then configured for ^{1}H, and the translation system was used to re-acquire the same experiment. The results are shown in Figure 3.7. The

small increase in SNR with the translation system can be attributed to a change in calibration of the ^{13}C transmit pulse between the two experiments.

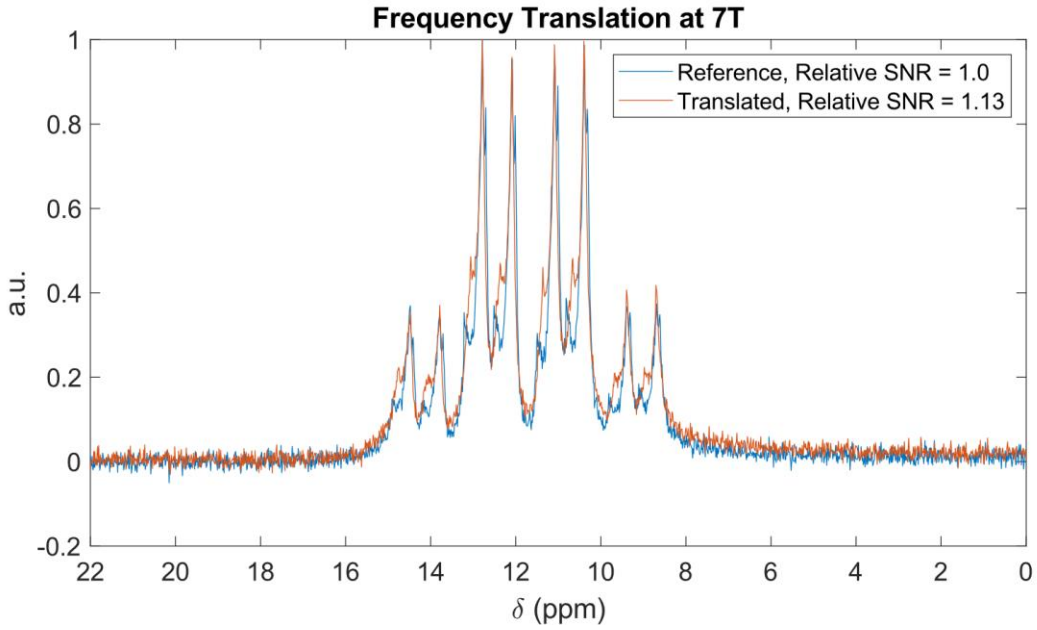

Figure 3.7: Translator performance comparison for ^{13}C at 7 T. Sample was 99% ^{13}C-enriched acetic acid. Spectra were acquired with 16 averages. No line broadening was applied.

To demonstrate the array receive capability enabled by the translation system, non-localized spectra were acquired from a 16-channel unilateral ^{13}C breast array coil. This coil includes a quadrature ^{13}C volume coil for transmit and collection of reference spectra as well as a 16-element soccer-ball geometry receive array. Isolating preamplifiers were used to supplement geometric decoupling and provide low noise performance.

The non-localized spectra from individual receive array elements are shown in Figure 3.8. In this preliminary result, there is significant signal variation due both to coil

orientation and differences in gain between channels on this test coil, but the result demonstrates the ability to detect signals from the 16-channel array.

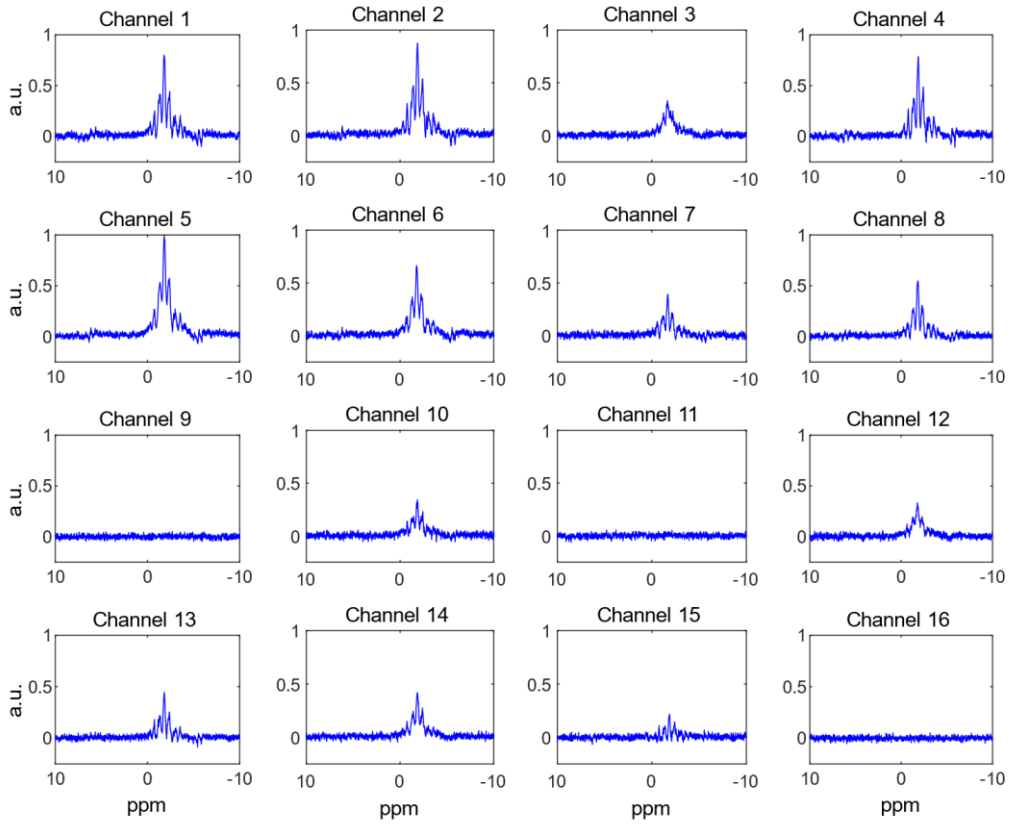

Figure 3.8: Spectra from individual ^{13}C array elements at 7 T. Sample was canola oil. 8 averages were acquired, and 3 Hz Gaussian line broadening was applied. Spectra have been normalized to have identical noise intensity.

Figure 3.9 compares the ^{13}C SNR obtained by the host system receiving from the volume coil and using the array coil through the translation system. In each case, the volume coil was used for transmit.

Before combination of the array data, the averaged signals from individual coils have a zero-order phase correction applied to correct for the relative phase between elements that arises due to variations in coil location and cable length. The averaged, phased signal from each coil is normalized to have the same noise level. For the SNR-weighted sum, each channel was multiplied by a factor equal to the ratio of its SNR to the SNR of the most sensitive channel before summing. Even for non-localized spectroscopy, use of 16-channel receive provides substantial gains in SNR: the simple sum increases SNR by a factor of 2.8, and the weighted sum increases SNR by a factor of 3.5.

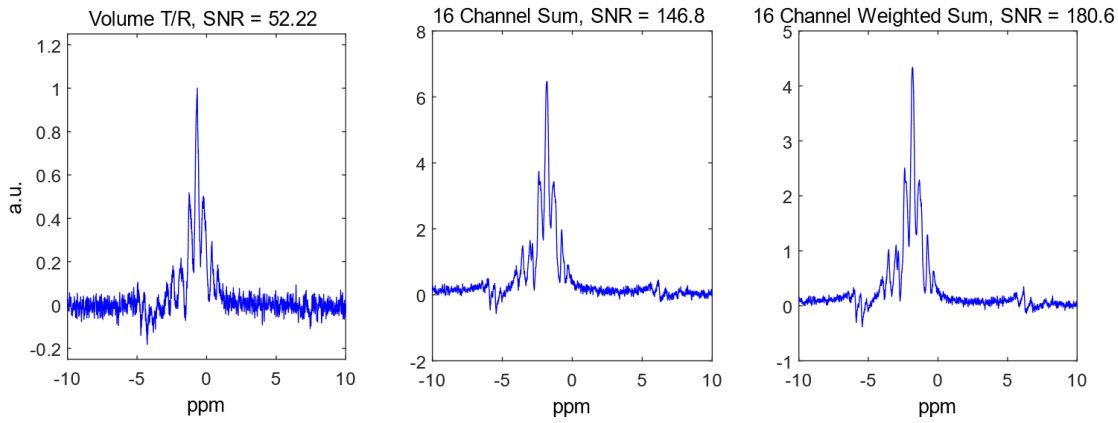

Figure 3.9: Comparison of data received by volume coil with data from 16-element receive arrays. Sample was canola oil. 8 averages were acquired, and 3 Hz Gaussian line broadening was applied.

To demonstrate the isolation provided by the translation system, spectra were acquired with the input of one channel of the translation system disconnected. The results of this experiment can be seen in Figure 3.10. Because no spectrum is visible in the

disconnected channel, the SNR of the received signal sets an upper bound on the isolation equal to the SNR of 35.6 dB.

In the future, we plan to fully utilize the sensitivity improvement promised by the 16-channel ^{13}C receive array using chemical shift imaging and localized spectroscopy.

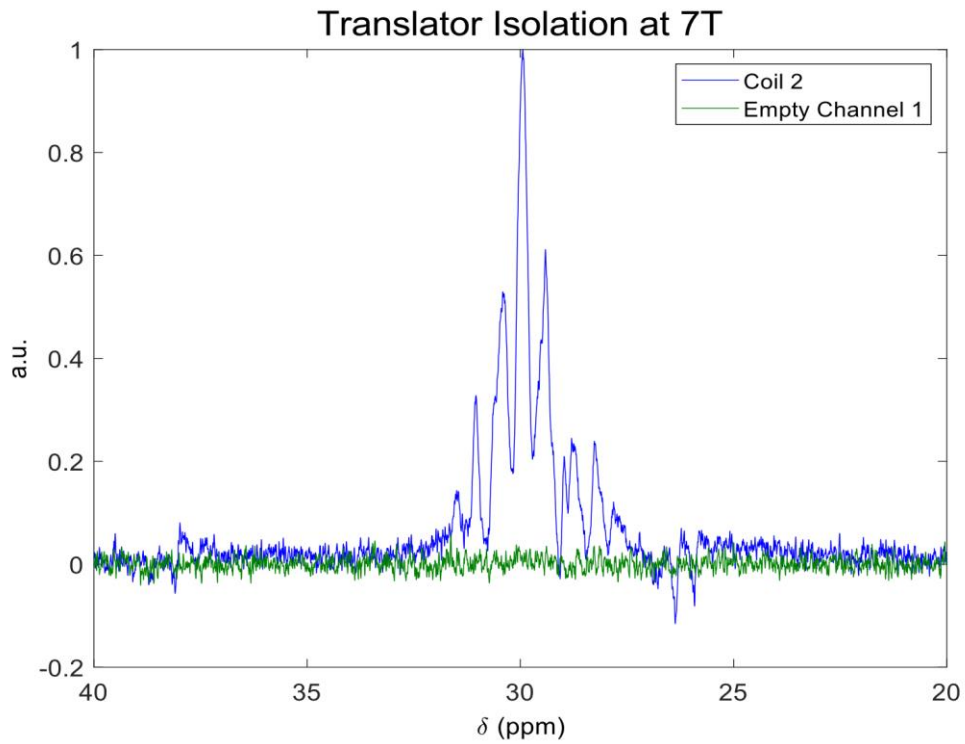

Figure 3.10: Demonstration of channel-to-channel isolation at 7T. The output of coil 1 after preamplification was unplugged from the input to the translation unit. No coupling can be seen, which sets a lower bound on channel-to-channel isolation of 35.6 dB.

3.3.4. Phase Coherence

Each of the two approaches to maintaining phase coherence has its strengths and weaknesses. If the approach of translating both the transmitted pulse and received signals is chosen, the scanner can be modified through the re-routing of a few cables to work with

a different nucleus without any changes being made to the pulse sequence. This allows simple pulse-and-acquire spectroscopy to be implemented without any programming changes. Mixing on both transmit and receive requires more equipment, as an additional mixing stage is needed to translate the transmitted pulse. Additionally, the host scanner is unaware of the change in nucleus, which invalidates calculations that include the gyromagnetic ratio. For example, this change affects the RF pulse amplitude calculation, the x-axis of spectra when displayed in parts-per-million (ppm), the apparent field-of-view when performing CSI, and the voxel size when using single-voxel techniques. For demonstration purposes and phantom studies this can be corrected by manually adjusting the acquisition parameters to compensate. For clinical use, modifying the pulse sequence to incorporate the change in gyromagnetic ratio is necessary. An additional complication is the impact of the change in transmit frequency on the host's built-in SAR monitoring. Presently, this would be addressed by operating far below the SAR limit, further aided by the reduced frequency of the X-nucleus, but for clinical use a more robust method must be developed.

The second approach requires modification only to the receive path of the system, but custom pulse sequences must be written to transmit at the frequency of the X-nucleus while receiving at the ^{1}H frequency. The difficulty of this depends on the pulse programming environment of the host scanner. The latter approach was straightforward on the spectroscopy-focused Varian Unity Inova imager, but the former approach was more easily achieved on the Philips 7T Achieva system.

3.4. Conclusion

3.4.1. Summary of Results

A frequency translation system was developed to adapt multi-channel ^{1}H receivers for use with X-nuclei. The system was designed to be flexible with regards to nucleus and B0 field strength and to accommodate ^{1}H-decoupling.

The system has been tested and shown to preserve the SNR of the received signal on both a 4.7T Varian Unity Inova small-animal scanner and a 7T Philips Achieva full-body imager. Additionally, ^{1}H-decoupling is easily accommodated by carefully filtering the received signal and translating it to a frequency slightly offset from the ^{1}H frequency.

Although non-localized spectroscopy benefits less than localized from the use of a receive array, a substantial increase in SNR has been shown using the translation system for 16-channel ^{13}C pulse-and-acquire spectroscopy.

3.4.2. Future and Ongoing Work

Development of a 16-channel ^{13}C unilateral breast array is nearly complete, and human testing should begin in the next few months including localized spectroscopy.

Work is being done to improve the usability of this translation system. A revised version is under development that will be able to interface directly with the Philips system without use of the Philips 16-channel ^{1}H interface. This will allow the system to be located at the head of the patient table, greatly easing setup. An improved control system with additional monitoring capabilities is being developed to improve the usability of the system.

4. A MULTINUCLEAR FREQUENCY TRANSLATION SYSTEM[2]

4.1. Motivation

Frequency Translation was developed to adapt multichannel receivers designed for only ^{1}H for use with other nuclei. Originally this was to enable use of small ^{23}Na and ^{31}P arrays [42], and in a previous chapter the development of a 16-channel Frequency Translation system was discussed. All of these systems were only shown to be capable of converting a single received nucleus to the ^{1}H frequency.

Arrays of receive coils have long been used to improve the SNR of imaging and spectroscopy [12, 13], and techniques have been developed to use array coils to accelerate imaging and spectroscopy [14, 15]. Experiments simultaneously examining multiple nuclei have long been of interest in spectroscopy and imaging [51, 56-58], but many MRI systems do not have the capability to simultaneously receive signals from multiple nuclei. Early work used two separate NMR spectrometers [56], and later work has made use of add-on systems to provide additional local oscillator frequencies [51].

There are multiple motivations for simultaneous interrogation of multiple nuclei. Early work was motivated by the desire to simultaneously obtain complementary information from both ^{1}H and ^{31}P [56], and recent developments in the field of magnetic resonance have made simultaneous acquisition of multiple nuclei more appealing.

---

[2] This is a draft of a paper intended for Submission to IEEE Access with a tentative title of "A Frequency Translation System for Simultaneous Multi-Channel Multi-Nuclear NMR and MRI".

4.1.1. Interleaved vs Simultaneous Imaging

Most NMR and MRI pulse sequences acquire data at a low duty cycle, often motivated by the need to wait for some amount of T_1 relaxation before exciting the sample again. Because of this, it was often determined to be easier to interleave multiple nuclei during each other's relaxation periods, much as multiple slices are interleaved in multi-slice imaging sequences [57, 59].

There have been a number of recent developments that have made simultaneous interrogation of multiple nuclei desirable. Recently, pulse sequences with high acquisition duty-cycles sequences such as MR Fingerprinting have been developed [60]. MR Fingerprinting cannot be extended to multiple nuclei by interleaving in the same fashion many other sequences can due its high acquisition duty cycle. Because these high-duty-cycle techniques use time very efficiently, there is insufficient down time between acquisitions in which a second nucleus could be acquired [50].

In addition, Hyperpolarization has become more accessible for clinical use, and that has led to a need for sequences that can quickly acquire signal from the rapidly decaying hyperpolarized nucleus while also acquiring reference signals or images from other nuclei. There has also recently been work on the simultaneous hyperpolarization of multiple nuclei, which would necessitate simultaneous imaging of multiple nuclei in order to acquire as much of the hyperpolarized signals as possible [61].

4.1.2. Frequency Translation

Frequency translation is a promising approach to adapting MR systems to be capable of simultaneous reception of multiple nuclei. It allows for continued use of the

host system's receivers, which reduces system cost and simplifies setup and data processing. Additionally, many systems are not capable of receiving data from more than a handful of non-^{1}H receive channels, so the use of a system to enable reception of data from x-nuclear arrays is likely to already be necessary.

The first-generation frequency translation system enabled the groundbreaking acquisition of 16-channel ^{13}C data, but it had a number of shortcomings that limited its potential uses. It was not particularly compact and required use of the host system's 16-channel ^{1}H interface box to interface with the scanner. This relegated the translation system to the rear of the magnet, adjacent to the bore. The placement of the translation system outside the magnet bore necessitated cable bundles running between the preamp box and the translator as well as between the translator and the host system interface box, each with 16 cables. These are bulky and must be manually guided each time the patient table is brought in or out of the magnet. Additionally, they require 64 connections to be made, not counting the 16 between the coil and the preamp unit, which is time consuming and introduces points for human error and mechanical failure.

4.1.3. Importance of Usability

The biggest shortcoming in the first translation system was usability. The system worked and performed as designed, but the system required an expert to set up and operate.

The first translation system provided rudimentary monitoring of the Local Oscillator (LO) output, but was limited to manually using a built-in SDR dongle to check the frequency of the LO. This was deemed sufficient, as many early problems arose from the LO being inactive or at the incorrect frequency, but a more sophisticated monitoring

system would greatly streamline debugging, especially when multiple nuclei are introduced.

4.2. Methods and Materials

4.2.1. Requirements

In order to be able to practically translate multiple nuclei, in a way that was easy to set up and operate, the following requirements were established:

- Compact – The translation system must be able to fit in the magnet bore along with all of the required interface hardware (e.g. LNAs). Ideally it could mount to the patient table in place of the scanner's coil interface box.
- Capable of direct interface – To improve ease of setup, it is desired for the translation system to interface directly with the proprietary coil connector on the host system's patient table without use of an additional interface box. In addition, as we work regularly with systems from several manufacturers, it is important that the translation system can be easily reconfigured to work with the clinical scanners at our collaborators' sites or our own small-bore imaging systems.
- Capable of translating multiple nuclei - There is a growing interest in the simultaneous study of multiple nuclei, and some hyperpolarization techniques are capable of simultaneously enhancing the polarization of multiple nuclei. To take advantage of this, the translation system must be capable of simultaneously translating multiple nuclei to the 1H frequency and compensating for the varying sensitivities of the different nuclei.

- Improved signal monitoring - With the increased complexity required to fulfil these requirements, we want an equally sophisticated monitoring system to catch and diagnose problems. Specifically, we want to be able to monitor signals at various points in the translation system and inject signals in to the input to test for proper functioning.
- User-friendly control software - The control software for the original system ran on a Raspberry Pi with a 3.5” (or 4.5”) touchscreen and keyboard. This software was only required to program the LO and check its frequency, but even this was cumbersome and patched-together. The new control software will run on a PC and be capable of controlling and monitoring the translator through a single interface.

4.2.2. Architecture

The basic architecture is depicted in Figure 4.1. The control unit contains a BeagleBone Black (BBB), a single-board computer (Texas Instruments, Dallas, TX, USA), and controls the LO generation, clock synthesis, and monitoring hardware and serves as a bridge to the microcontroller in the frequency translation unit. It is controlled by a PC running in-house software over a wired ethernet connection and controls the frequency translation unit over an optical interface.

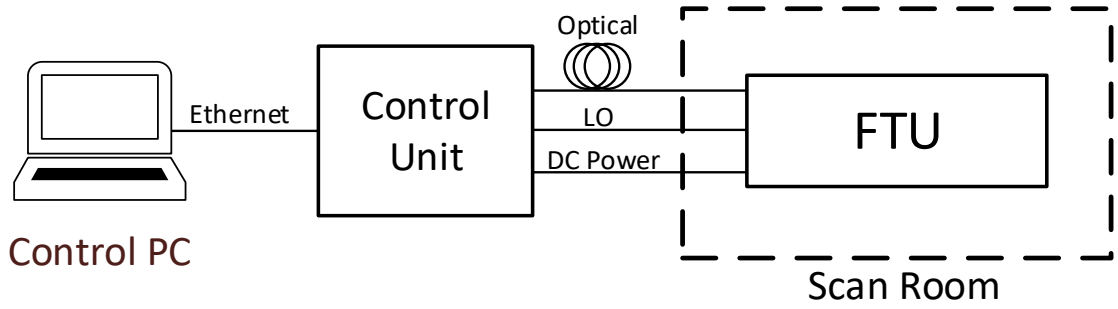

Figure 4.1: Multinuclear translation system block diagram.

Graphical control software, written in Python, runs on a control PC. This software provides a user interface for controlling LO generation, gain of the translation channels, and options for generating monitoring signals and measuring their intensity. This software interfaces with the control unit over ethernet using the ZeroMQ protocol (zeromq.org), which provides a robust and easy-to-implement control and data passing protocol. Robustness of the link is ensured by requiring each message sent by the control PC to receive a reply from the control unit. If no reply is received, an error will be raised on the control software on the PC.

The control unit serves as a bridge between the control PC and the frequency translation unit (FTU). An optical interface was chosen between the control unit and FT to minimize the potential for interference from the gradients or RF coils and to eliminate the possibility of coupling noise into the scan room. A lightweight proprietary protocol is used over a bi-directional UART connection. In a manner similar to the link between the control PC and control unit, each message sent by the control unit to the FTU must receive a reply, or an error will be raised. The physical interface is provided by a fiber optic link over polymer optical fiber for robustness.

4.2.2.1. Control PC Software

The Control PC Software is written in Python and uses the Qt framework (via the pyQt interface) for GUI development (The Qt Company, Espoo, Finland). The user interface is provided by ManualControlWindow.py, which provides for manual control of the Frequency Translation System. The GUI can be seen in Figure 4.2.

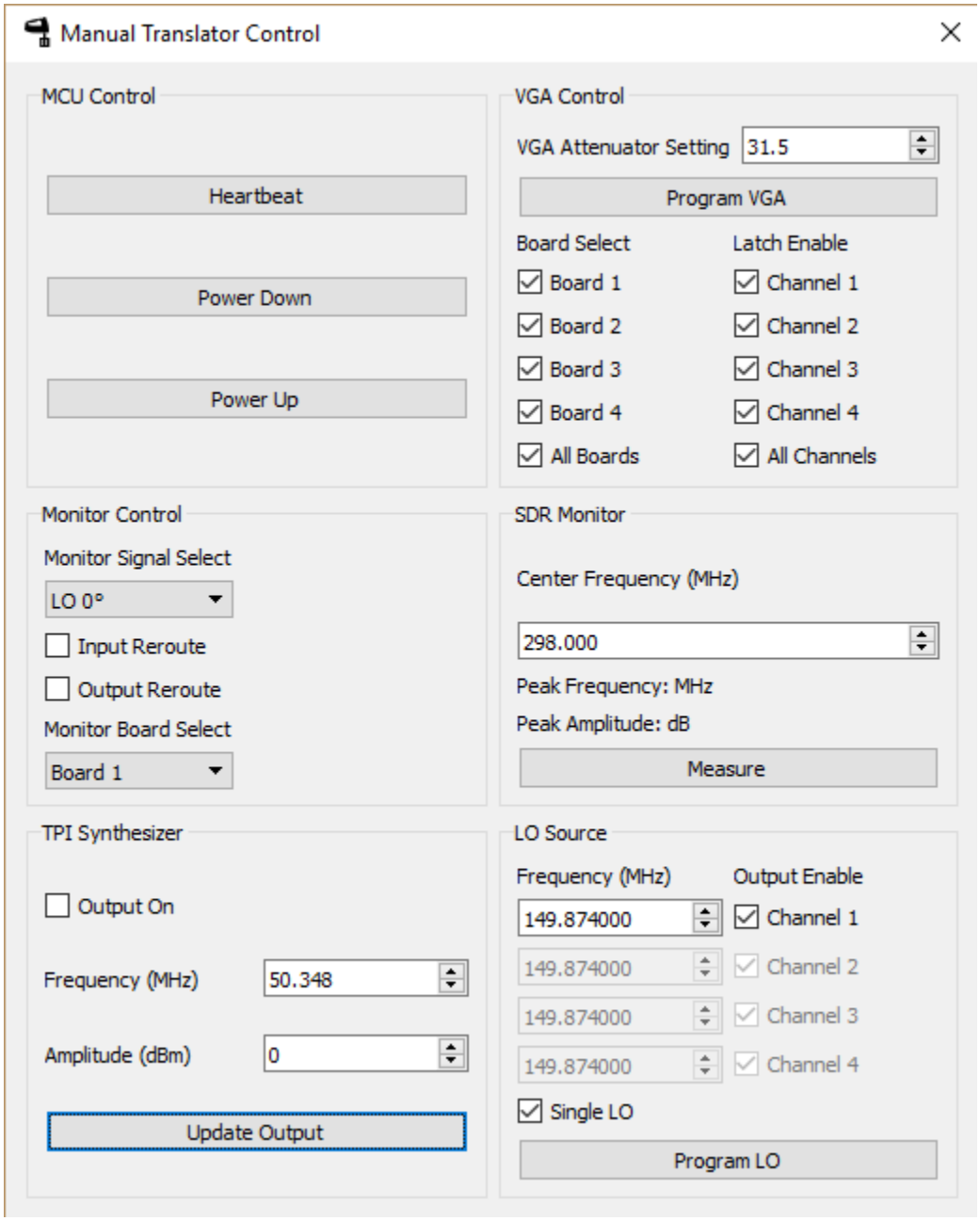

Figure 4.2: Manual Translator Control GUI. Settings shown are a typical configuration for 16 ^{13}C channels at 4.7T.

The functionality of the GUI is divided up into six major components which we will discuss from left to right, top to bottom.

- The MCU Control section contains the functions that interface directly with the microcontroller in the translation unit.
- The VGA Control section allows for selection of and programming of the variable gain amplifiers on the frequency translation boards. The checkboxes allow for selection of which boards and channels will be programmed with the specified gain setting when the button is clicked.
- The Monitor Control section controls the RF switches that make up the monitoring system. The Monitor Select, Input Reroute, and Output Reroute switches control the SP4T and SPDT RF switches on all four translation boards, and the Monitor Board Select switch controls the standalone SP4T switch board that selects which translation board has its monitor output routed to the monitoring system.
- The SDR Monitor section contains control for the SDR peak finder and displays its output. The approximate center frequency is input, and the peak of the SDR output is given along with its amplitude.
- The TPI Synthesizer section contains all of the needed controls for the TPI RF synthesizer.
- The LO Source section contains controls for enabling each LO channel and setting its frequency. When the Single LO checkbox is checked, all four LO outputs share the same frequency and output enable state. This helps streamline setups in which all channels share the same nucleus.

ManualControlWindow.py allows two command-line options that configure the software on startup. Using the -v or –verbose flags enables a much more detailed logging mode which can be helpful for system development and debugging. The -b or –b0 tags can be used with a B0 field strength to configure the clock generation board and LO synthesizer clock for the optimal rates for the specified field strength. At present, only 4.7T and 7T are supported.

4.2.2.2. Control Unit Software

The microcontroller program is written in C and primarily interrupt-driven. After initialization, the MCU waits for input over the optical serial link. The MCU is capable of powering itself down, to be woken up when an extra optical link is brought low. While powered down, the MCU's clock turns off. Details about the control unit software and the communication protocols used over the ZeroMQ and optical links are provided in Appendix A.

4.2.3. Construction

The control and power supply units are mounted in a 4U rack case, that can be seen in Figure 4.3. The empty 1U slot at the top is for a transmit translation system, if required.

Figure 4.3: Control unit, containing, from top to bottom, empty slot for transmit translation unit, translator control unit, and power supply unit.

4.2.3.1. Control Unit

The control unit is an 8” deep, 2U rack unit that contains all of the hardware necessary to control the translation unit, generate the local oscillators, and monitor the translation unit. It is the middle unit in Figure 4.3, and the interior of it can be seen in Figure 4.4.

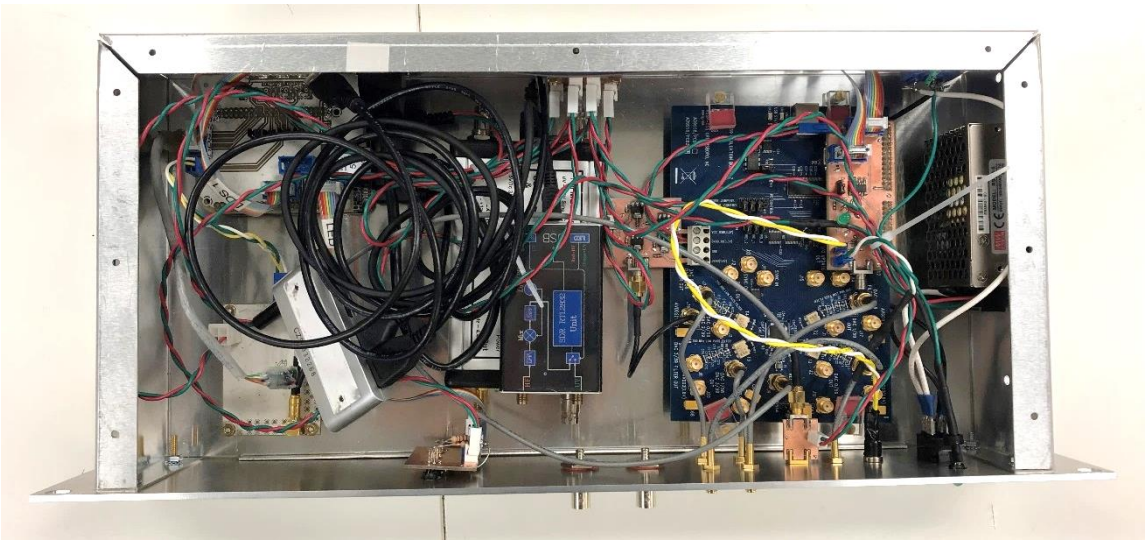

Figure 4.4: Interior of control unit.

4.2.3.1.1. BeagleBone Black

The BeagleBone Black is the core of the control unit. It serves as a bridge between the client computer and the boards and modules necessary to control the frequency translation system. The board runs the Debian distribution of GNU/Linux, and runs a set of custom Python programs to control the various portions of the translation system in response to commands received over its network connection.

4.2.3.1.2. BeagleBone Black Optical Interface Cape

Mezzanine Boards for the BeagleBone series of boards are commonly referred to as “Capes”. In order to interface the optical connection to the BBB as well as to bring out the SPI and I^2C busses and some spare digital lines, a custom cape was developed. This cape connects the optical transceivers to the UART pins of the BBB and re-arranges the serial bus and digital I/O lines into more convenient form factors. Additionally, the inputs/outputs to the optical interfaces are brought out to pin headers.

4.2.3.1.3. AD9959 DDS RF Synthesizer

LO generation is performed by the AD9959 (Analog Devices, Norwood, MA, USA), which provides four local oscillator outputs. Instead of developing and debugging a complicated PCB to support this device, it was decided that it was more cost-effective to simply use an evaluation board which already included the AD 9959 and its required support components. Additionally, the evaluation board provides a USB interface, which while not used in the final version of the translation system, was useful in development and testing of the system.

The AD9959 was chosen because it can provide four LO outputs, has a maximum DDS clock of 500 MHz, and can arbitrarily reset the phase of the LO outputs in response to a trigger. The 500 MHz maximum core frequency is sufficiently high such that at 4.7 T all LO frequencies are below the Nyquist frequency, and at 7 T most relevant LO frequencies fall in the first image band for undersampling.

There are two custom support PCBs to interface the AD9959 evaluation board to the rest of the Control Unit. The evaluation board requires four separate power supplies: two at +3.3 V and two at +1.8 V. A small board was developed to generate these voltages from the +5 V supply that mounts directly to the evaluation board's power connector using separate regulators for each supply (LD1117S33 for +3.3V and LD1117S18 for +1.8V, both STMicroelectronics, Geneva, Switzerland).

The second board was developed to provide a more compact control interface for the AD9959 evaluation board. The evaluation board has two 26-pin headers for control, but our application only requires a handful of these pins, so the interface board allows use

of only two 8-pin headers for control. Additionally, the interface board includes support for a reset button and logic to allow for an external TTL signal to arbitrarily reset the phase of the local oscillators.

4.2.3.1.4. Clock Generation Board

The AD9959 can be operated at a core frequency of up to 500 MHz. It has a built-in PLL clock multiplier, but the multiplication factor is limited to factors of 4-20. We desire to operate the AD9959 at close to its maximum core frequency to increase its maximum output frequency, but the reference oscillator from the host system is only 10 MHz, so it is necessary to boost the reference clock frequency used by the AD9959.

The clock generation board is based on the CDCE706 programable PLL clock synthesizer (Texas Instruments) and was originally developed for the broadband system. The device is configured by the BeagleBone Black over the I^2C interface, using a binary configuration file stored on the BeagleBone Black. The programable PLL is used to multiply the frequency of the input clock signal, which is typically at 10 MHz. The PLL is configured based on the B_0 field strength and the nuclei of interest.

The clock generation board is a two-layer board that was designed in-house, sent out for manufacture, and populated in-house.

4.2.3.1.5. TPI 1002-A RF Synthesizer

A TPI 1002-A Signal Generator (RF Consultant, Austin, TX, USA) is included as a test source for debugging the translation system. The synthesizer has a frequency range of 35-4400 MHz and is controllable over USB. A Windows GUI is available and was used for development purposes, but for embedding into the control unit, a custom Python

interface was written to control the synthesizer from the BeagleBone Black over USB. Implementation of the Python interface was straightforward, as the device uses a standard serial control interface with well-documented commands.

The TPI synthesizer is powered off of its USB connection from a powered USB hub included in the control unit. The synthesizer also can share the host system's 10 MHz reference for improved frequency stability.

4.2.3.1.6. RTL-SDR Dongle

Also attached to the powered USB hub is a RTL.SDR+ Upconverter USB SDR dongle. This is used in conjunction with the TPI synthesizer to debug the translation system. At present, this can be used to find the peak frequency and amplitude in a region around a specified center frequency

4.2.3.1.7. +5 V DC Power Supply

The Control Unit has its own power supply, allowing it to be operated independently from the translation system for development and debugging purposes. The MEAN WELL RS-25-5 (New Taipei City, Taiwan) power supply provides a maximum output of 5 A and can operate off of 120-240 VAC 1 and 2-phase supplies at 50-60 Hz. A standard IEC C14 power inlet is used for compatibility with a wide variety of systems.

4.2.3.2. Power Supply Unit

All of the power supplies chosen for the power supply unit can operate off of 120-240 VAC 1 and 2-phase supplies at 50-60 Hz. A standard IEC C14 power inlet is used for compatibility with a wide variety of systems. An unswitched IEC C13 outlet is also provided for powering the control unit without use of a power strip.

4.2.3.2.1. +/- 7.5 V DC Power Supplies

The main power supplies for the translation system are two 7.5 VDC MEAN WELL RSP75-7.5 supplies, each rated for 10 A. One of these supplies is configured to supply +7.5 VDC to power most of the translation system. The other supply is configured to supply -7.5VDC for the negative rail of a bi-polar op-amp supply as well as the forward bias supply for the PIN diode driver.

4.2.3.2.2. + 15 V DC Power Supply

A small +15V Power Supply LRS35-15 rated for 2.3 A is included to provide the reverse bias voltage supply for the PIN diode driver. This supply can also be used to supply power to preamplifiers, which frequently require a small amount of current at 10-15 VDC.

4.2.3.2.3. +5 V Voltage Regulator Board

A small amount of current is needed to operate the transmit-side translation stage (if needed). Instead of including an additional power supply, a small +5 V regulator (LD1085, STMicroelectronics) is included to power the transmit-side translator from the +7.5 V supply.

4.2.3.3. Translation Unit

The translation unit resides in the scan room, typically installed on or attached to the head of the patient table. The translation unit contains the active frequency translation boards, a PIN diode driver for the coil, and control, support, and monitoring hardware. Figure 4.5 shows the exterior of the multinuclear frequency translation unit. The tabs at the front are for mounting the unit directly to the head of the Philips Achieva 7T patient

table, and adapters could be constructed for other scanners. Figure 4.6 shows the interior of the translation unit. The scanner interface cable has not been installed in this picture.

Figure 4.5: Exterior of multinuclear frequency translation unit.

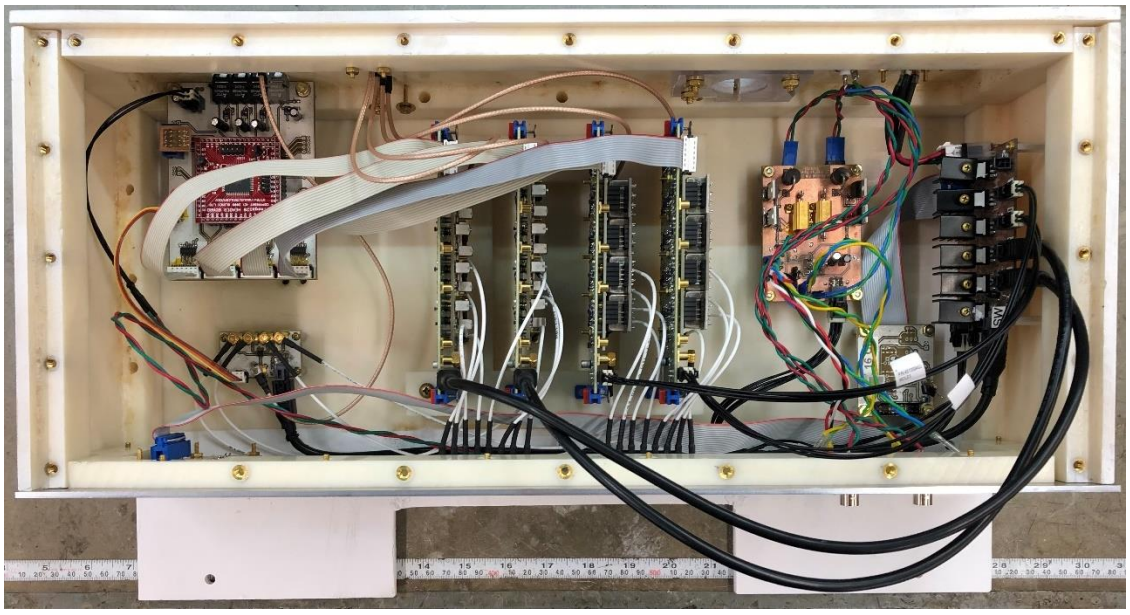

Figure 4.6: Interior of multinuclear frequency translation unit.

4.2.3.3.1. Voltage Regulation Board

The voltage regulation board contains 14 voltage regulators to provide regulated power supplies to each translator board, the control board, the RF switch, and the PIN diode driver as well as a spare output capable of supplying an additional translator board. Each output has its own +5 V voltage regulator. The LD1085 is used for the control board and translation boards, heat sunk and designed to supply 1.5 A. The LP2950 is used for the SP4T RF switch and PIN diode driver, designed to supply 50 mA. Each translator board has its own -5 V voltage regulator, the XC6902N501, designed to supply 100 mA. The control and SP4T RF switch do not require a -5 V supply in their current designs, so they share a -5 V supply using the XC6902N501 for future-proofing.

The +15 V and -7.5 V outputs for the PIN diode driver board are not regulated, as the PIN diode driver is best operated with the maximum forward and reverse bias voltages available.

A connector is provided to supply an output for LED indicators, one for each channel. With the indicators, the regulator board requires approximately 20 mA on the +15 V supply, 200 mA on the +7.5 V supply, and 200 mA on the -7.5 V supply. The voltage regulation board is a two-layer board that was designed, milled, and assembled in-house.

4.2.3.3.2. Control Board

The control board serves as the interface between the control unit and the translation and switch boards in the translation unit. It is based on an ATmega128

microcontroller (Microchip Technology, Chandler, AZ, USA), which runs C code developed in-house that communicates with the control unit over a fiber optic connection.

Based on the received commands, the control board programs the settings of the translator boards and the SP4T RF switch board. The control board microcontroller has three sets of additional outputs that have been brought to pin headers. Four digital I/O lines have been brought out and are presently used as to drive LED status indicators. The ATmega128 also has a SPI port and an I2C port that are presently unused.

A single synchronous serial bus is used to program all of the variable gain amplifiers on the translator boards, but a combination of board and channel select lines allows for individual control over the VGAs. Digital outputs on the MCU are used to configure the positions of the monitoring switches on the translation boards. The switches on all four boards are controlled in parallel, and the separately controlled SP4T RF switch is used to select the monitor output to send back to the control system. The SP4T RF switch is also controlled by MCU digital outputs.

The control board requires a +5 V power supply at approximately 500 mA. Its two-layer board was designed in-house, sent out for PCB manufacture, and assembled in-house.

4.2.3.3.3. Scanner Interface Board

The Scanner Interface Board is responsible for providing the correct identification and status signals to the host scanner. Up to now, only an interface board for the Philips Achieva has been developed, but development of circuits for other systems would be straightforward. The interface board for the Philips Achieva is powered directly from the

scanner and is a two-layer board was designed in-house, sent out for PCB manufacture, and assembled in-house.

4.2.3.3.4. SP4T RF Switch Board

The SP4T RF switch board is designed to select one of the monitoring outputs of the four translation boards for routing back to the control unit. It is based on the SKY13384-350LF RF switch (Skyworks Solutions, Woburn, MA, USA). This switch terminates the isolated RF inputs in 50 Ω to eliminate impedance mismatches which could affect performance.

The SP4T RF Switch Board requires a +5 V power supply at approximately 30 mA and is a two-layer board was designed in-house, sent out for PCB manufacture, and assembled in-house.

4.2.3.3.5. Translation Boards

The translation board is designed to perform frequency translation on four received channels. The block diagram of the board can be seen in Figure 4.7. The LO and one of the channels can be sampled with monitoring switches, which can be remotely controlled to verify performance of the translation system.

The four channels share a single LO, which is also split for monitoring. Upon arriving at the translation board, a circuit based on a high-speed fully-differential op-amp (ADA4932, Analog Devices) is used to generate a differential clock signal. This signal will be divided five ways (between the monitor and four translation signals), so two GALI-52+ monolithic amplifiers (Mini-Circuits) are used to boost the signal before splitting with

a resistive power divider. Although a resistive divider is inefficient, it is broad banded, has no magnetic components, and is compact to implement.

The received RF signal flow through each channel is as follows. The received signal is converted from single-ended to differential using the same circuit as the LO input. The signal is mixed to the ^{1}H frequency by the active mixer (ADL5801, Analog Devices) before being converted back to single-ended by a circuit based on the ADA4857 high-speed op-amp (Analog Devices). The single-ended ^{1}H signal is filtered by an interchangeable bandpass filter cell. After this, a GALI-52+ is used in conjunction with a DVGA2-33A+ (Mini-Circuits) to provide a variable gain stage to provide 10.5 to 42 dB of gain in 0.5 dB increments. The output of this variable gain stage is routed to the host system's 1H receiver.

One of the channels on each board is equipped with two switches which allow the RF input and translated output to be bypassed and routed to the monitoring switch. The bypass switch (AS169-17LF, Skyworks Solutions) has a typical insertion loss of 0.3 dB, which is easily compensated for by adjustment of the VGA.

The SKY13384-350LF (Skyworks Solutions) terminates the isolated RF ports in 50 Ω, so the LO level is independent of the state of the on-board SP4T RF switch.

The translation boards require approximately 1.5A at +5 V and 100 mA at -5 V each and were designed in-house and sent out for PCB manufacture and assembly. An assembled translation board can be seen in Figure 4.8.

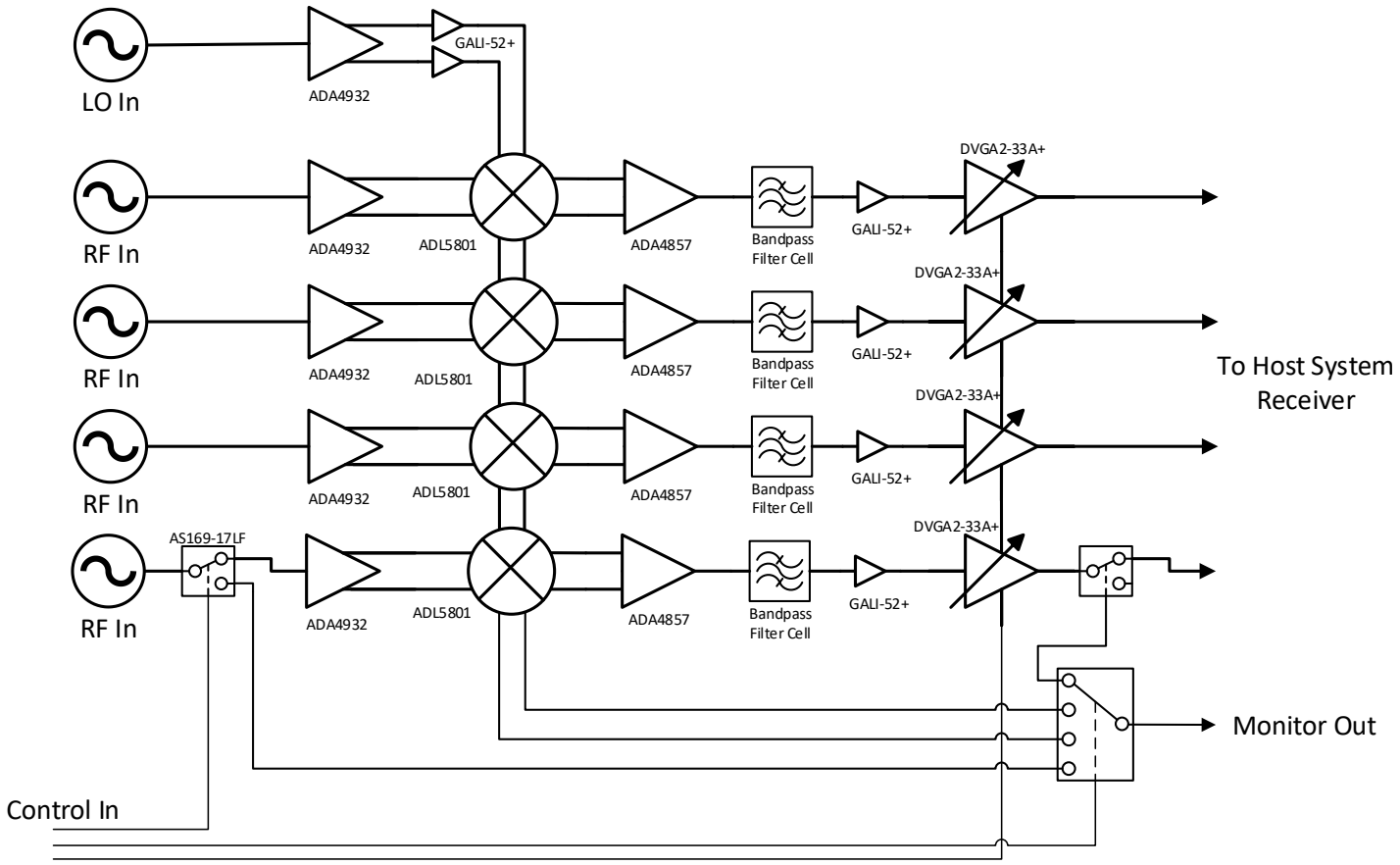

Figure 4.7: Block diagram of 4-channel translation board.

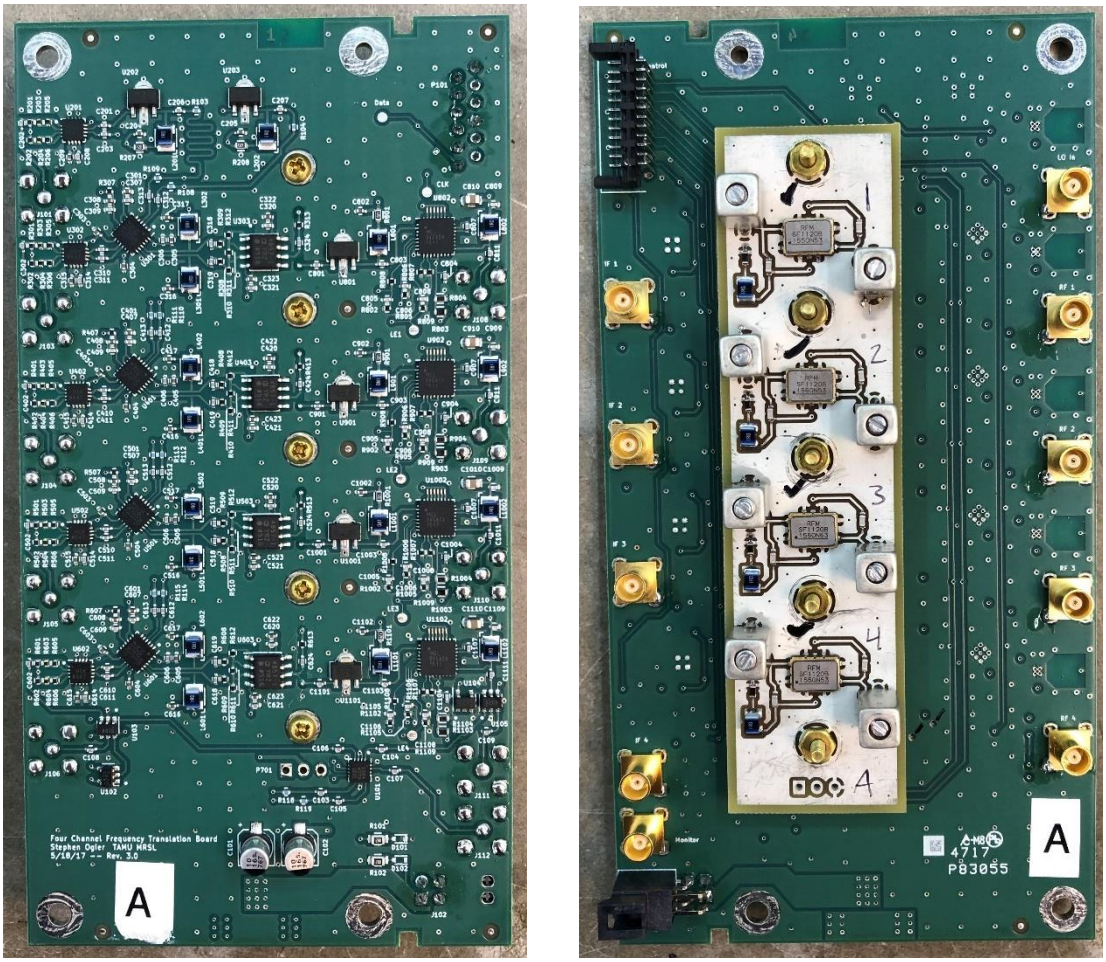

Figure 4.8: 4-Channel Frequency Translation board for Multinuclear Translation System. Left photo is front of board, with inputs on the left and outputs on the right. Right photo is rear of board, with a 298 MHz filter board installed.

4.2.3.3.6. PIN Diode Driver

The PIN diode driver is designed to provide reliable forward and reverse biasing for two opposite outputs. The forward and reverse bias voltages were chosen to be approximately -5 V and + 15 V, respectively. These are the same voltages used by the Philips Achieva system for compatibility for reference imaging. The driver is designed to source 2 A per output when forward biased, and a negligible amount of current for reverse.

The driver uses an unregulated forward bias supply, which gives a slightly larger output voltage of approximately -6.4 V unloaded.

The circuit is based on circuit D.1 from the PIN Diode Designers' Handbook [53], with modifications to allow it to drive more current and be better suited to our application. The single output transistor has been replaced with a Darlington Pair to increase the maximum output current. Additionally, the PNP transistors in the original design have been replaced with NPN devices to accommodate the negative forward bias and positive reverse bias voltages. The silicon diode specified has been replaced with a high-current Schottky diode to reduce the voltage drop in the driving circuit during forward bias.

The PIN diode driver can be controlled manually via toggle switch or by a TTL-compatible system control input. Manual or system control can be chosen via a second toggle switch. System control can be active-high or active-low, selectable by an on-board jumper. Manual control of coil state is useful for volume T/R experiments or when checking the tuning of the transmit and receive coils. Driver circuits for LED indicators are included to display the current state of each output of the driver.

The switching time of the PIN diode driver was characterized with the output unloaded, which can be seen in Table 4.1. The switching time to the forward biased state was defined as the time between the beginning of the input transition to the output reaching a steady voltage, approximately -6.4 V for both drivers. The switching time to the reverse biased state was defined as the time between the beginning of the input transition and the output reaching +14 V.

System Input	Output 1	Output 2
Rising	736 ns to Forward Bias	84 µs to Reverse Bias
Falling	46 us to Reverse Bias	712 ns to Forward Bias

Table 4.1: Pin Diode Driver switching performance

A dummy load was used to test the performance of each output at full current. The system input was used to drive the outputs at a 50% duty cycle at 100 Hz. The dummy load was constructed of a 2 Ω high-power resistor in series with a 1N5408 diode and was measured to draw approximately 2 A during forward bias.

No heat sinks were mounted on any of the devices in the PIN diode driver. The maximum temperature reached, as measured by a FLIR i7 (Wilsonville, OR, USA) was 81°C on the low-side output transistors. The high-side output transistors only reached a maximum of 33°C, and the Schottky diode reached a maximum of 43°C.

4.2.4. Operation

4.2.4.1. Choice of Local Oscillator Frequency

Although one's first instinct is often to use the highest available clock frequency, for this application careful choice of clock frequency is imperative.

One constraint on the clock frequency is that for phase resetting to work, the clock frequency must be a multiple of 10 MHz. The AD9959 is configured to sample its control inputs at the $1/4^{th}$ of the clock frequency, and the host system generates its triggers in synchrony with its 10 MHz clock, so in order for the timing between the phase reset signal and the resetting of the output phase to be consistent, the core frequency must be a multiple of 40 MHz.

Another constraint on the clock frequency arises when it is necessary to undersample the LO output. The output of a DDS system will be modulated by the envelope

$$A = \frac{\sin\left(\pi \frac{f_{out}}{f_s}\right)}{\pi \frac{f_{out}}{f_s}}$$

where f_s is the sampling frequency of the DDS system [36]. Because of this, there are some choices for clock frequency that would result in low LO amplitudes.

When using one of the DDS image outputs as an LO source, spurious outputs become more of an issue than they are when operating below the Nyquist frequency. Major spurs appear at frequencies given by

$$f_{spur} = nf_s \pm f_{out}$$

where *n* is a positive integer [36].

At 4.7T, the ^{1}H frequency is approximately 200 MHz, so any required LO will be below the Nyquist frequency if a DDS clock frequency of over 400 MHz is used. In practice, to separate the LO outputs as far as possible from major spurs, it is advisable to use a clock frequency close to the highest available, typically 480-500 MHz.

At 7T, even if a 500 MHz clock is used, the required LOs for several nuclei (including ^{2}H and ^{15}N) fall above the Nyquist frequency. In order to compute the best DDS clock frequency, a spreadsheet was developed to compute the spurs and relative amplitudes for multiple nuclei, which is shown in Figure 4.9. Two factors were considered in the selection of the DDS clock frequency: the minimum distance of any nucleus of interest to a major spur and the minimum relative LO amplitude.

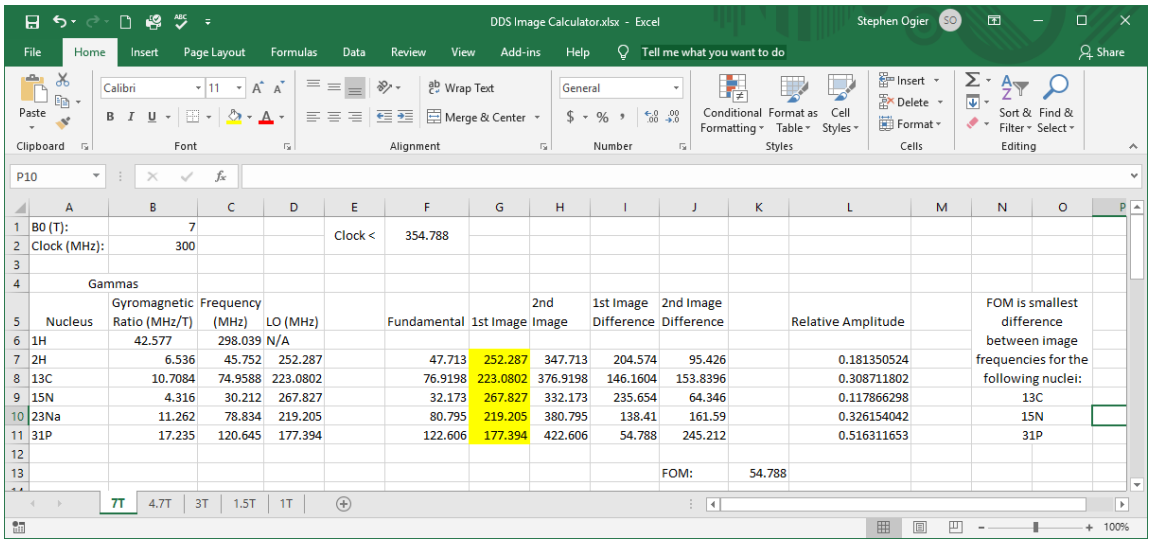

	A	B	C	D	E	F	G	H	I	J	K	L	M	N	O
1	B0 (T):	7			Clock <	354.788									
2	Clock (MHz):	300													
3															
4		Gammas													
5	Nucleus	Gyromagnetic Ratio (MHz/T)	Frequency (MHz)	LO (MHz)		Fundamental	1st Image	2nd Image	1st Image Difference	2nd Image Difference		Relative Amplitude		FOM is smallest difference between image frequencies for the following nuclei:	
6	1H	42.577	298.039	N/A											
7	2H	6.536	45.752	252.287		47.713	252.287	347.713	204.574	95.426		0.181350524			
8	13C	10.7084	74.9588	223.0802		76.9198	223.0802	376.9198	146.1604	153.8396		0.308711802			
9	15N	4.316	30.212	267.827		32.173	267.827	332.173	235.654	64.346		0.117866298		13C	
10	23Na	11.262	78.834	219.205		80.795	219.205	380.795	138.41	161.59		0.326154042		15N	
11	31P	17.235	120.645	177.394		122.606	177.394	422.606	54.788	245.212		0.516311653		31P	
12															
13										FOM:	54.788				

Figure 4.9: Spreadsheet calculator for optimizing DDS clock frequency.

For ^{13}C and ^{15}N, a DDS clock of 320 MHz was chosen, putting both nuclei in the first image band. This choice of clock resulted in a minimum distance to a major spur of 104 MHz, and a lowest relative amplitude of 0.22, for ^{15}N. For ^{13}C, ^{15}N, and ^{31}P, a DDS clock of 300 MHz was chosen putting all three in the first image band. This choice of clock resulted in a minimum distance to a major spur of 55 MHz, and a lowest relative amplitude of 0.12, for ^{15}N.

This spreadsheet was designed as a development tool. When setting up the system for operation at a new field strength, the optimal clock frequency can be determined. These calculations only have to be performed once when the system is initially being configured for a new field strength. In actual operation, the clock frequency is pre-programmed and set by use of a startup parameter.

4.2.4.2. Hardware Setup

For setup on a human imaging system, the control unit is set up in the equipment room, while the translation unit is installed in the magnet on the patient table. For control, a Cat 5 cable is run from the control unit to a laptop running the control GUI in the control room.

The control unit is set up in the equipment room, where it has easy access to the host system's 10 MHz reference and phase reset trigger (if applicable). The LO and power outputs, and monitoring connections are routed through the penetration panel. The optical control lines are routed through the waveguide into the scan room.

Inside the scan room, the LO, power, monitoring lines, and control lines are routed to the translation unit, typically through the magnet bore. To keep the lines in place and ease use, they are mounted to in a flexible plastic cable carrier that is mounted to a non-magnetic frame set up at the rear of the magnet.

4.2.4.3. Software Setup

Software setup is straightforward. The control software on the BeagleBone Black starts automatically on power-up. The client software is presently started with a command-line function, with an option to specify the nominal B_0 strength of the magnet so that the clock frequencies and LO calculations will be properly configured.

4.3. Results

4.3.1. Bench Performance

Performance of the Multinuclear Translation System was evaluated on the bench, using a test signal, spectrum analyzer, and oscilloscope. The results of the characterization can be seen in Table 4.2.

	^{13}C AT 4.7T	^{13}C AT 7T
Conversion Gain	9.23 dB	-4.5 dB
0.1 dB Input Compression Point	-2.99 dBm	-7.75 dBm
Isolation at ^{1}H frequency	45.89 dB	54.12 dB

Table 4.2: Multinuclear Translator Performance

To demonstrate the capability of the Multinuclear Translation System to simultaneously convert multiple nuclei to the ^{1}H frequency, a test was done in which signals were inserted into the translation system at 20.3 and 50.3 MHz, which correspond to ^{15}N and ^{13}C at 4.7T. The 20.3 MHz test signal was generated by a PTS-250 frequency synthesizer and had an amplitude of -0.6 dBm, and the 50.3 MHz test signal was generated by the built-in TPI RF synthesizer and had an amplitude of 2.74 dBm. An oscilloscope capture of the input signals is shown in Figure 4.10. It is important to note that the although the input signals are well above the 0.1 dB compression point, they still can show the capabilities of the translation system. In actual operation it would be best to avoid inputs with such large amplitudes.

Because each four-channel translation board shares the same LO between all channels, the two test signals were inserted into the inputs of two different four-channel boards. The LO source was configured for outputs at 179.7 and 149.7 MHz, which were routed to the FTU.

In order to compensate for the difference in input level, the VGAs on the board to which the 50.3 MHz signal was input were set to their lowest gain, approximately 10.5 dB, while the VGAs on the other board were set to 12.0 dB of gain. The outputs can be seen in Figure 4.11. Some distortion can be seen in the 50.3 MHz signal. This distortion is from non-linearities in the TPI RF synthesizer. It could be filtered out, but the harmonics of 50.3 MHz are mixed out-of-band, so no filtering is necessary.

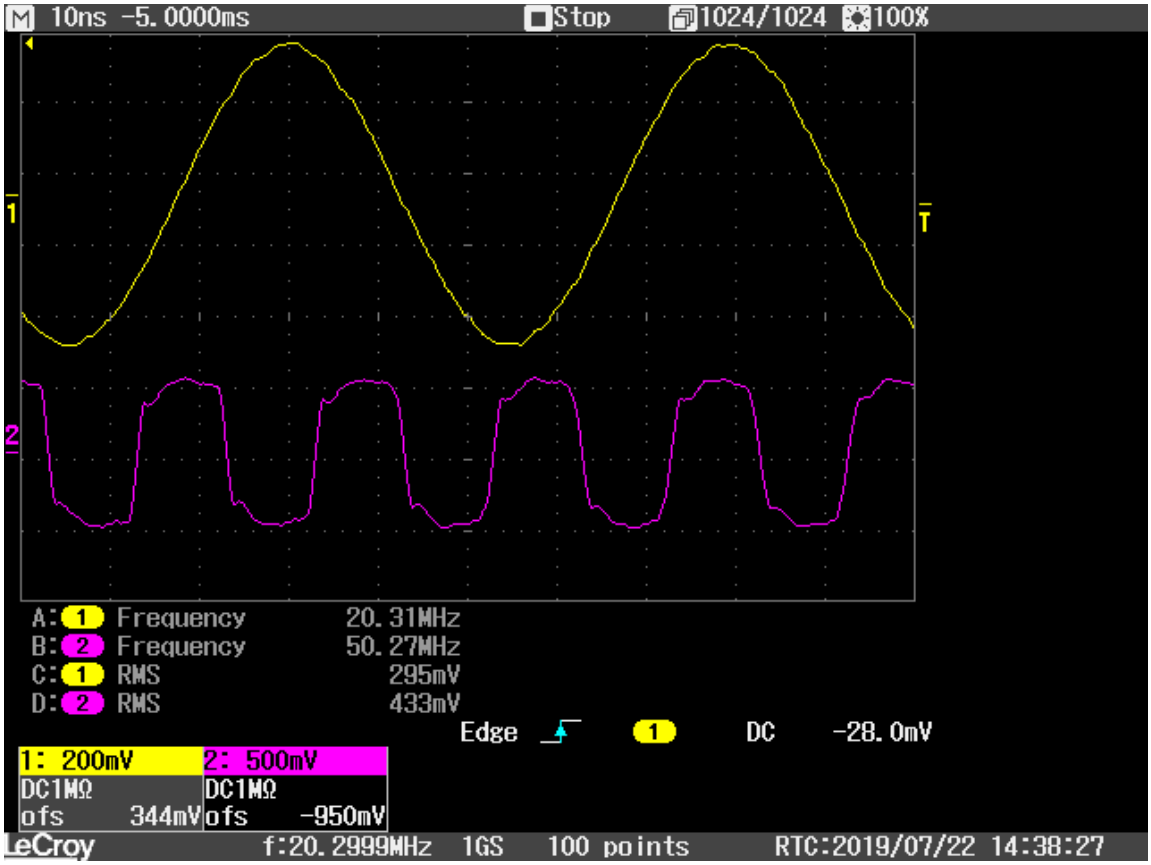

Figure 4.10: Test inputs to multinuclear translation system. Top trace is at 20.3 MHz, and bottom trace is at 50.3 MHz.

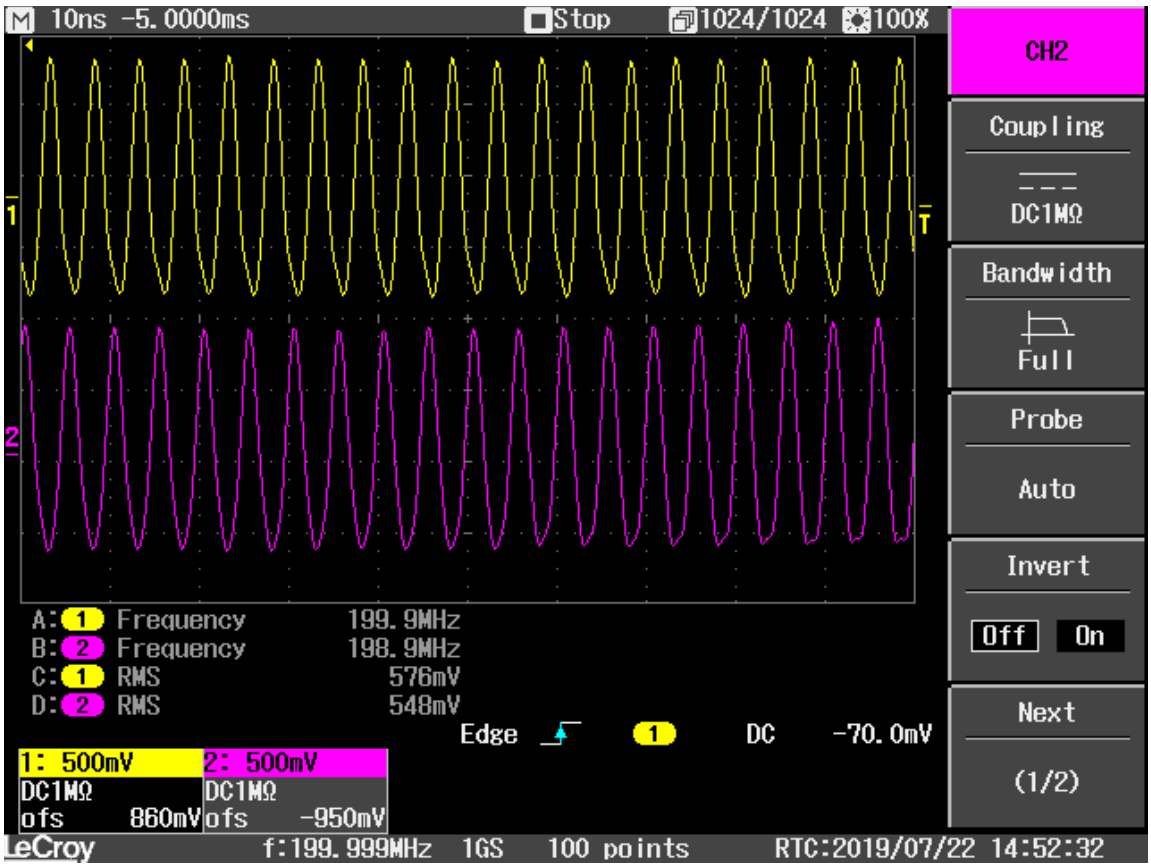

Figure 4.11: Test outputs of multinuclear translation system. Both outputs have been translated to 200 MHz, and the gains of the translation channels have been adjusted to compensate for the different input levels.

4.3.2. 4.7 T Performance

Performance of the system was evaluated on a 4.7T small-bore imaging system. The host spectrometer was a Varian Unity Inova, which made for easy setup, as the translation system can easily be inserted between the Varian LNA and the rest of the Varian receive system.

The host system's 10 MHz reference was used to generate the DDS clock, and a programmable trigger line was used to reset the phase of the LO before each acquisition.

To demonstrate the phase coherence of the system, spectra were acquired from a sample of 91% isopropanol in water with 1, 2, 4, 8, and 16 averages. The SNR of the averaged spectra is proportional to the square root of the number of averages, and if the translation system is phase coherent, that trend should be clear.

All spectra had 0-order phase correction, 3 Hz Gaussian line broadening, and DC offset correction applied. The phase correction term was found by using the jMRUI program to manually phase each spectrum.

Reference spectra were acquired with the system in a stock configuration. The same pulse sequence was used as for frequency translation, but the transmit and receive frequencies were both set to the ^{13}C frequency. The reference spectra can be seen in Figure 4.12. In order to ensure the full dynamic range of the Varian receiver was utilized, a Miteq AU-1114-BNC LNA (L3 Narda-MITEQ, Hauppauge, NY, USA) with 28 dB of gain was inserted. Gain was reduced with the addition of attenuation after the LNA by 5 dB for the reference data and 6 dB for the translated in order to bring both received signals to approximately the same level (within 2dB of each other).

Translated spectra were acquired using a single channel of the Multinuclear Translation System to convert the preamplified ^{13}C signal from the Varian LNA to the ^{1}H frequency. The translated and filtered signal was then inserted into the Varian receive path. The VGA in the translation channel was configured for minimum gain in order to avoid overflowing the host system receiver. The s2pul_SO_translate pulse sequence was used to acquire the translated spectra. This pulse sequence can be seen in Appendix D.

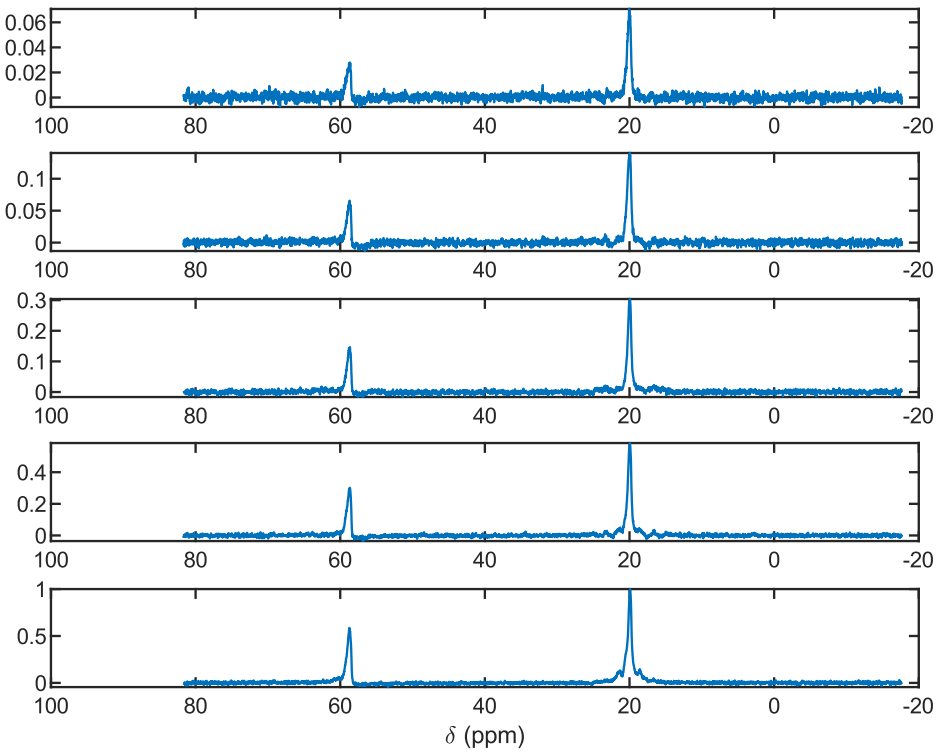

Figure 4.12: Reference isopropanol spectra. From top to bottom, spectra were acquired with 1, 2, 4, 8, and 16 averages. Spectra were scaled to the peak intensity of the 16-average dataset.

The translated spectra can be seen in Figure 4.13. The spectra clearly show SNR improvement as the number of averages increases, but the SNR improvement does not appear to be as dramatic as in the reference data. Additionally, the zero-order phase correction term shows a great deal more variation than with the reference spectra.

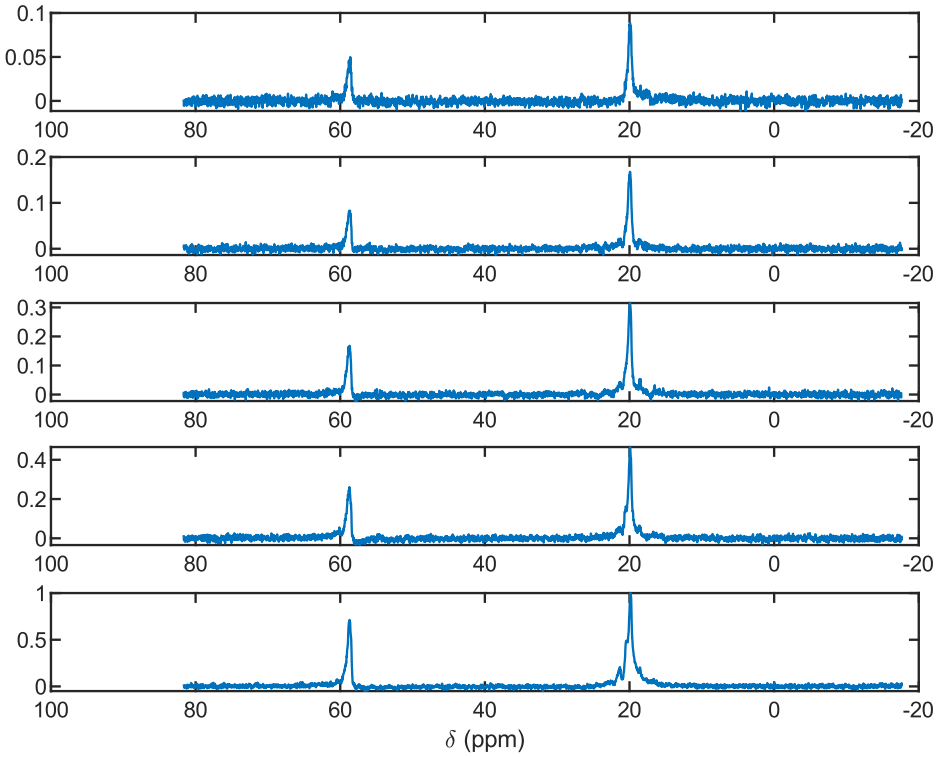

Figure 4.13: Translated isopropanol spectra. From top to bottom, spectra were acquired with 1, 2, 4, 8, and 16 averages. Spectra were scaled to the peak intensity of the 16-average dataset.

The results of the phase coherence analysis can be seen in Figure 4.14. The SNR of both the reference data from the stock Varian system and the Varian system with the translation system inserted show a clear trend of SNR increasing with number of averages. The lower plot shows the SNR versus $\sqrt{NSA}$, where *NSA* is the number of signal averages. This is expected to be a linear relationship, but the SNR of the translated data doesn't seem to reflect that. The degradation in SNR from the addition of the translation system is ranges from -0.7099 dB to -5.0651, with the degradation generally getting worse as the number of averages increases.

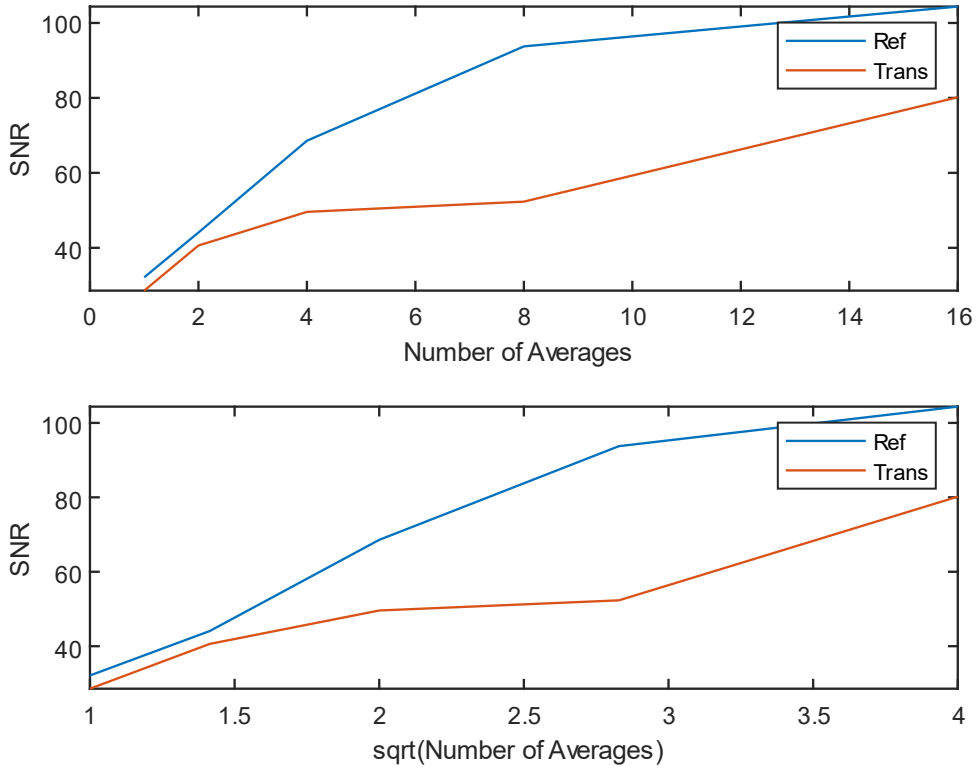

Figure 4.14: SNR versus number of averages for stock Varian system and Varian system with Multinuclear Translation System inserted.

The variation in the zero-order phase correction term and the abnormality in the SNR improvement with averaging suggests that the phase resetting of the LO is working inconsistently. A 16 average data set was acquired without phase correction and showed much more severe SNR degradation, which suggests the phase resetting is providing some benefit, but it is not producing its theoretical results.

To isolate the problem, the LO source from the original frequency translation system was substituted for the source in the multinuclear translation system. The

averaging results of this can be seen in Figure 4.15. The SNR is improved over the built-in LO source, and averaged results show a clear linear trend versus $\sqrt{NSA}$. The SNR difference between the translated and reference spectra ranges from -0.18 dB to +3.6 dB. The improved SNR for low numbers of averages could be because of slight differences in overall signal level between the reference and translated signals, but it is unclear why the translation system has better performance with high numbers of averages. It could be that the Varian system's receiver has better phase coherence at 200 MHz than at 50 MHz.

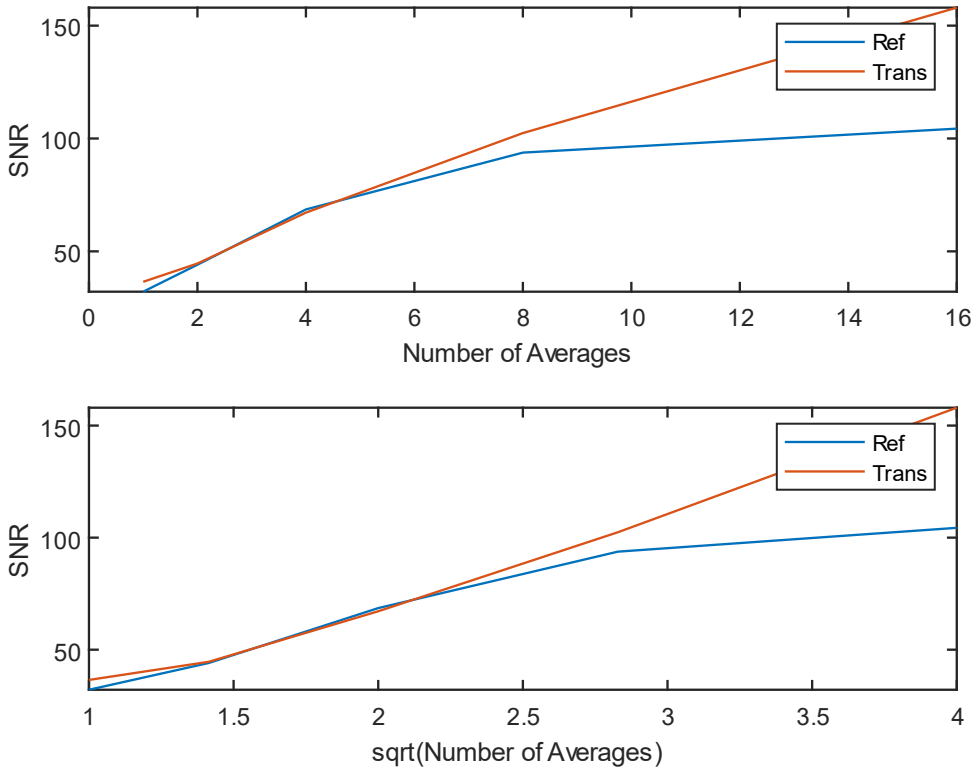

Figure 4.15: SNR versus number of averages for stock Varian system and Varian system with Multinuclear Translation System with the original version's LO source.

4.4. Conclusion and Discussion

The Multinuclear Frequency Translation System has been shown to be able to convert multiple input frequencies to the ^{1}H frequency, without significant degradation of SNR. The phase coherence issue in the built-in LO source needs to be addressed, but it is likely a simple issue with the triggering circuit that can be easily fixed.

This system is a significant improvement over the original translation system, as it is capable of translating multiple received nuclei. Using the Multinuclear Translation System is also much easier than using its predecessor, as it has more sophisticated controls, is capable of directly interfacing with the host system, and has built-in monitoring equipment.

The ability to simultaneously receive multiple nuclei has become more important in recent years, as the clinical application of hyperpolarization and the development of Simultaneous Multinuclear MR Fingerprinting have increased the need for systems that can acquire multiple nuclei truly simultaneously.

4.4.1. Future Work

The built-in signal generation and monitoring capabilities of the Multinuclear Translation System present an enormous amount of promise for semi-automated calibration and debugging tools. At present, the control software is only capable of operating the TPI synthesizer and SDR receiver manually, but a more sophisticated interface could be developed to help less technically proficient users calibrate and debug the system.

An additional feature that would improve usability would be the ability to save configuration profiles. This would streamline setup, as one would not have to start from the default configuration each time the system is restarted.

4.4.2. Future Expansion

In order to simultaneously study multiple nuclei on a system with a single transmit channel, the transmit-side translation system would need to be upgraded. In order to accomplish this, the transmit-side translation stage must be made to be capable of translating the ^{1}H RF pulse from the host system to 2-3 different frequencies, as well as provide a buffered output for the incoming ^{1}H pulse. In order to better accommodate the different sensitivities of different nuclei, the gain of each output should be able to be controlled independently by the control system.

Additionally, in order to achieve compatibility with non-Philips host systems, interface circuitry must be devised to accommodate each system. This is a minor change, and simply requires replacing the interface cable and board with ones matched to the new host system.

5. A STANDALONE BROADBAND MRI SYSTEM[3]

5.1. Introduction

The broadband system was developed as a platform to expand the capabilities of the MRI systems in the MRSL as well as a platform on which new technologies and approaches could be tested.

The broadband system needed to be compatible with two 4.7T small-bore imaging systems and a 1T human extremity scanner. The 1T system is very compact and doesn't require a great deal of RF power or gradient current to operate, so compact RF and gradient amplifiers were included to allow the broadband system to function without needing any parts of the system that came with the 1T. The 4.7T systems require more RF power and gradient current and have a more modular construction, so it was decided to have the broadband system interface with the existing RF and gradient amplifiers.

Aside from needing to work across two different field strengths, the broadband system needed to be truly broadband in order to work with a large variety of nuclei. To date, it has studied ^{1}H, ^{2}H, ^{13}C, ^{15}N, ^{23}Na, and ^{31}P. The gyromagnetic ratios of these nuclei vary widely, so in order to cover all of these nuclei at both field strengths it must be capable of operating over a frequency range of 4.3 to 200 MHz.

The broadband system was designed and constructed under the direction of Dr. Steven M. Wright by the post-doctoral research Dr. John C. Bosshard as well as a number of graduate students, including Dr. Neal Hollingsworth, Scott Blaczyk, Brian Bass, and

[3] This is a draft of a paper intended for Submission to IEEE Transactions on Biomedical Engineering with a tentative title of "A Stand-alone Broadband MRI System for Simultaneous Multinuclear Imaging".

the author. The triple-tuned coil was developed principally by Hongli Dong with assistance by the author, and the triple-nucleus receiver front-end was developed by Dr. Chung-Huan “Tim” Huang.

5.2. Broadband System Architecture

Instead of the console-spectrometer architecture common in many analytical and clinical systems, the broadband system uses a single PC for control and signal acquisition. An external set of rack units contain hardware for generating and amplifying the RF transmit pulses, gradient amplifiers, and power supplies for the high-power amplifiers. A block diagram of the broadband system as used for simultaneous imaging and spectroscopy at 4.7T is shown in Figure 5.1.

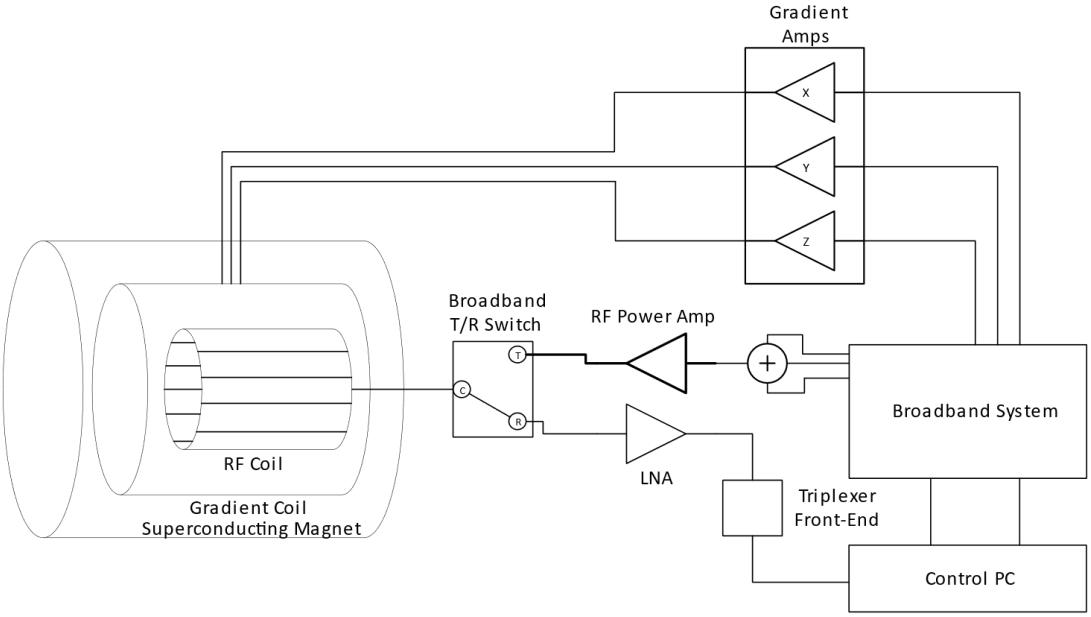

Figure 5.1: Block diagram of broadband system.

5.2.1. Host PC

The host PC contains two PCIe cards that serve as the core of the broadband system. The NI PCIe-6363 (National Instruments, Austin, Texas, USA) generates the gradient waveforms as well as controlling RF waveform generation, clock generation, and all of the other small-signal components. Digitization is performed by an UltraView 4-channel 16-bit digitizer card (Berkeley, CA, USA). The host PC runs control software written in LabView (National Instruments) that generates and plays out the pulse sequence and acquires the received signals.

5.2.2. NI PCIe-6363

The NI PCIe-6363 is used to control everything other than digitization of the received signal. Three analog outputs are used for controlling the gradient amplifiers. Digital outputs are used to control RF waveform generation. The DDS synthesizer is controlled by the PCIe-6363 as well as the blanking switch and variable gain amplifier. In order to maintain synchronization with the generated RF pulses and digitized data, it uses a 10 MHz reference oscillator from the clock synthesizer board.

5.2.3. UltraView Digitizer

The UltraView, along with the DDS synthesizer, is one of two components that allow this system to be truly broadband. Its sampling rate is limited to 250 MS/s, but it has a front-end bandwidth of 700 MHz that allows it to undersample signals without significant SNR penalty. It can generate its own sample clock for operation at 250 MS/s, but in order to reduce the data size by undersampling, it requires an externally generated clock that is supplied by the clock synthesizer board.

5.2.4. Small Signal Unit

The small signal unit, the top unit of the full broadband system shown in Figure 5.2, contains the hardware required to generate and condition the RF and gradient small-signal waveforms. All of the broadband system controls go to the small signal unit, and the outputs of the small signal unit are routed to the RF and gradient power amplifiers. The interior of the small signal unit can be seen in Figure 5.3.

Figure 5.2: Front of full broadband system. Units are, from top to bottom, small signal unit, power amplifier unit, and power supply unit.

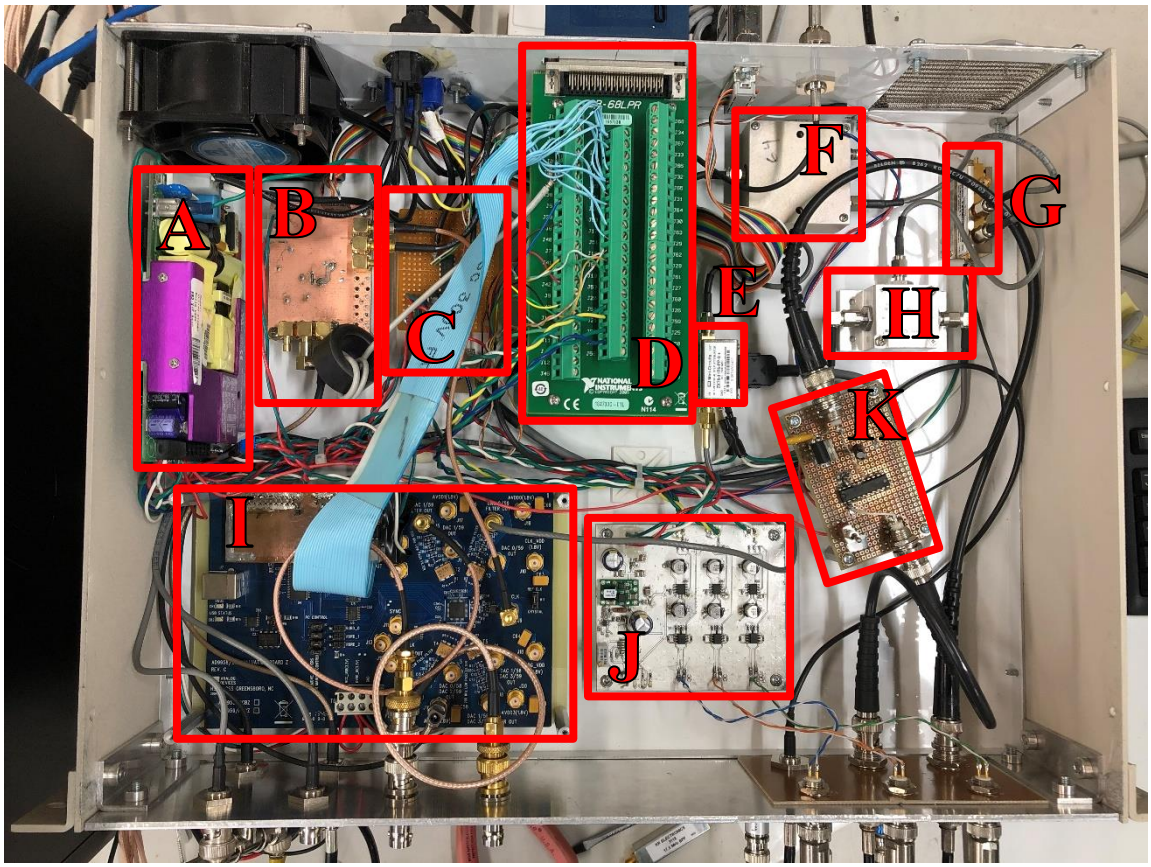

Figure 5.3: Interior of broadband system small signal unit. A is the DC power supply, B is clock synthesizer board, C is control buffer board, D is breakout board for connecting to NI PCIe-6363 board, E is the variable attenuator, F is the fixed gain stage, G is the RF blanking switch, H is the directional coupler, I is the AD9959 RF generator, J is the gradient conversion and monitoring board, and K is trigger conditioning board.

5.2.4.1. AD9959 DDS RF Synthesizer

The second key to truly broadband operation is a direct digital synthesis (DDS) RF synthesizer based on the AD9959 (Analog Devices, Norwood, MA, USA). This synthesizer has four RF outputs capable of operating independently and supports full modulation control over a quad-SPI digital interface. Broadband operation is achieved because of its high maximum clock frequency, 500 MHz, which is sufficient for 4.7T

without undersampling. Additionally, this device supports triggerable resetting of the output phase, which is necessary for some approaches to maintaining phase coherence.

In was deemed more cost and time-effective eschew designing a circuit board that would include the AD9959 and instead an evaluation board manufactured by Analog Devices that includes the device was installed in the broadband system. The evaluation board allows for USB control of the DDS device, which was used in evaluation and initial debugging. In actual operation, the AD9959 is controlled over a quad-SPI interface by the PCIe-6363. An interface mezzanine board was designed and installed to convert the 5V logic level used by the PCI3-6363 to the 3.3V level used by the AD9959.

5.2.4.2. Digital Step Attenuator

Because the DDS only has 10 bits of amplitude modulation, using DDS modulation for gain control reduces the resolution of the amplitude modulation. A digital step attenuator (ZX76-31R5-PP-S+, Mini-Circuits, Brooklyn, NY, USA) provides 31.5 dB of programmable attenuation in 0.5 dB steps, allowing for fine control over the transmit power. The attenuator is controlled by the NI PCIe-6363 over a parallel interface, and is powered by a +3.3V DC power supply.

5.2.4.3. Fixed Gain Stage

The digital step attenuator is followed by a fixed gain stage, based on the Gali-74+ monolithic amplifier (Mini-Circuits).

5.2.4.4. RF Blanking Switch

The blanking switch is performed after the fixed gain stage by a SPDT RF switch (ZX80-DR-230-S+, Mini-Circuits). This switch has a built-in driver that allows it to be

directly controlled by the NI-PCIe-6363. It terminates un-connected outputs in 50Ω, so when the output of the previous gain stage is disconnected, the input to the radiofrequency power amplifier (RFPA) sees 50Ω at its input. The switch has a second throw, which would it allow it to select between two RF sources in addition to blanking the RFPA if that were ever required.

5.2.4.5. Directional Coupler

A directional coupler (ZFDC-20-4-S+ Mini-Circuits) is the last stage in the RF small-signal path. Both the main and coupled outputs of the directional coupler are routed to the front panel. This coupler is included to allow for monitoring of the generated RF pulse without interference with the RF transmit path.

5.2.4.6. Clock Synthesizer

The clock synthesizer board was not originally a part of the system and was added when it was determined that a more powerful and flexible clocking solution was needed to drive the AD9959 and enable undersampling with the UltraView. It is controlled over I^2C by a NI USB-8451 (National Instruments) USB to I^2C/SPI interface connected via USB to the host PC. Because this board is also a part of the multinuclear frequency translation system, further details have been included in Appendix C.

5.2.4.7. Gradient Conversion and Monitoring Unit

This board is responsible interfacing the single-ended gradient control outputs from the NI PCIe-6363 with both single-ended and differentially driven gradient amplifiers. Fully differential op-amps (THS4131, Texas Instruments, Dallas, TX, USA) are used to convert the single-ended input to a differential output, as seen in Figure 5.4.

Because gradient signals range in frequency from DC to ~20 kHz, it is not possible to use a magnetic transformer or balun to convert the signal to differential. Both phases of the differential output can be used to drive a differential input gradient amplifier (e.g. the Performance Controls, Inc. amplifiers used with the Varian imaging systems) or only the positive phase can be used to drive a single-ended input gradient amplifier (e.g. the compact gradient amplifiers in the broadband system).

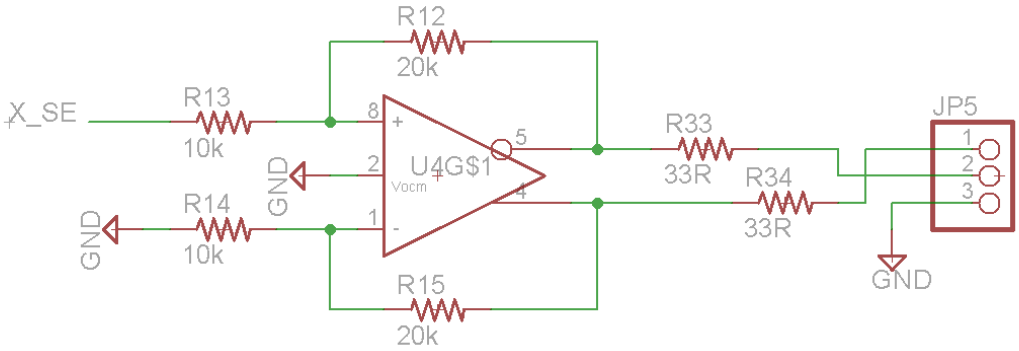

Figure 5.4: Gradient single-ended to differential converter.

Although it is not at present fully implemented, this board also includes monitoring circuitry to protect the gradient amplifiers and coils. The gradient amplifiers on the two Varian 4.7T systems are incredibly powerful, and if the gradient waveform generating software or hardware were to fail in a way that left a gradient on in a high-current state, the gradient coil or amplifier could overheat and be damaged or destroyed. In order to prevent this, an analog supervisory circuit based on the AD736 RMS to DC converter (Analog Devices, Norwood, MA, USA) was developed that would trigger a shutdown line if the RMS voltage of any of the gradient channels exceeded a preset threshold. The

gradient monitoring circuit can be seen in Figure 5.5. The output of this circuit was compared to a threshold, and if the threshold was exceeded, a shutdown line was pulled low.

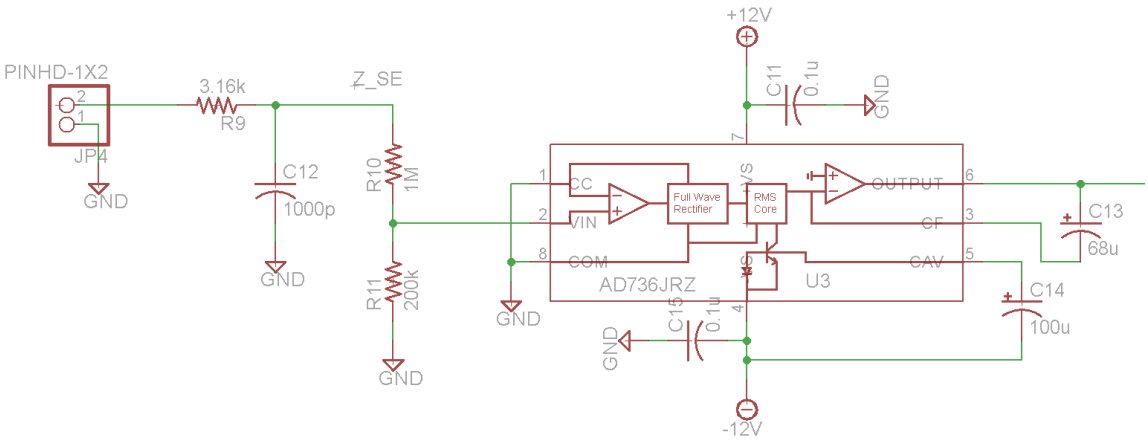

Figure 5.5: Gradient RMS conversion circuit.

The single-ended to differential conversion and watchdog circuits require a ±12V DC bipolar power supply, but the power supply in the small signal unit can only supply +12V. The negative voltage rail is generated by a built-in buck-boost modular switching regulator (PTN78000A, Texas Instruments) that can generate a negative power supply from a positive input voltage.

5.2.4.8. Control Buffer Board

This board serves as a buffer for digital control lines.

5.2.4.9. Trigger Conditioning Board

This one provides signal conditioning for the trigger signal for the UltraView to ensure consistent triggering.

5.2.4.10. Power Supplies

The small signal unit is powered entirely by a single power supply that has +12V, +5V, and +3.3V outputs. The case fan is located directly adjacent to the supply to keep it from overheating.

5.2.5. Power Amplifiers

In order to avoid interference with the small-signal portions of the broadband system and keep the system modular, the RF power amplifiers and gradient amplifiers are housed in a separate rack unit, which can be seen in Figure 5.6.

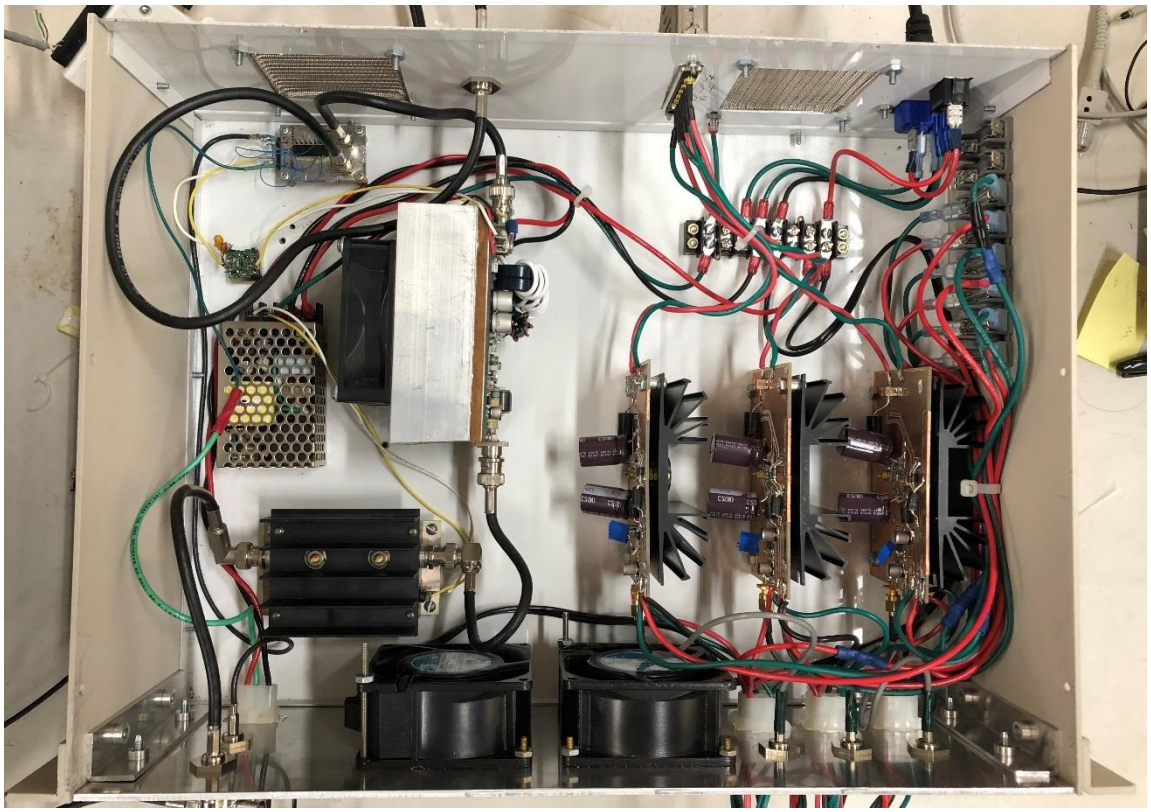

Figure 5.6: Power amplifier unit.

.

5.2.5.1. Gradient Amplifiers

The gradient amplifiers were constructed in-house using a circuit based on the Apex PA12A high-power operational amplifier. The circuit used is a derivative of the Improved Howland Current Pump, and is capable of producing a maximum output of ±15 A. Additional protection diodes and an R-C snubbing circuit were added to protect against voltage spikes and oscillation from the inductive load of the gradient coils.

5.2.5.2. RF Power Amplifiers

Broadband power amplification is provided for use with the 1T system and is accomplished by two stages of RF amplifier. The final gain stage of the small signal unit has a maximum output power of +19.2 dBm, which is far less than the approximately +30 dBm necessary to fully drive the power amplifier. To increase the input signal to the RFPA to a sufficient level, a Mini-Circuits ZHL-3A is used to boost the signal to a sufficient level. The ZHL-3A has a maximum output power of 29.5 dBm, which is sufficient to achieve sufficient output power to observe gain compression. It has a specified bandwidth of 400 kHz to 150 MHz, which is more for up to 3T.

The RF power amplifier is a 500W pallet amplifier (CAP1075-500, Communication Amplifiers, LLC, Terrell, TX, USA). This amplifier is rated from 10-75 MHz, but has been verified to perform well down to 5 MHz. It has a large heatsink and fan mounted directly to it to cool it during operation and in testing, it was able to achieve 450 W for both ^{1}H and ^{2}H at 1T.

5.2.5.3. Amplifier Blanking Switch

Because RFPAs produce broadband noise at all times they are biased, a blanking switch is necessary after the RFPA to block the noise it produces when there is no active transmit pulse.

5.2.6. Power Supplies

Power Supplies for the power amplifiers are housed in a separate unit from the rest of the system, which can be seen in Figure 5.7. The gradient amplifiers require ±48 V DC and ±12V DC, and the RF power amplifier requires +48 V DC.

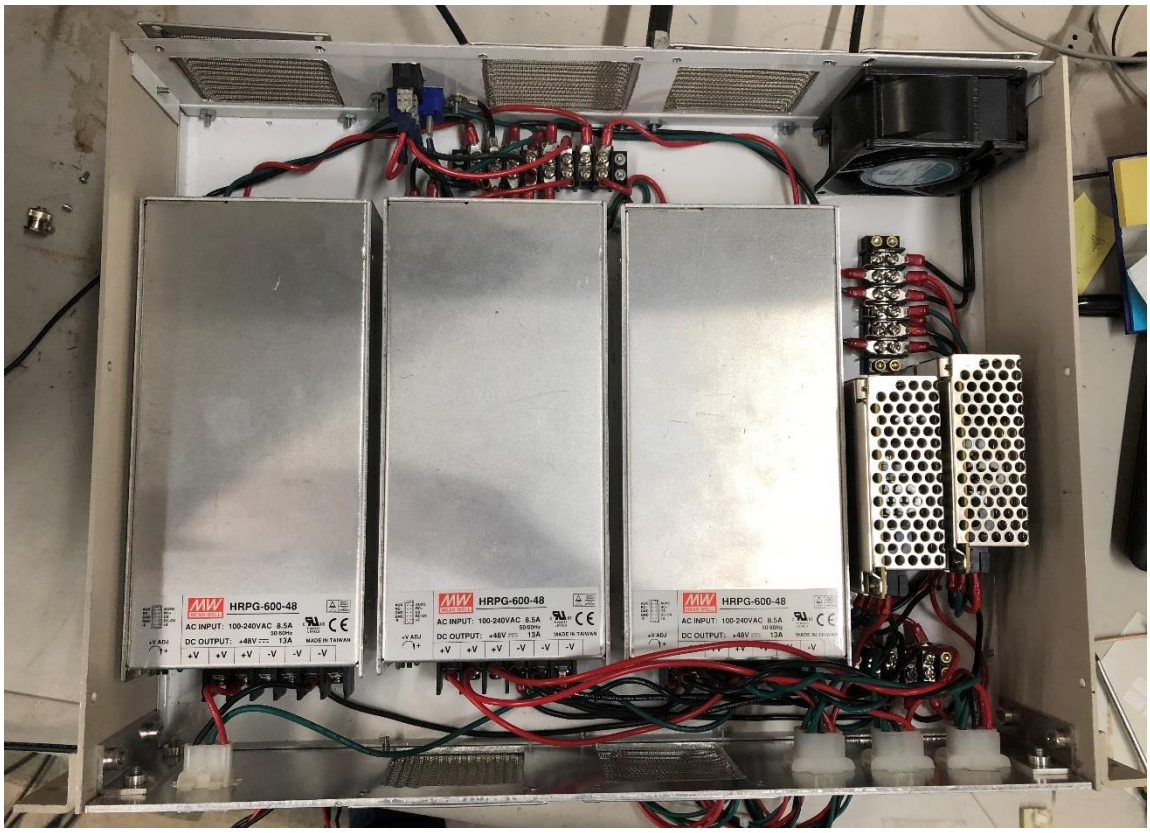

Figure 5.7: Power supply unit. 48V DC supplies are on the three on the left, and 12V DC supplies are the two on the right.

5.3. Triple-Tuned Receiver Front-End

One of the primary motivations for the development of this system is simultaneous imaging of multiple nuclei with multi-tuned, single-port coils. Dual-tuned coils with multiple ports are in common use [62-64], but our desire is to simplify construction of multi-tuned arrays through the use of multi-tuned coils in which all nuclei share a single port. A triple-tuned single-port coil for ^{1}H, ^{23}Na, and ^{2}H can be seen in Figure 5.8.

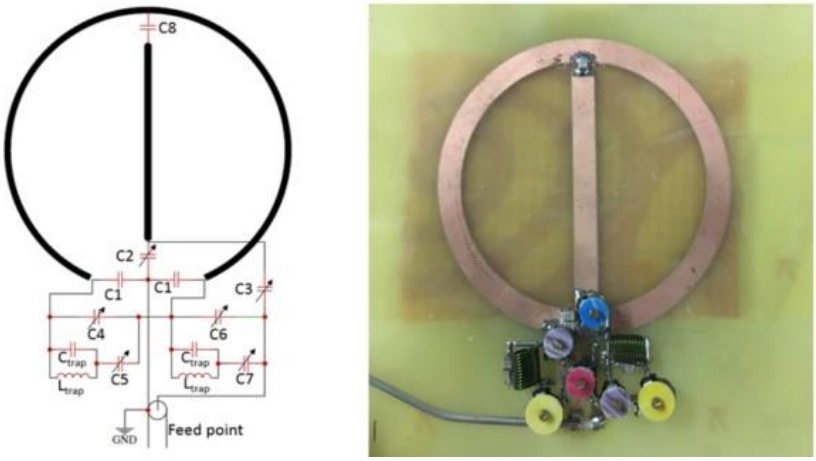

Figure 5.8: Triple-tuned single-port coil designed for ^{1}H, ^{23}Na, and ^{2}H.

Although having all nuclei share a single port makes array design more straightforward, it adds complications to the design of the broadband receiver. Different nuclei have vastly varying abundances and sensitivities, so in order to best utilize the limited dynamic range of the receiver, it is necessary to apply different gains to the separate nuclei. Additionally, if the received signal is to be undersampled, it is necessary to separately filter the different nuclei to reduce the amount of out-of-band noise that will alias into the received signal.

To accomplish both of these goals, it is necessary to separate multi-nuclear received signal from the low-noise amplifier into separate channels for each nucleus for amplitude adjustment and bandpass filtering. Commercially available diplexers and triplexers are typically designed for ham radio use and have bands that are ill-suited to our application.

Our lab has developed a receiver front-end that allows us to split the incoming multinuclear signal into three paths for amplitude adjustment and filtering [65]. The architecture is based on a design used in ultra-wideband systems [66] and allows for easy construction and re-configuration through the swapping of transmission line segments and bandpass filters. The architecture of this triplexer can be seen in Figure 5.9. The front-end can be seen along with a broadband T/R in Figure 5.10. The transmission line segments are chosen such that at the input to each bandpass filter, the shorted transmission line is λ/4 long and presents and open circuit at the tee connection before the filter.

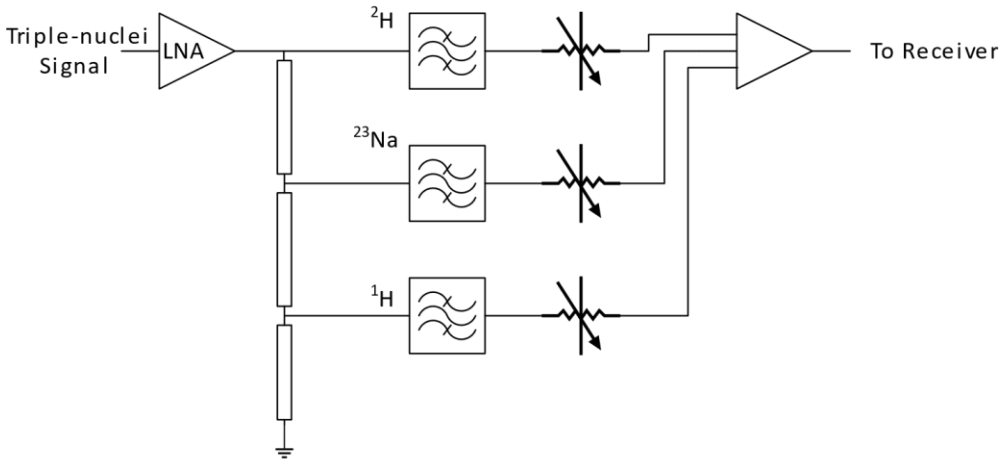

Figure 5.9: Block diagram of flexible triplexer.

Figure 5.10: Triplexing front-end and broadband T/R switch. Top units are, from left-to-right, the broadband signal combiner and the broadband T/R switch. The bottom unit is the signal triplexer and preamplifier unit.

After amplitude adjustment and bandpass filtering, the signals are re-combined with an active three-port combiner, based on the OPA843 (Texas Instruments) operational amplifier.

5.4. Pulse Programming

Because this is a research and development system, it was considered imperative that the pulse sequence programming environment be user-friendly and flexible. Inspired by the pulse sequence programming environment used by Tecmag (Houston, TX, USA) a spreadsheet-based programming environment was developed. A CSV spreadsheet is used to specify a number of time intervals of configurable but fixed duration. During each

interval, the activity of the RF pulse generator, gradient output axes, and digitizer can be specified. These spreadsheets can be generated manually using an editor such as Excel, or they can be generated by helper programs. LabView VIs were developed to automatically generate pulse sequence CSV files based on desired imaging parameters to streamline the creation of routine imaging sequences. The pulse sequence is played out by a LabView GUI that directly controls the spectrometer hardware.

5.5. Transmit Considerations

Using a single-port multi-tuned coil for transmit greatly simplifies the design of the transmit system, but the nonlinearity of the RFPA introduces complications when RF pulses at different frequencies are transmitted simultaneously [67]. Simultaneously amplifying two shaped pulses results in pulse distortion, reduced gain, and the introduction of additional output frequencies arising from intermodulation distortion. A simulation of this behavior can be seen in Figure 5.11.

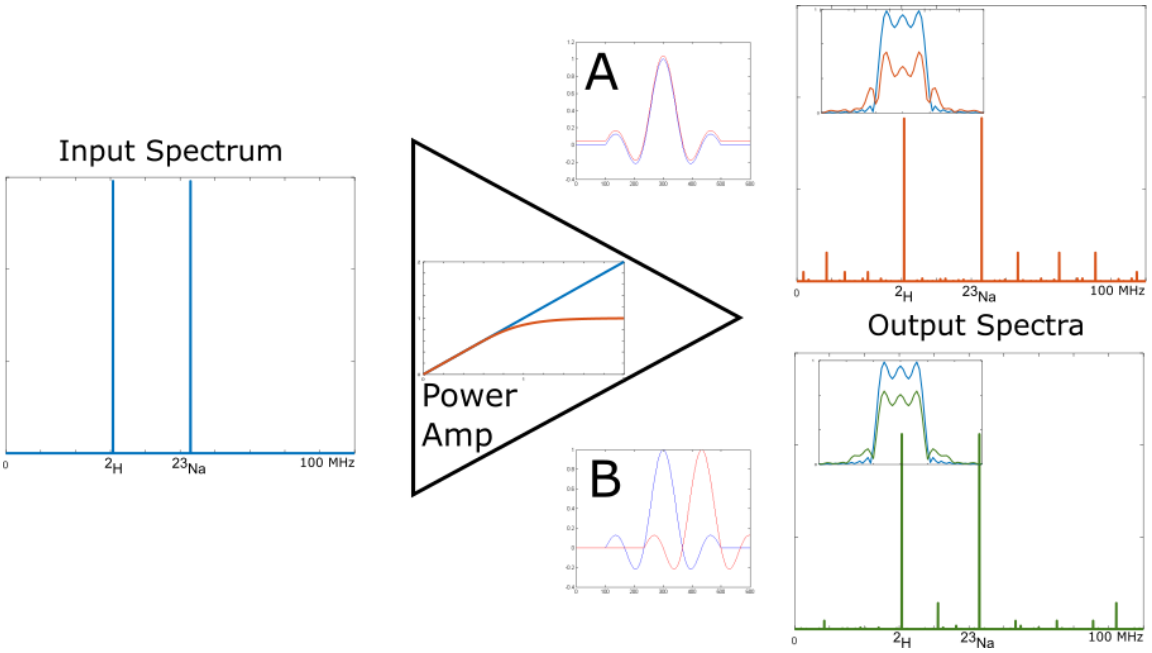

Figure 5.11: How offsetting simultaneous RF pulses can reduce the error in tip angle by reducing maximum instantaneous power. All pulses are five-lobe sinc pulses with durations of 4 ms. The input spectrum is shown on the left. The output spectra are shown on the right after passing through a simulated nonlinear amplifier with the gain curve shown. A depicts the result when the two pulses are not offset in time. B shows the improvement from offsetting the two pulses by the width of the main lobe.

The severity of this problem can be reduced by simply offsetting the two RF pulses in time. This greatly reduces the amplifiers peak output power while only altering the TE or echo timing by a few milliseconds or less.

This was demonstrated with the broadband system and a dual-tuned transmit-receive volume coil was tuned for ^{2}H and ^{23}Na at 4.7T. To measure the effects of nonlinearity, the RF gain necessary to produce a 90° tip in ^{23}Na was measured with singly excited nucleus and with the two nuclei excited with simultaneous RF pulses as well as two offset pulse variants.

Reference data were acquired from by initially only exciting ^{23}Na. Initially, no power was applied at ^{2}H and a calibration curve for ^{23}Na was obtained, tip angle vs. RF power as measured in dB of attenuation. Next, the ^{23}Na was calibrated again while simultaneously applying a high power sinc pulse at ^{2}H. This was repeated with the ^{2}H sinc pulse offset from the ^{23}Na pulse by half the width and the entire width of the main lobe of the sinc pulse, as seen in Figure 5.11. Approximately 200W of power was necessary to achieve a 90° tip in ^{23}Na (with no ^{2}H excitation) and a 700W ^{2}H pulse was applied (lower gyromagnetic ratio nuclei require more current to achieve the same tip angle). In order to accentuate the effects of nonlinearity, a 6 dB high-power attenuator was placed between the RFPA and the coil to simulate the higher power requirements of a larger coil.

Figure 5.12 shows the results of this experiment. As expected, the RF calibration curve with ^{23}Na alone demonstrates the expected sinusoidal behavior, indicating constant amplifier gain with increasing input power. When the simultaneous ^{2}H pulse is added, the calibration curve is distorted, requiring greater input power to reach the same tip angle, indicating saturation of the amplifier. The calibration curve with the shifted RF pulse, shifted only by the minor lobe width, is much closer to the original curve.

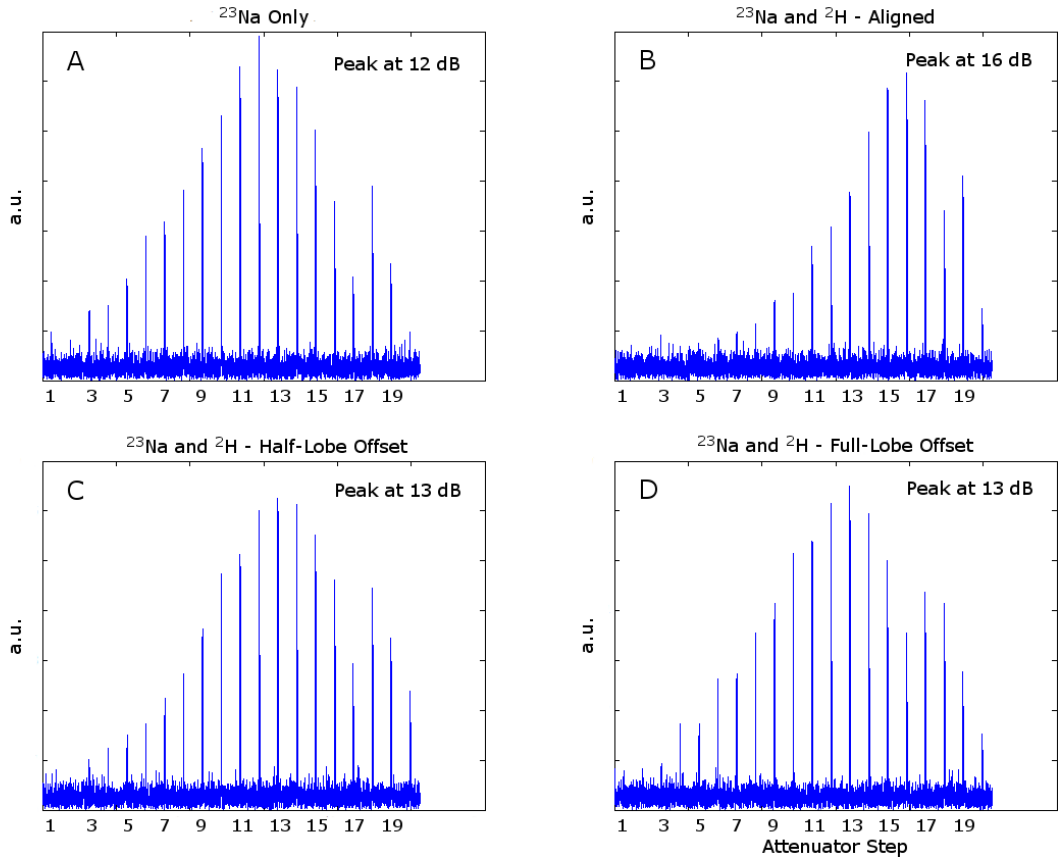

Figure 5.12: Comparison of 23Na pulse calibration series acquired with only a 23Na pulse (A) and simultaneous 23Na and 2H pulses (B-D). The pulse envelopes are shown in Figure 1. In B, the pulses are fully overlapped, causing a 4 dB shift in the amount of power needed to achieve a spin echo. In C and D, the pulses are offset to reduce the change in required power to only 1 dB by shifting the 2H pulse over the width of half or all of the main lobe (respectively).

5.6. Results

A large variety of work has been conducted using this system [63, 68], but two illustrative results have been included that demonstrate the full capabilities of this system. Both results were acquired on a 4.7T small-bore magnet.

5.6.1. Simultaneous Imaging Results

The coil triple-tuned for ^{1}H, ^{23}Na, and ^{2}H was used to acquire simultaneous ^{1}H, ^{23}Na, and ^{2}H images from the phantom shown in Figure 5.13. Simultaneous images were acquired with the triplexer front-end and with a 200 MHz low-pass filter (BLP-200+, Mini-Circuits) for comparison. For reference, images were acquired one-at-a-time of each nucleus on the Varian imaging system. A gradient echo sequence was used with a TR of 1000 ms and a TE of 12 ms.

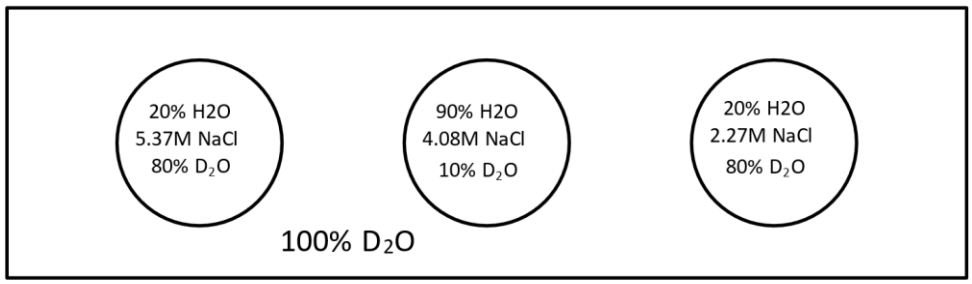

Figure 5.13: Cross-sectional diagram of phantom used for simultaneous imaging of ^{1}H, ^{23}Na, and ^{2}H.

The resulting images can be seen in Figure 5.14. The three images have been scaled and cropped to have the same field of view, so the images from the nuclei with lower gyromagnetic ratios have lower resolutions. The fields of view obtained for ^{1}H, ^{23}Na, and ^{2}H were 100 mm, 378 mm, and 651 mm square, respectively. Because the nuclei were excited simultaneously, their slice thicknesses are also dependent on the gyromagnetic ratio. ^{1}H, ^{23}Na, and ^{2}H have slice thicknesses of 1.79 mm, 6.75 mm, and 11.63mm, respectively. Table 5.1 contains a comparison of the SNRs of images in Figure

5.14. For the X-nuclei, the triplexer front end provides a higher SNR than the reference Varian system. For ^{1}H, it only degrades the SNR by 0.84 dB. The images acquired with a lowpass filter have an inferior SNR in all cases.

Using the broadband system with the triplexer front-end allows us to simultaneously image three nuclei without a significant SNR penalty. Imaging the three nuclei simultaneously cuts the required imaging time in three, which is important when imaging dynamic processes or hyperpolarized substances.

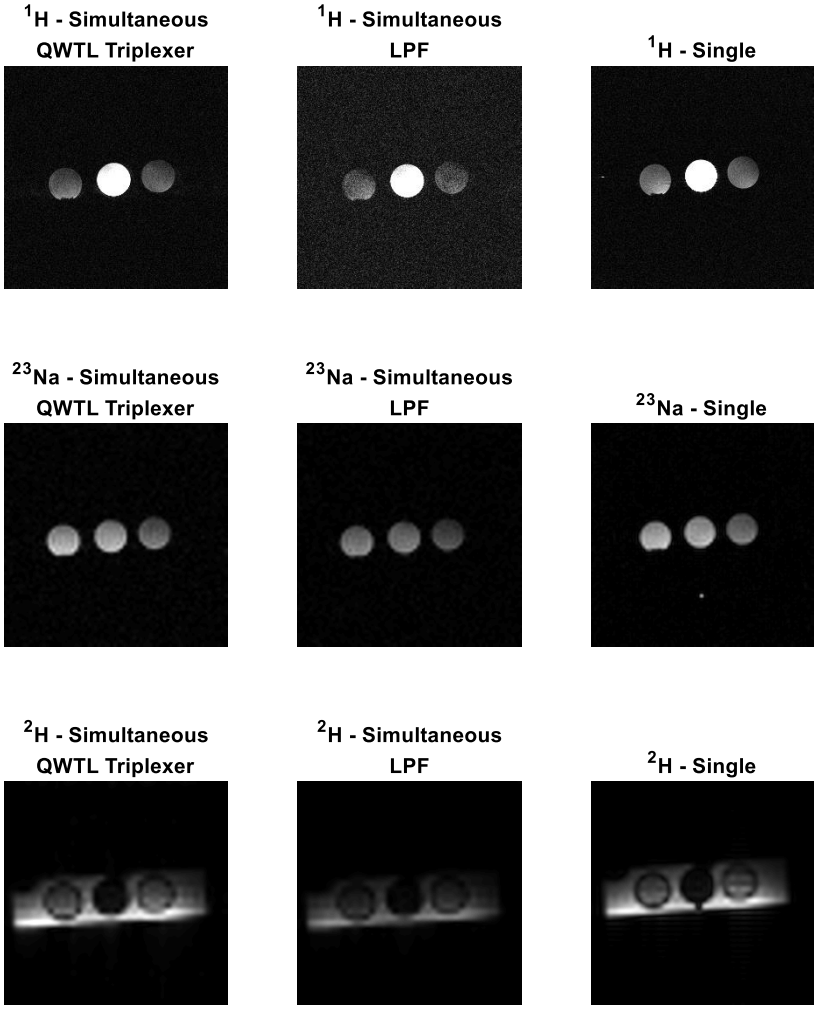

Figure 5.14: Simultaneous ^{1}H, ^{23}Na, and ^{2}H images acquired with the lab-developed triplexer, a lowpass filter, and singly-acquired reference images taken on the Varian imager.

	Maximum SNR		
	Triplexer front-end Simultaneous	Low-pass filter Simultaneous	Varian Single Nucleus
^{1}H	426	185	469
^{23}Na	296	167	274
^{2}H	723	598	700

Table 5.1: SNR comparison of images in Figure 5.14.

5.6.2. Simultaneous Spectroscopy Results

One of the main aims of the broadband system and triplexing front end were that they both be easily reconfigurable for different nuclei and types of experiments. To demonstrate the spectroscopic capabilities of the system, spectra were acquired simultaneously from ^{1}H, ^{13}C, and ^{15}N, using the phantom seen in Figure 5.15 and a coil similar to that in Figure 5.8, but tuned for ^{1}H, ^{13}C, and ^{15}N. Enriched samples of ^{13}C and ^{15}N were used to simplify the experiment, as the low natural abundances of both of these nuclei make spectroscopy of them challenging.

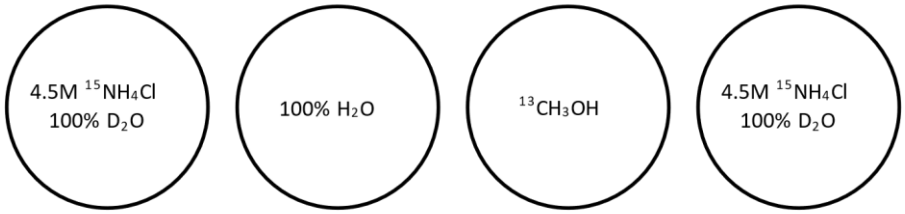

Figure 5.15: Cross-sectional diagram of phantom used for simultaneous imaging of ^{1}H, ^{13}C, and ^{15}N.

Spectra were collected with a simple pulse-and-acquire sequence with a single average. Because hard RF pulses for spectroscopy are of much shorter duration than the sinc pulses used in imaging, it is acceptable to put the RF pulses in succession in order to avoid problems that may occur when sending pulses at different frequencies through a single RFPA [67]. The resulting spectra can be seen in Figure 5.16. The broadband system offers a significant SNR for the X-nuclei in both configurations. The broadband system has slightly lower SNR (0.63 dB) when acquiring ^{1}H spectra.

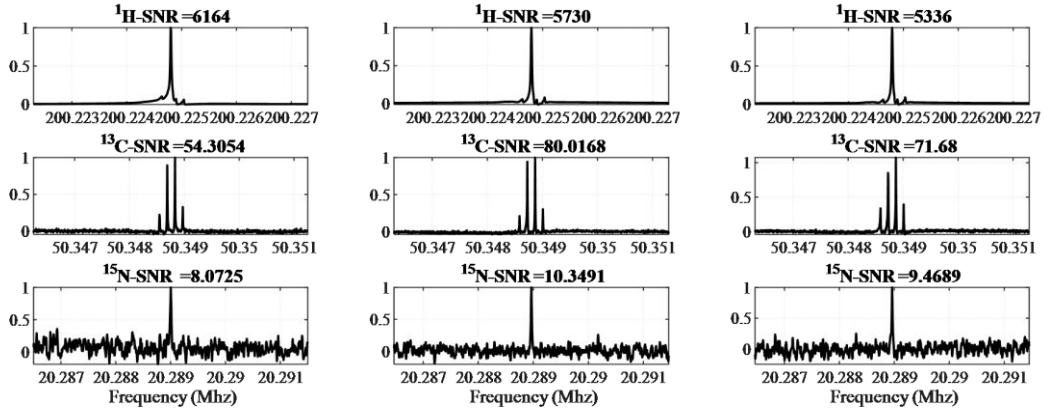

Figure 5.16: Comparison of ^{1}H, ^{13}C, and ^{15}N acquired on broadband system to Varian reference. From left to right, spectra were acquired with the Varian system, the broadband system with all nuclei sharing a single ADC channel, and the broadband system with individual ADCs for each nucleus.

5.7. Conclusion and Discussion

A standalone broadband system for NMR and MRI has been developed and demonstrated with both spectroscopy and imaging. By using direct digital synthesis for transmit and a high-speed multi-channel digitizer for receive, it is possible to operate the same system across a variety of nuclei at 1T and 4.7T with minimal reconfiguration. The broadband system contains compact RF and gradient amplifiers for directly driving a 1T human extremity scanner and can easily be interfaced to the RFPA and gradient amplifiers of a Varian 4.7T small-bore imaging system. Pulse sequence programming is done through a flexible spreadsheet-based interface, and helper programs have been written to generate routinely used sequences.

The system has enabled substantial research at 1T [68]. At 4.7T, the broadband system shows comparable or better SNR for X-nuclei (^{2}H, ^{13}C, ^{15}N, and ^{23}Na) and only a

slight degradation of SNR for ^{1}H. Simultaneous imaging or spectroscopy enables more dense collection of time points in dynamic studies and more efficient use of the magnetization in studies involving hyperpolarized agents.

At present, simultaneous imaging sequences have truly simultaneous excitations, which results in un-equal slice thicknesses and differing fields-of-view based on gyromagnetic ratio, and additional complications arising from the non-linearity of the RFPA. Future work includes the development of pulse sequences that will overcome this limitation, potentially by offsetting the RF excitation pulses [57]. Additionally, we wish to extend the single triple-tuned coils into an array of triple-tuned coils to expand the FOV and improve SNR for multinuclear imaging or CSI.

6. CONCLUSIONS AND DISCUSSION

A variety of technologies for enabling the development and use of array coils for X-nuclei have been presented. Two generations of frequency translating receiver front-ends have been developed and demonstrated. By using active mixers, we can install a system in the scan room that converts the signal received from a non-^{1}H nucleus to the ^{1}H frequency, enabling it to be received by the host MRI system. Using a frequency translating front end allows us to add multinuclear receive capability to a ^{1}H array receiver with a minimum of additional complexity. Using direct digital synthesis for LO generation allows control of the LO phase, enabling us to maintain phase coherence with the add-on system.

The original translation system enabled the first known acquisition of data from a 16-channel ^{13}C coil. Even without using any form of localization, an enormous SNR improvement was demonstrated in a phantom study with a unilateral breast array coil. The second-generation translation system added improved control and monitoring and the ability to translate multiple nuclei to ^{1}H at the same time. By directly interfacing with the host scanner, setup is greatly simplified.

Additionally, a broadband imaging system has been developed to enable the development of techniques and technologies related to simultaneous multi-nuclear imaging and spectroscopy. A broad-band high-speed digitizer and flexible DDS RF pulse synthesizer make this system incredibly flexible.

The gains in SNR from X-nuclear array coils will be even greater for localized spectroscopy. In order to make full use of this, methods for calculating the optimal combination of received signals will need to be further developed.

The development of these systems is important for both natural abundance and hyperpolarized *in vivo* NMR. For natural abundance and enriched studies of thermally polarized nuclei, the improved sensitivity provided by the array reduces the number of averages required to obtain an acceptable SNR. For hyperpolarized studies, the receive arrays can be used to improve resolution from an undersampled signal.

The ultimate goal with all of these applications is the study of metabolism and disease *in vivo*. The huge improvements in SNR that can be provided by X-nuclear receive arrays have the potential to enable more sensitive detection of biomarkers associated with disease processes and improve the resolution of NMR imaging.

REFERENCES

[1] F. Bloch, "Nuclear Induction," *Physical Review,* vol. 70, no. 7-8, pp. 460-474, 10/01/ 1946, doi: 10.1103/PhysRev.70.460.

[2] E. M. Purcell, H. C. Torrey, and R. V. Pound, "Resonance Absorption by Nuclear Magnetic Moments in a Solid," *Physical Review,* vol. 69, no. 1-2, pp. 37-38, 01/01/ 1946, doi: 10.1103/PhysRev.69.37.

[3] W. D. Knight, "Nuclear magnetic resonance shift in metals," *Physical Review,* vol. 76, no. 8, p. 1259, 1949.

[4] W. Dickinson, "Dependence of the F 19 nuclear resonance position on chemical compound," *Physical Review,* vol. 77, no. 5, p. 736, 1950.

[5] N. Muller, P. C. Lauterbur, and J. Goldenson, "Nuclear magnetic resonance spectra of phosphorus compounds," *Journal of the American Chemical Society,* vol. 78, no. 15, pp. 3557-3561, 1956.

[6] P. C. Lauterbur, "C13 nuclear magnetic resonance spectra," *The Journal of Chemical Physics,* vol. 26, no. 1, pp. 217-218, 1957.

[7] B. D. Ross, G. K. Radda, D. G. Gadian, G. Rocker, M. Esiri, and J. Falconer-Smith, "Examination of a case of suspected McArdle's syndrome by 31P nuclear magnetic resonance," *New England Journal of Medicine,* vol. 304, no. 22, pp. 1338-1342, 1981.

[8] C. T. Moonen, R. J. Dimand, and K. L. Cox, "The noninvasive determination of linoleic acid content of human adipose tissue by natural abundance carbon-13 nuclear magnetic resonance," *Magnetic resonance in medicine,* vol. 6, no. 2, pp. 140-157, 1988.

[9] R. Gruetter *et al.,* "Direct measurement of brain glucose concentrations in humans by 13C NMR spectroscopy," *Proceedings of the National Academy of Sciences,* vol. 89, no. 3, pp. 1109-1112, 1992.

[10] A. Madden, M. Leach, J. Sharp, D. Collins, and D. Easton, "A quantitative analysis of the accuracy of in vivo pH measurements with 31P NMR spectroscopy: assessment of pH measurement methodology," *NMR in Biomedicine,* vol. 4, no. 1, pp. 1-11, 1991.

[11] R. A. De Graaf, *In vivo NMR spectroscopy: principles and techniques*. John Wiley & Sons, 2007.

[12] P. B. Roemer, W. A. Edelstein, C. E. Hayes, S. P. Souza, and O. Mueller, "The NMR phased array," *Magnetic resonance in medicine,* vol. 16, no. 2, pp. 192-225, 1990.

[13] S. M. Wright and L. L. Wald, "Theory and application of array coils in MR spectroscopy," *NMR in Biomedicine,* vol. 10, no. 8, pp. 394-410, 1997.

[14] D. K. Sodickson and W. J. Manning, "Simultaneous acquisition of spatial harmonics (SMASH): fast imaging with radiofrequency coil arrays," *Magnetic resonance in medicine,* vol. 38, no. 4, pp. 591-603, 1997.

[15] K. P. Pruessmann, M. Weiger, M. B. Scheidegger, and P. Boesiger, "SENSE: sensitivity encoding for fast MRI," *Magnetic resonance in medicine,* vol. 42, no. 5, pp. 952-962, 1999.

[16] M. P. McDougall and S. M. Wright, "64-channel array coil for single echo acquisition magnetic resonance imaging," *Magnetic Resonance in Medicine: An Official Journal of the International Society for Magnetic Resonance in Medicine,* vol. 54, no. 2, pp. 386-392, 2005.

[17] C. J. Hardy, P. A. Bottomley, K. W. Rohling, and P. B. Roemer, "An NMR phased array for human cardiac 31P spectroscopy," *Magnetic resonance in medicine,* vol. 28, no. 1, pp. 54-64, 1992.

[18] A. Arunachalam *et al.*, "Accelerated spectroscopic imaging of hyperpolarized C-13 pyruvate using SENSE parallel imaging," *NMR in Biomedicine,* vol. 22, no. 8, pp. 867-873, 2009.

[19] J. Tropp *et al.*, "Multi-channel metabolic imaging, with SENSE reconstruction, of hyperpolarized [1-13C] pyruvate in a live rat at 3.0 tesla on a clinical MR scanner," *Journal of magnetic resonance,* vol. 208, no. 1, pp. 171-177, 2011.

[20] Z. Zhu *et al.*, "Coil Combination Methods for Multi-Channel Hyperpolarized 13C Imaging Data from Human Studies," *Journal of Magnetic Resonance,* 2019.

[21] J. D. Kaggie *et al.*, "A 3 T sodium and proton composite array breast coil," *Magnetic resonance in medicine,* vol. 71, no. 6, pp. 2231-2242, 2014.

[22] R. B. Hansen *et al.*, "Coil profile estimation strategies for parallel imaging with hyperpolarized 13C MRI," *Magnetic Resonance in Medicine,* 2019.

[23] J. H. Ardenkjær-Larsen *et al.*, "Increase in signal-to-noise ratio of> 10,000 times in liquid-state NMR," *Proceedings of the National Academy of Sciences,* vol. 100, no. 18, pp. 10158-10163, 2003.

[24] D. G. Gadian, K. S. Panesar, A. J. P. Linde, A. J. Horsewill, W. Köckenberger, and J. R. Owers-Bradley, "Preparation of highly polarized nuclear spin systems using brute-force and low-field thermal mixing," *Physical Chemistry Chemical Physics,* vol. 14, no. 16, pp. 5397-5402, 2012.

[25] J. Kurhanewicz *et al.*, "Analysis of cancer metabolism by imaging hyperpolarized nuclei: prospects for translation to clinical research," *Neoplasia,* vol. 13, no. 2, pp. 81-97, 2011.

[26] C. R. Bowers and D. P. Weitekamp, "Parahydrogen and synthesis allow dramatically enhanced nuclear alignment," *Journal of the American Chemical Society,* vol. 109, no. 18, pp. 5541-5542, 1987.

[27] K. Golman, O. Axelsson, H. Jóhannesson, S. Månsson, C. Olofsson, and J. Petersson, "Parahydrogen-induced polarization in imaging: Subsecond 13C angiography," *Magnetic Resonance in Medicine: An Official Journal of the International Society for Magnetic Resonance in Medicine,* vol. 46, no. 1, pp. 1-5, 2001.

[28] J.-B. Hövener *et al.*, "PASADENA hyperpolarization of 13C biomolecules: equipment design and installation," *Magnetic Resonance Materials in Physics, Biology and Medicine,* vol. 22, no. 2, pp. 111-121, 2009.

[29] J. F. Colell *et al.*, "Generalizing, extending, and maximizing nitrogen-15 hyperpolarization induced by parahydrogen in reversible exchange," *The Journal of Physical Chemistry C,* vol. 121, no. 12, pp. 6626-6634, 2017.

[30] J. S. Waugh, "Theory of broadband spin decoupling," *Journal of Magnetic Resonance (1969)*, vol. 50, no. 1, pp. 30-49, 1982/10/15 1982, doi: http://dx.doi.org/10.1016/0022-2364(82)90029-4.
[31] J. S. Waugh, "Systematic procedure for constructing broadband decoupling sequences," *Journal of Magnetic Resonance (1969)*, vol. 49, no. 3, pp. 517-521, 1982.
[32] A. Shaka, J. Keeler, and R. Freeman, "Evaluation of a new broadband decoupling sequence: WALTZ-16," *Journal of Magnetic Resonance (1969)*, vol. 53, no. 2, pp. 313-340, 1983.
[33] P. C. Lauterbur, "Image Formation by Induced Local Interactions: Examples Employing Nuclear Magnetic Resonance," *Nature*, vol. 242, no. 5394, pp. 190-191, 1973/03/01 1973, doi: 10.1038/242190a0.
[34] D. Guilfoyle and P. Mansfield, "Chemical-Shift Imaging," *Magnetic resonance in medicine*, vol. 2, no. 5, pp. 479-489, 1985.
[35] B. Gilbert, "A precise four-quadrant multiplier with subnanosecond response," *IEEE journal of solid-state circuits*, vol. 3, no. 4, pp. 365-373, 1968.
[36] Analog Devices, *A Technical Tutorial on Direct Digital Synthesis*. 1999.
[37] S. M. Wright, M. P. McDougall, K. Kurpad, and D. G. Brown, "Parallel imaging: system design and limitations," in *IEEE International Symposium on Biomedical Imaging: Nano to Macro 2004*, 15-18 April 2004 2004, pp. 1200-1203 Vol. 2, doi: 10.1109/ISBI.2004.1398759.
[38] D. G. Brown, "Instrumentation for parallel magnetic resonance imaging," Texas A&M University, 2007.
[39] P. P. Stang, S. M. Conolly, J. M. Santos, J. M. Pauly, and G. C. Scott, "Medusa: a scalable MR console using USB," *IEEE transactions on medical imaging*, vol. 31, no. 2, pp. 370-379, 2012.
[40] C. E. Hayes, N. Hattes, and P. B. Roemer, "Volume imaging with MR phased arrays," *Magnetic resonance in medicine*, vol. 18, no. 2, pp. 309-319, 1991.
[41] S. E. Ogier and S. M. Wright, "A frequency translation approach for multichannel 13 C spectroscopy," in *2015 37th Annual International Conference of the IEEE Engineering in Medicine and Biology Society (EMBC)*, 2015: IEEE, pp. 1564-1567.
[42] R. F. Lee, R. Giaquinto, C. Constantinides, S. Souza, R. G. Weiss, and P. A. Bottomley, "A broadband phased-array system for direct phosphorus and sodium metabolic MRI on a clinical scanner," *Magnetic resonance in medicine*, vol. 43, no. 2, pp. 269-277, 2000.
[43] B. Razavi, *RF microelectronics*. Pearson Education, 2012.
[44] Analog Devices. ADL5801 [Online] Available: https://www.analog.com/media/en/technical-documentation/data-sheets/adl5801.pdf
[45] D. M. Pozar, *Microwave Engineering*, 2nd ed. John Wiley & Sons, 1998.
[46] R. E. Collin, *Foundations for microwave engineering*. John Wiley & Sons, 1992.

[47] R. J. Ordidge, A. Connelly, and J. A. Lohman, "Image-selected in vivo spectroscopy (ISIS). A new technique for spatially selective NMR spectroscopy," *Journal of Magnetic Resonance (1969)*, vol. 66, no. 2, pp. 283-294, 1986.

[48] P. A. Bottomley, "Spatial localization in NMR spectroscopy in vivo," *Annals of the New York Academy of Sciences*, vol. 508, no. 1, pp. 333-348, 1987.

[49] J. D. Kaggie *et al.*, "Synchronous radial 1H and 23Na dual-nuclear MRI on a clinical MRI system, equipped with a broadband transmit channel," *Concepts in Magnetic Resonance Part B: Magnetic Resonance Engineering*, vol. 46, no. 4, pp. 191-201, 2016.

[50] Z. Yu, G. Madelin, D. K. Sodickson, and M. A. Cloos, "Simultaneous proton MR fingerprinting and sodium imaging," in *International Society for Magnetic Resonance in Medicine Annual Meeting & Exhibition*, Montreal, 2019, p. 0488. [Online]. Available: https://index.mirasmart.com/ISMRM2019/PDFfiles/0488.html. [Online]. Available: https://index.mirasmart.com/ISMRM2019/PDFfiles/0488.html

[51] M. Meyerspeer, A. W. Magill, A. Kuehne, R. Gruetter, E. Moser, and A. I. Schmid, "Simultaneous and interleaved acquisition of NMR signals from different nuclei with a clinical MRI scanner," *Magnetic resonance in medicine*, vol. 76, no. 5, pp. 1636-1641, 2016.

[52] J. Keeler, *Understanding NMR spectroscopy*. John Wiley & Sons, 2011.

[53] Microsemi Corp., "The PIN Diode Designers' Handbook," 1998. [Online]. Available: https://www.ieee.li/pdf/essay/pin_diode_handbook.pdf

[54] T. DiCola. "Freq Show: Raspberry Pi RTL-SDR Scanner." Adafruit. https://learn.adafruit.com/freq-show-raspberry-pi-rtl-sdr-scanner/overview (accessed.

[55] R. A. de Graaf, "Theoretical and experimental evaluation of broadband decoupling techniques for in vivo nuclear magnetic resonance spectroscopy," *Magnetic resonance in medicine*, vol. 53, no. 6, pp. 1297-1306, 2005.

[56] K. R. Thulborn, N. F. Soffe, and G. K. Radda, "Simultaneous in vivo measurement of oxygen utilization and high-energy phosphate metabolism in rabbit skeletal muscle by multinuclear 1H and 31P NMR," *Journal of Magnetic Resonance (1969)*, vol. 45, no. 2, pp. 362-366, 1981.

[57] O. Gonen *et al.*, "Simultaneous and interleaved multinuclear chemical-shift imaging, a method for concurrent, localized spectroscopy," *Journal of Magnetic Resonance, Series B*, vol. 104, no. 1, pp. 26-33, 1994.

[58] J. Keupp *et al.*, "Simultaneous dual-nuclei imaging for motion corrected detection and quantification of 19F imaging agents," *Magnetic resonance in medicine*, vol. 66, no. 4, pp. 1116-1122, 2011.

[59] O. Gonen, J. Hu, J. Murphy-Boesch, R. Stoyanova, and T. R. Brown, "Dual interleaved 1H and proton-decoupled-31P in vivo chemical shift imaging of human brain," *Magnetic resonance in medicine*, vol. 32, no. 1, pp. 104-109, 1994.

[60] D. Ma *et al.*, "Magnetic resonance fingerprinting," *Nature*, vol. 495, no. 7440, pp. 187-192, 2013.

[61] B. E. Kidd *et al.*, "Toward Cleavable Metabolic/pH Sensing “Double Agents” Hyperpolarized by NMR Signal Amplification by Reversible Exchange," *Chemistry–A European Journal,* vol. 24, no. 42, pp. 10641-10645, 2018.

[62] M. R. Smith *et al.*, "In Vivo Imaging and Spectroscopy of Dynamic Metabolism Using Simultaneous 13C and 1H MRI," *IEEE Transactions on Biomedical Engineering,* vol. 59, no. 1, pp. 45-49, 2011.

[63] S. E. Ogier, J. C. Bosshard, and S. M. Wright, "A Broadband Spectrometer for Simultaneous Multinuclear Magnetic Resonance Imaging and Spectroscopy," in *International Society for Magnetic Resonance in Medicine,* 2016.

[64] N. V. Anisimov and O. S. Pavlova, "Simultaneous Recording of NMR Signals from Nuclei with Different Gyromagnetic Ratios Using Undersampling Technique," *Applied Magnetic Resonance,* pp. 1-10, 2018.

[65] C.-H. Huang, S. E. Ogier, M. Gu, and S. M. Wright, "Flexible RF Filtering Front-End For Simultaneous Multinuclear MR Spectroscopy," in *2018 40th Annual International Conference of the IEEE Engineering in Medicine and Biology Society (EMBC)*, 2018: IEEE, pp. 1368-1371.

[66] M. Karlsson, A. Serban, J. Osth, and S. Gong, "Frequency triplexer for ultra-wideband systems (6–9 GHz)," *IEEE Transactions on Circuits and Systems I: Regular Papers,* vol. 60, no. 3, pp. 540-547, 2012.

[67] S. E. Ogier, H. Dong, S. M. Wright, and J. C. Bosshard, "RF Power Considerations for Simultaneous Multi-Nuclear MRI/MRS," in *International Society for Magnetic Resonance in Medicine*, 2017, p. 2700.

[68] M. Gu *et al.*, "Dynamic 31P MRS of Skeletal Muscle with a 1 Telsa Extremity Scanner," in *International Society for Magnetic Resonance in Medicine,* 2019.

APPENDIX A

CONTROL SCHEME FOR MULTINUCLEAR TRANSLATION SYSTEM

A-1. Control Unit Software

bbb_server.py is the main program that runs on the BBB. It must do the following:

- Drive the optical UART
- Program the AD9959 to provide the LO
- Control the TPI RF synth.
- Interface with the RTL-SDR

bbb_server.py opens a ZMQ socket, which the client can connect to. The client connects to this socket and sends commands over this link. The BBB server replies to each command – the ZMQ REP-REQ connection requires a response from the server before the client can send a message again.

bbb_server.py also initializes the RTL-SDR server. This runs in the background and doesn't connect to our ZMQ socket. All that's required is to run it at the start and close it when the program terminates.

bbb_server.py parses the commands from the ZMQ socket to determine whether they are for the FTU or the TPI. The commands are prefixed with four characters.

- FTU: Precedes a command for the FTU Control Board (MCU). This command is passed to an FTUBridge object that controls the optical link to the FTU Control Board
    - FTU:POWER UP Reply for Power Up is FTU Control Wakeup Complete!

        - FTU:POWER DOWN Reply for Power Down is FTU Control Shutdown Complete!
        - For all other commands, the FTUBridge object checks by default to make sure the FTU MCU replies with the same command that was sent. If there's no response, the FTUError is raised with message "No heartbeat response". If the response is to resend the last command, the BBB will resend the last command. If this fails, FTUError will be raised with message "MCU not receiving valid command". If the heartbeat response is different from the sent message, FTUError will be raised with message "Incorrect heartbeat response". If the heartbeat response is correct, the reply is FTU Write Successful!
        - If the FTUBridge has been configured not to check the heartbeat response, the reply will always be FTU Write Unknown Result?
- TPI: Precedes a command for the TPI Synthesizer. This command is passed to a TPIBridge object that controls the USB serial link to the TPI Synthesizer.
    - TPI:WRITE:[message] Writes [message] to TPI synthesizer. Reply is TPI Write Complete!
        - If message is output on or off command, the bbb_server also turns the TPI Output On indicator LED on or off.
    - TPI:READ:[int] Reads [int] bytes from TPI synthesizer. Reply is TPI Data Read:[bytes read]

- DDS: Precedes a command for AD 9959 DDS Frequency Synthesizer. This command is passed to a DDSBridge object that controls the SPI link to the 9959.
    - DDS:WRITE:[message] Writes [message] to AD 9959
    - DDS:READ:[register][length] Reads [length] bytes from [register]
    - DDS:RESET Toggles line to reset AD 9959
- PLL: Precedes a command for CDCE706 PLL Frequency Synthesizer. This command is passed to a PLLBridge object that controls the SMBus/I2C link to the CDCE706.
    - PLL:WRITE:[message] Writes a series of bytes to CDCE706 starting with register 0
    - PLL:READ:[register] Reads a single byte from specified register
    - PLL:BREAD Block read of all bytes of CDCE706, starting from register 1. Register 0 can only be read with byte read command.
- BBB: Precedes a command for the Beaglebone Black. This command isn't passed to anything.
    - BBB:HEARTBEAT Checks that BBB is still responding. Reply is HEARTBEAT

Errors are handled in a way that attempts to keep the bbb_server.py running. If the exception is raised by one of the device control objects (FTUError, TPIError, DDSError, or PLLError), bbb_server.py will catch it, send the error message back with a preface indicating the type of exception. For example, if the FTUBridge object doesn't

receive a heartbeat response from the FTU MCU, it will raise the exception FTUError with the message “No heartbeat response”. This would be caught by bbb_server.py, and the message FTU Error: No heartbeat response would be sent to the client.

Invalid messages are handled without raising an exception by sending a reply to the client. If bbb_server.py is unable to determine which device the command is for, it replies Invalid command of unknown type. If it can determine which device the command is for, the reply will take the form Invalid [DEV] command:[message], where [DEV], is the three-letter-acronym for the device the command was intended for and [message] is the message as received by the BBB. For example, an invalid DDS command would generate the reply Invalid DDS command:DDS:WRONG.

The exception to this is for the FTU. The FTU MCU only supports write operations and power up/down commands. If the command isn’t a power up or down command, the bbb_server.py simply forwards it to the FTU MCU, so it isn’t possible to generate an Invalid FTU command:[…] message.

A-2. Optical Interface

The optical link has four polymer optical fibers (POFs) that connect Control Unit and the FTU. The function of each fiber is specified in Table A-1.

Fiber	Direction	Function
1	FTU->CU	Data return (UART)
2	CU->FTU	Data send (UART)
3	CU->FTU	Blanking (Active High)
4	CU->FTU	Wake-Up

Table A-1: Optical Interface Description

A-3. FTU MCU Control Scheme

Bit								Function
7	6	5	4	3	2	1	0	
1	1	[VGA Setting, 6b]						Program VGA(s)
1	0	0	0	[LE Setting, 4b]				Set active LE bits
1	0	0	1	[BS Setting, 4b]				Set active BS bits
1	0	1	0	VC2	VC1	S2	S1	Set board-level switches
1	0	1	1	R*	R*	MS2	MS1	Set monitoring switch (chooses board)
0	0	0	1	1	1	0	0	Heartbeat
0	0	0	0	0	1	1	0	Power Down
0	0	0	0	0	0	0	1	Resend last byte

*Reserved

Table A-2: Optical Interface Command Scheme

All unspecified commands are presently unallocated.

A-3.1 Power Up

To wake up the MCU, the wake-up line is brought low. This triggers an interrupt that wakes up the MCU.

A-3.2 Power Down

To power down the MCU, the wake-up line is brought high, then the shutdown command is sent to the microcontroller over the serial link.

APPENDIX B

PIN DIODE DRIVER FOR MULTINUCLEAR TRANSLATION SYSTEM

B-1. Design

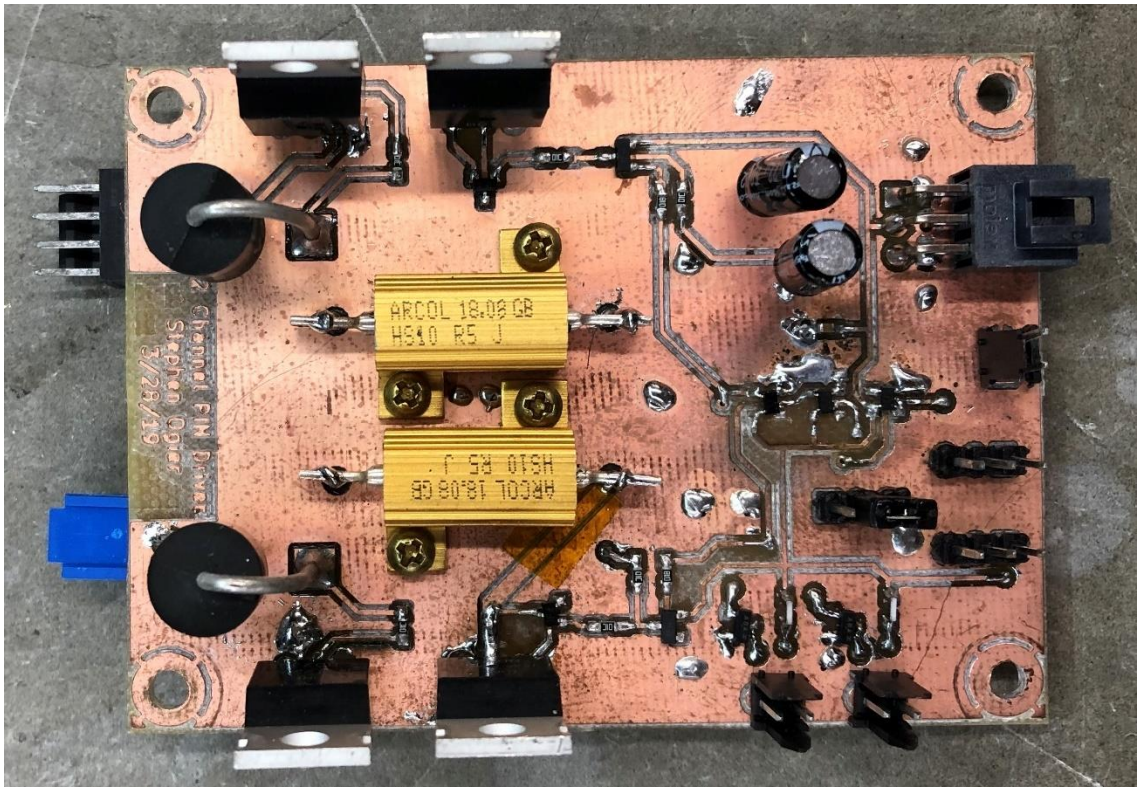

This PIN diode driver was designed to provide a more robust driver for array coils compatible with the Philips Achieva 7T system. The Philips system uses -5 V for forward bias and approximately +15 V for reverse bias. This circuit uses similar voltages, although in order to increase the forward bias current of our receive elements, the forward bias voltage was increased to approximately -6.5 V.

The driver has two complimentary outputs, one for the transmit coil, and one for the receive array. Controlling both PIN driver outputs from a single input ensures that at

no point are both the transmit and receive elements tuned, other than briefly during switching.

Manual control of the state of the transmit and receive coils has proven helpful when testing the coils on the bench and during setup. In order to streamline this, a switch was included to switch the input from the system's TTL control line to a manual switch that can select the transmit or receive states.

The gating signal from the Philips Achieva 7T is low during transmit. Other systems, including the Varian Unity Inova systems in the MRSL, have high gating signals during transmit. This is accommodated for by a jumper, which enables bypassing an inverter to allow both polarity control signals to be used. This inverter is after the manual control logic, so changing its configuration also reverses the sense of the manual control. This is easily fixed by flipping the connector on the cable for the manual control switch.

B-2. Schematics

Figure B-1 shows the top-level schematic of the PIN diode driver. The TTL control input is on the left, and the two PIN diode driver output circuits are the blocks on the right.

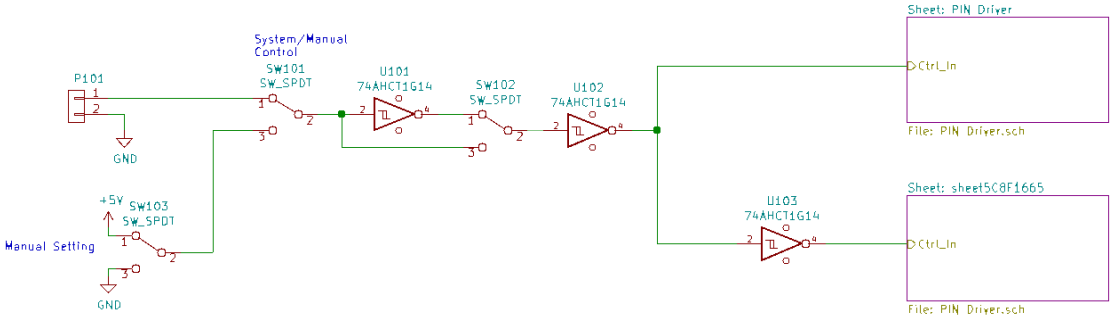

Figure B-1: Overview Schematic

Figure B-2 shows the schematic of an individual PIN diode driver channel. The control input on the left is a TTL-compatible signal. Each channel has two outputs: the top output is the PIN diode drive voltage, and the bottom output is to drive an indicator LED.

A Darlington pair is used for the PIN diode drive transistor to allow for a small control current to provide a large maximum output current.

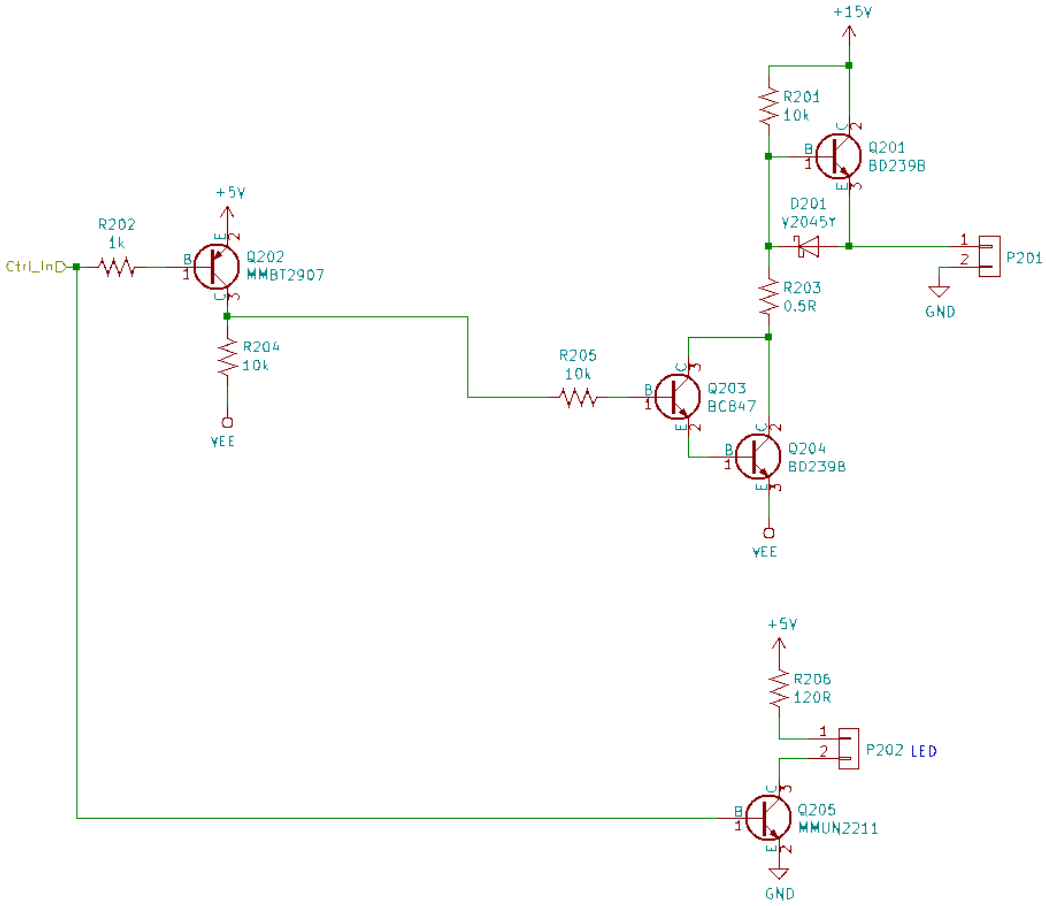

Figure B-2: PIN diode and LED driver circuits.

APPENDIX C

MULTI-PURPOSE CLOCK SYNTHESIS BOARD

C-1. Overview

The initial version of the Broadband System used a single 10 MHz TCXO with several buffered outputs as the system frequency reference. As the system grew in capability, it became necessary to generate clock signals at other frequencies, for example to supply the reference oscillator for the AD9959 or the sampling clock for the UltraView acquisition board. A clock source with multiple, independently programmable outputs was needed that also had 10 MHz reference outputs for synchronizing other devices.

The Multi-Purpose Clock Synthesis board is based around the CDCE706 programmable PLL clock synthesizer. This IC has three internal PLLs and from which up to 6 outputs can be derived. It can take operate off of an on-board 10 MHz TCXO or an external oscillator. The board also includes an NB3L553 clock fanout buffer to provide three extra 10 MHz outputs for synchronization and future use.

This board later found use in the Multinuclear Frequency Translation System where it increases the frequency of the reference oscillators so that it can be further stepped up by the AD9959's built-in PLL.

C-2. Schematics

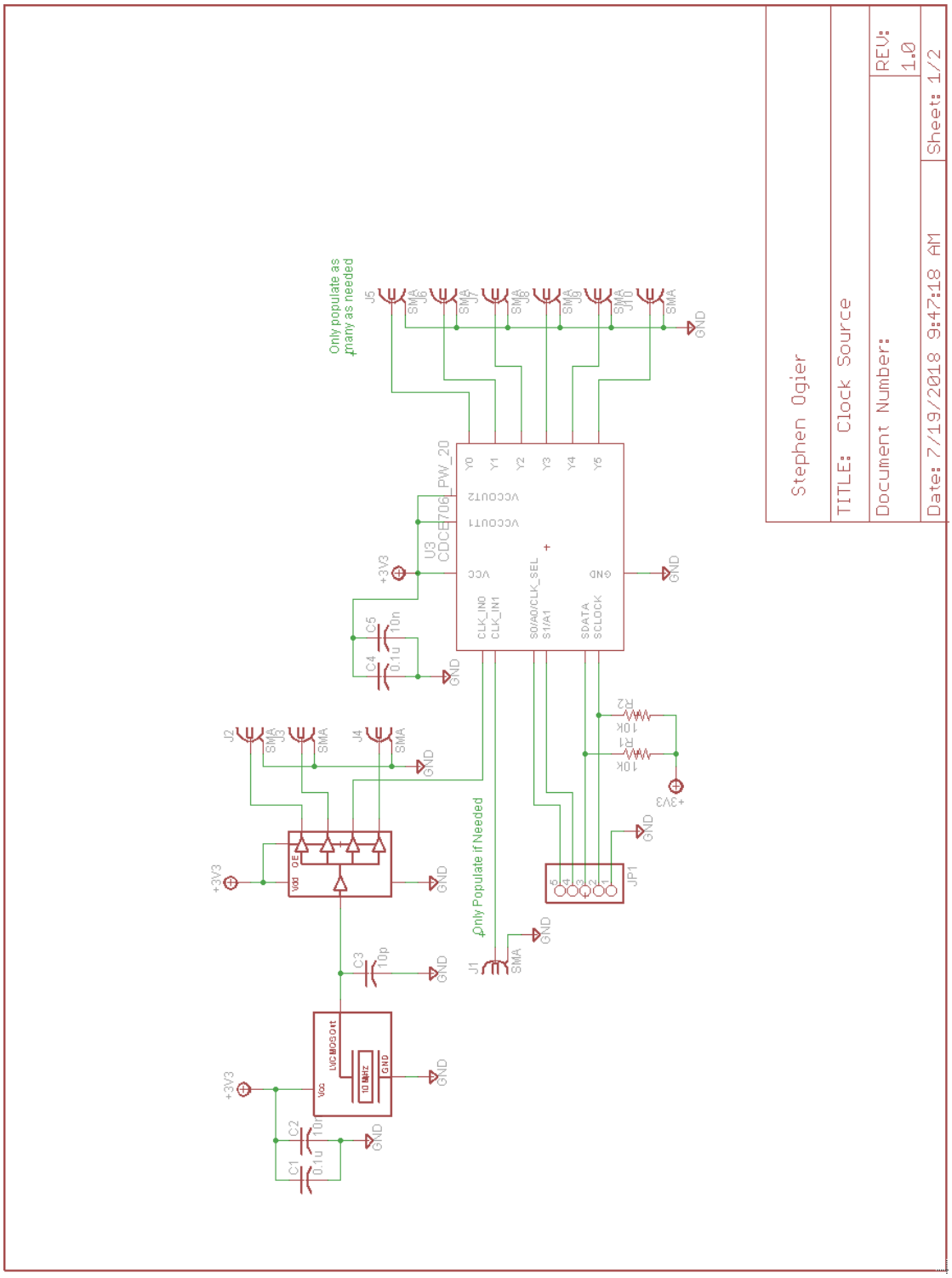

Figure C-1: Clock Synthesizer Schematic

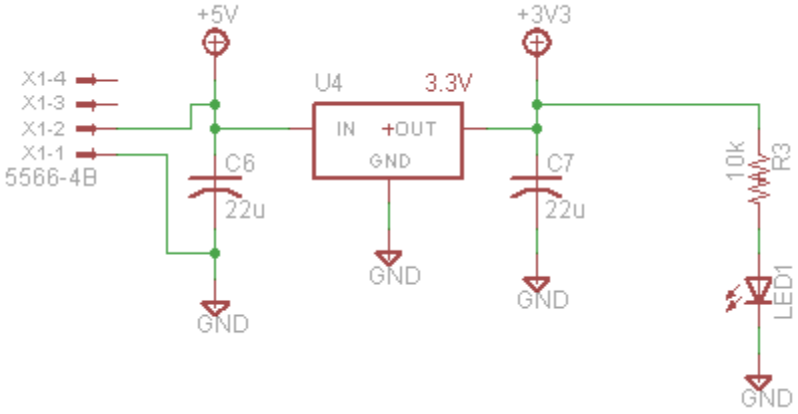

Figure C-2: Clock Synthesizer Voltage Regulation

C-3. Assembly Options

If the PLL is only going to be operated from an external reference oscillator (as is done in the Multinuclear Frequency Translation System), then it is not necessary to populate the parts responsible for generating and splitting the built-in oscillator. This allows one to omit the 10 MHz temperature-controlled crystal oscillator and 4-way active clock splitter.

C-4. Programming

The PLL IC in is programmed over the I^2C interface, which enables it to be easily integrated into a system. The configuration parameters are in a dense, proprietary format, so a script was written by Dr. John Bosshard to generate hexadecimal control files that can be written to the PLL over an I^2C link with minimal overhead. This script can be run in either the Matlab or Octave environments.

APPENDIX D

VARIAN UNITY INOVA FREQUENCY TRANSLATION PULSE SEQUENCE

This is a version of the Varian s2pul.c pulse sequence that has been modified to support frequency translation. Two principle changes have been made:

- The sequence has had the transmit and receive frequencies hard-coded so that the system frequency can be changed during the pulse sequence so that the transmit pulse is at the frequency of the X-nucleus (^{13}C for most of this work), and the received signal is at the ^{1}H frequency.
- Statements have been added to turn a spare TTL line (spare 2) on and off before each acquisition. This was done in order to provide a means of resetting the phase of the translator's LO to ensure phase coherence of the system.

This pulse sequence was also used to collect reference data. To do this, the only required modification was to change both the transmit and receive frequencies to be the frequency of the X-nucleus.

```
#ifndef LINT
static char SCCSid[] = "@(#)s2pul.c 14.1 12/08/98 Copyright
(c) 1991-1996 Varian Assoc.,Inc. All Rights Reserved";
#endif

/*  s2pul - standard two-pulse sequence */

#include <standard.h>
```

```
pulsesequence()
{

   double freqs[2] = {200.222, 50.348};
   create_freq_list(freqs ,2 ,OBSch ,0);

   v1 = zero;
   /* equilibrium period */
   sp2on();          /* Added 09-09-14 to reset LO source */
   status(A);
   hsdelay(d1);
   sp2off();   /* Added 09-09-14 to reset LO source */

   /* --- tau delay --- */

   incr(v1);
   vfreq(0, v1);

   status(B);
/* pulse(p1, zero);  Removed unused pulse 09-09-14 */
   hsdelay(d2);

   /* --- observe period --- */
   status(C);
   pulse(pw, oph);
   /* Added 09-09-14 to force TX to 13C */
   decr(v1);
   vfreq(0, v1);
   rcvron();
   txphase(zero);
   decphase(zero);
   delay(alfa+(1.0/(beta*fb)));
   acquire(np,1.0/sw);

   }
```

APPENDIX E

MATLAB FUNCTIONS FOR SPECTRAL DATA PROCESSING

E-1. phasing.m

```
function [ phased ] = phasing( spectra, phases )
%phasing Applies 0-order phase correction to an array of spectra or
FIDs.
% Uses default number of points and sampling rate
% np = 32768

np = size(spectra,1);

phases_0 = ones(np,1)*phases;

pc = exp(-1i*phases_0*pi/180);

phased = spectra .* pc;

end
```

E-2. lb.m

```
function [ widened ] = lb(FIDs, sw, width)
%lb Performs exponential line broadening.
%   Can operate on arrays of FIDs
%   Time is in first dimension
%   Array is in second dimension
%
%   sw is spectral width aka sampling rate
%   width is line broadening width in Hz


np = size(FIDs,1);
t = (0:np-1)/sw;

weight = exp(-t*width)'* ones(1,size(FIDs,2));

widened = FIDs.*weight;

end
```

E-3. snr.m

```
function [ snr ] = snr( data )
%Calculates Peak/standard deviation SNR

s = max(real(data));

n = std(real(data(end-1000:end)),[],1);

snr = s./n;

end
```